Raul Corrêa Silva

Quantum interference of force, Hanbury Brown and Twiss interference with electrons, and photon reflection by a quantum mirror

Tese apresentada ao Programa de Pós-Graduação em Física do Instituto de Ciências Exatas da Universidade Federal de Minas Gerais como requisito parcial para obtenção do título de Doutor em Ciências.

Supervisor: Pablo Lima Saldanha

Belo Horizonte

2019

Dados Internacionais de Catalogação na Publicação (CIP)

Silva, Raul Corrêa.

S586q Quantum interference of force, Hanbury Brown and Twiss with electrons, and photon reflection by a quantum mirror/ Raul Corrêa Silva. – 2019.
92 f. il.

Orientador: Pablo Lima Saldanha.
Tese (doutorado) – Universidade Federal de Minas Gerais – Departamento de Física.
Bibliografia: f. 81 -89.

1. Interferência quântica. 2. Óptica quântica. 3. Elétrons. Tese. I.Título. II. Saldanha, Pablo Lima.

CDU – 535 (043)

Elaborada pela Biblioteca Professor Manoel Lopes de Siqueira da UFMG.

Universidade Federal de Minas Gerais
Instituto de Ciências Exatas
Programa de Pós-Graduação em Física
Caixa Postal 702
30.123-970 Belo Horizonte - MG - Brasil

Telefone (xx) (31) 3409 5637
(xx) (31) 3409 5633
Fax (xx) (31) 3409 5688
(xx) (31) 3409 5600
e-mail pgfisica@fisica.ufmg.br

ATA DA SESSÃO DE ARGUIÇÃO DA 352ª TESE DO PROGRAMA DE PÓS-GRADUAÇÃO EM FÍSICA, DEFENDIDA POR Raul Corrêa Silva orientado pelo professor Pablo Lima Saldanha para obtenção do grau de **DOUTOR EM CIÊNCIAS, área de concentração Física**. Às 09:00 horas de vinte e sete de fevereiro de dois mil e dezenove na sala 4129 do Departamento de Física da UFMG, reuniu-se a Comissão Examinadora, composta pelos professores **Pablo Lima Saldanha** (Orientador - Departamento de Física/UFMG), **Leonardo Teixeira Neves** (Departamento de Física/UFMG), **Reinaldo Oliveira Vianna** (Departamento de Física/UFMG), **Stephen Patrick Walborn** (Instituto de Física/UFRJ) e **Gabriela Barreto Lemos** (International Institute of Physics - UFRN) para dar cumprimento ao Artigo 37 do Regimento Geral da UFMG, submetendo o Mestre **Raul Corrêa Silva** à arguição de seu trabalho de Tese de Doutorado, que recebeu o título de **"Quantum interference of force, Hanbury Brown and Twiss interference with electrons, and photon reflection by a quantum mirror".** Às 14:00 horas do mesmo dia o candidato fez uma exposição oral de seu trabalho durante aproximadamente 50 minutos. Após esta, os membros da comissão prosseguiram com a sua arguição e apresentaram seus pareceres individuais sobre o trabalho, concluindo pela aprovação do candidato.

Belo Horizonte, 27 de fevereiro de 2019.

Prof. Pablo Lima Saldanha
Orientador do estudante
Departamento de Física/UFMG

Prof. Stephen Patrick Walborn
Instituto de Física/UFRJ

Prof. Leonardo Teixeira Neves
Departamento de Física/UFMG

Dra. Gabriela Barreto Lemos
International Institute of Physics/UFRN

Prof. Reinaldo Oliveira Vianna
Departamento de Física/UFMG

Candidato Raul Corrêa Silva

Agradecimentos

Antes de tudo agradeço ao Pablo, que me orientou desde o mestrado e por todo o doutorado, sempre com a disponibilidade e estímulo necessários. Sua orientação, apoio e conselhos acadêmicos, científicos e profissionais certamente tornaram esse processo mais tranquilo, evitando sempre obstáculos desnecessários. Foi um prazer o trabalho durante todo esse tempo!

Agradeço aos professores, colegas e amigos do Enlight, por proporcionarem um ambiente de trabalho sempre agradável e estimulante. Aos colegas e amigos físicos que sempre reencontro pelas conferências. Aos amigos Denise e Davi pelo companheirismo, carinho, cafés e constante troca de idéias de sempre! Esse doutorado tem muitas boas marcas de vocês.

Agradeço aos meus pais, irmão e demais familiares pelo amor fundamental de sempre, pelo apoio na carreira e pela compreensão das peculiaridades da minha profissão. Aos amigos sempre tão importantes e centrais na minha vida, Carol, Cris, Lilian, Gabo, Lulis, Tomaz, Thyer, Ian, Augusto, Felipe, Hélio, e todos os que estiveram presentes de algum modo. And Kah Chun Pau, you know how important you were to me during our time together and after. All that we shared makes you an essential piece of this thesis.

I immensely thank Joachim, who received me so well in his group in Erlangen for the 12 months that I have been there. The welcoming was a big help in making me feel comfortable when I was so far from home. My sincere gratitude also to my group colleagues, who were always very kind and helpful to me, and provided such an exciting work environment of constant exchange of ideas about physics and everything else.

Obrigado a toda a equipe de trabalhadores do Departamento de Física da UFMG, secretarias, colegiados, biblioteca, professores, às equipes de limpeza e segurança do ICEx, todos são fundamentais para proporcionar um ambiente de trabalho funcional e estimulante na Universidade.

Agradeço ao CNPq e à CAPES pelo apoio financeiro durante o doutorado realizado no Departamento de Física da UFMG, através das bolsas de doutorado e taxa de bancada. Agradeço à CAPES pelo apoio financeiro oferecido durante o período de estágio no exterior, através do Programa de Doutorado Sanduíche no Exterior (PDSE), processo número 88881.134204/2016-01.

Resumo

A presente tese apresenta trabalhos realizados em três assuntos. O primeiro assunto tratado diz respeito a interferência quântica. Mostramos que uma partícula quântica em um interferômetro Mach-Zehnder, sob a ação de uma força positiva em um dos braços do interferômetro e uma força nula no outro, pode receber na média uma transferência de momento negativa quando sai do interferômetro por uma porta específica. Nesse cenário, um conjunto de partículas pode na média ganhar momento no sentido oposto ao da força aplicada devido a interferência quântica, um comportamento sem análogo clássico. Chamamos esse efeito de "interferência quântica de força", e apresentamos três possibilidades de implementação experimental para detectar tal efeito, com elétrons ou nêutrons em um interferômetro Mach-Zehnder, e com átomos de um condensado de Bose-Einstein. Em seguida discutimos o caso de dois elétrons propagando no mesmo interferômetro Mach-Zehnder e mostramos que, devido ao mesmo efeito de interferência quântica de força, os dois elétrons podem sofrer uma atração efetiva. O segundo assunto tratado é o desenvolvimento de uma proposta experimental para detectar interferência de Hanbury Brown e Twiss com elétrons se propagando no espaço livre. Recentemente surgiram dúvidas sobre experimentos do tipo realizados anteriormente, cujos resultados podem ser explicados como causados por repulsão Coulombiana ao invés de um efeito de interferência de duas partículas. Na nossa proposta, os dois efeitos podem ser diferenciados claramente, o que abre caminho para o desenvolvimento de uma técnica de imagem com fontes incoerentes de elétrons. Finalmente, o terceiro assunto diz respeito à derivação por primeiros princípios do momento trocado entre um fóton e um espelho quântico após o primeiro ser refletido pelo segundo. Para isso, usamos as condições de contorno impostas pela superfície do espelho sobre a equação de onda do fóton. Mostramos que o sistema em geral termina em um estado emaranhado, a menos que a incerteza em posição do espelho seja muito menor do que o comprimento de onda do fóton, caso em que o espelho se comporta classicamente. O nosso tratamento leva diretamente à conclusão de que o momento do fóton é $\hbar\mathbf{k}$, e isso nos permite dar uma contribuição ao histórico debate Abraham–Minkowski sobre o momento da luz em um meio material. A configuração que usamos revela o momento de Minkowski, em que o momento da luz é proporcional ao índice de refração do meio.

Palavras-chave: Óptica quântica, Interferência quântica, Interferência de matéria, Interferência de Hanbury Brown e Twiss, Interferência de dois elétrons, Função de onda de fóton, Momento do fóton.

Abstract

This Thesis contains work developed in three subjects. In the first of them, we show that a quantum particle under the action of a positive force in one path of a Mach-Zehnder interferometer and a null force in the other path may receive a negative average momentum transfer when it leaves the interferometer by a particular exit. In this scenario, an ensemble of particles may receive an average momentum in the opposite direction of the applied force due to quantum interference, a behavior with no classical analogue. We name this effect as "quantum interference of force", and discuss some experimental schemes that could verify the effect with current technology, with electrons or neutrons in Mach-Zehnder interferometers in free space and with atoms from a Bose-Einstein condensate. We then discuss the case of two electrons propagating in the same Mach-Zehnder interferometer and show that, due to the same quantum interference of force effect, the two electrons can sometimes suffer an effective attraction. The second subject is the development of an experimental proposal to detect the Hanbury Brown and Twiss interference with electrons propagating in free space. In previously realized experiments, doubts were casted upon the results, which may be explained as caused by Coulomb repulsion of the electrons instead of a two-particle interference effect. In our proposal, the two effects can be clearly distinguished, opening the path for imaging with incoherent electron sources. Finally, the third subject concerns the derivation from first principles of the momentum exchange between a photon and a quantum mirror upon reflection, by considering the boundary conditions imposed by the mirror surface on the photon wave equation. We show that the system generally ends up in an entangled state, unless the mirror position uncertainty is much smaller than the photon wavelength, when the mirror behaves classically. Our treatment leads us directly to the conclusion that the photon momentum has the known value $\hbar\mathbf{k}$, and this allows us to contribute to the longstanding Abraham–Minkowski debate about the momentum of light in a medium. We show that in our setting the Minkowski momentum is revealed, in which the light momentum is proportional to the medium refractive index.

Keywords: Quantum optics, Quantum interference, Matter interference, Hanbury Brown and Twiss interference, Two-electron interference, Photon wave function, Photon momentum,.

Contents

1 Introduction

The present Thesis is composed of three different branches. The three of them can be joined under the broad umbrella of Theoretical Quantum Mechanics, but the difference between them is large enough so that there will not be a common introduction to them all. Each of the three subjects will be treated in a different chapter, and the necessary detailed historic and scientific introduction will be made in each of them.

In chapter 2 we present a curious effect that arises when the quantum superposition principle encounters the concept of force acting on a particle. Namely, we discuss the situation in which a quantum particle is in a superposition of two states, while a force acts on only one of them. We show that if the force is for instance positive, then this superposition of a positive force with no force at all on the same particle may lead to a negative momentum transfer to that particle, which goes against the classical intuition. This happens because of an interference effect, more specifically a destructive interference effect. We show that it is purely quantum effect, in the sense that classically no statistical sum of such two situations (a positive force and a zero force acting on a particle) could lead to that anomalous momentum transfer to the particle. For all these reasons, we name the effect as *quantum interference of force*. Three possible experimental setups that could detect it are proposed, one that uses electrons, one with neutrons, and another one with atoms from a Bose-Einstein condensate.

As a spin off of the quantum interference of force, we also discuss in chapter 2 the case in which the force is caused by the interaction with another quantum particle. In this two-particle setting, we specifically address the case in which two electrons propagate simultaneously in the same Mach-Zehnder interferometer. The superposition is then of states in which they propagate through different interferometer paths and do not interact, with states in which they propagate through the same path and suffer Coulomb repulsion. We show that quantum interference can cause an effective attraction between the two electrons, once again going against the classical intuition. An experimental implementation of this proposal is also discussed. The presentation of the effect we call quantum interference of force is published as an article in the journal Quantum [1], and the effective attraction between two electrons due to it is discussed in a pre-print available on the online platform ArXiv [2], and it is currently under review for publication.

Chapter 3 contains the work developed during the Sandwich PhD period of April 2017 to March 2018 at the University of Erlangen-Nuremberg (Germany), under the supervision of Prof. Joachim von Zanthier. We discuss an experimental proposal for the detection of Hanbury Brown and Twiss interference in free space with electrons. This

two-particle interference effect was originally detected using two-intensity correlation measurements with classical light in the 1950s [3–6], and used for imaging with incoherent light sources. Extensions of this effect for electrons have been successfully done on chip in 1999 [7, 8], but this setup forbids their use for imaging, while the success of a 2002 free space implementation [9] has recently been questioned [10, 11]. The critics argue that the Coulomb repulsion and not an interference effect could have been responsible for the detected pattern. We propose an experimental setup that could unambiguously distinguish between the Coulomb repulsion and the genuine interference effect that arises from the extension of the Hanbury Brown and Twiss effect for fermions.

In order to develop our experimental proposal, we first present a brief review of two-intensity correlation measurements and of the Hanbury Brown and Twiss original experiments, all under the point of view of classical optics. Following, we show the traditional way to quantize the electromagnetic field, since we want to extend the Hanbury Brown and Twiss interference for fermions, which cannot be described classically. The bunching and anti-bunching effects for light are then discussed, since they are central in two-intensity correlation measurements and the latter shows exclusively quantum features of the electromagnetic field – it will also be present in the electron field extension. We finally present the experimental setup that could detect the Hanbury Brown and Twiss effect, and that should be the basis for imaging with incoherent electron sources in the near future. The experimental realization of the proposal is on the way, in collaboration with the group of Prof. Peter Hommelhoff at the University of Erlangen-Nuremberg.

Finally, chapter 4 is concerned with the reflection of a single photon by a quantum mirror. By quantum mirror we mean that we are using quantum mechanics to treat its motion and interaction with the photon, and we will be specially interested in exclusively quantum effects there. We use a photon wave function formalism [12–15] in order to derive the quantum state of the photon-mirror system after the reflection, and this formalism allows us to treat the problem with boundary conditions on the surface of the mirror, bypassing the difficulties of doing such with electromagnetic field operators [16–19]. The photon wave function formalism of Bialynicki-Birula and Sipe [12, 13] is the basis for the calculations of this chapter, and we present its core in a section within the chapter.

As results, we show that the final state of the photon-mirror system is in general entangled, and we discuss the limits in which this entanglement could be detected – unfortunately, it is beyond the reach of current technology. Our treatment naturally provides a derivation of the momentum of the photon, even if it propagates through a medium on its way to be reflected by the mirror. Then the historical Abraham–Minkowski debate is addressed [20, 21], in which the two physicists, Max Abraham and Hermann Minkowski, propose different expressions for the momentum carried by the electromagnetic field when it propagates through a material medium. The setup we analyze has the spirit of

historically known experiments that try to probe the light momentum in a medium [22,23], and we show that in this quantum version the mirror gains the Minkowski momentum in the reflection process, which is proportional to the medium refractive index. The results of chapter 4 are published as an article in the journal Physical Review A [24].

2 Quantum interference of force

Interference phenomena on quantum systems can lead to extremely curious physics. The most canonical example is the double-slit experiment, which according to Feynman "has in it the heart of quantum mechanics" [25–27]. Other intriguing examples are delayed-choice experiments [28–31], quantum erasers [32–35], "interaction-free" measurements [36–38], and quantum delayed-choice experiments [39–41], among many others.

In this chapter we discuss another very curious quantum interference effect inspired on a work by Aharonov et al. [42]. In their article, the authors show that the classical limit of quantum optics is achieved in a strange way when we look at how photons transfer momentum to a mirror inside an interferometer, if the mirror position is treated quantum-mechanically. They showed that, depending on by which port of the interferometer the photon exits, it may transfer to the mirror an average momentum in the opposite direction that one would expect, due to an interference effect. This can be seen as a quantum random walk in the momentum space [43], in which the interferometer beam splitters play the role of a quantum coin that decides whether the mirror will be pushed by the photon or not, while under suitable post-selection it ends up being pulled.

We generalize this result upon considering anomalous momentum transfers to general quantum objects and by considering that the momentum transfer in one of the arms of the interferometer may be of the same order of magnitude than the initial momentum uncertainty of the quantum object, not necessarily in the weak interaction regime considered in Ref. [42]. These generalizations lead us to some proposals for feasible experiments that could observe an anomalous momentum transfer to a quantum object due to the quantum interference of force. Some of them one use quantum particles (electrons or neutrons) propagating in a Mach-Zehnder interferometer in free space, with a force that acts only in one of the interferometer arms. Another one uses an interferometer based on the internal degrees of freedom of atoms from a Bose-Einstein condensate, with a force that acts differently on these internal states.

With an appropriate post-selection, the quantum superposition of a positive force with no force in an ensemble of quantum particles may generate a negative average momentum transfer to these particles. No classical system can present this behavior, such that the quantum interference of force that we discuss here is a genuinely quantum effect.

Furthermore, we discuss the situation in which the force that acts on a particle is caused by the interaction with another quantum particle. Namely, we investigate what happens when two electrons propagate through a Mach-Zehnder interferometer side by side. We propose an experiment in which the superposition of the electrons repelling each

other (when they propagate through the same path) with them not interacting at all (when they propagate through different paths) may lead to an effective attraction between them, when the appropriate post-selection is made.

The results presented in this chapter are available in two papers: the one published in Ref. [1] presents the quantum interference of force with a single particle, and one available as a pre-print in Ref. [2] discusses the effective attraction of two electrons due to this effect.

2.1 Aharonov et al.'s thought experiment

We begin by reviewing the results of the 2013 paper authored by Aharonov et al. [42] that motivated our own results. The authors consider the modified Mach-Zehnder interferometer displayed in Fig. 1 for their thought experiment. The light enters the interferometer and is split into paths A and B by beam splitter BS_1. On path B, the light hits the mirror M from the inside at an angle α and can exchange momentum with it. A second beam splitter BS_2 interferes the light from the two paths towards two interferometer exits. Some of the light leaves the interferometer directly towards detector D_2, but the light from the other exit is redirected via path C to the back of the mirror M and is reflected once again by it at an angle β before it reaches detector D_1. Both beam splitters have reflection and transmission coefficients ir and t respectively, with r and t real positive numbers, and $r^2 + t^2 = 1$.

Let us first consider that the incident light is a classical beam with energy U during the length of the experiment. The momentum carried by this beam is thus U/c, where c is the speed of light in vacuum. Upon reflection, the beam transfers a momentum to the mirror M that depends on the angle of incidence α of the beam, since only the momentum component perpendicular to the surface of M will be inverted. The fraction t^2U of the light energy that is transmitted by BS_1 is the one reflected by M, such that one can write the momentum that the light transfers to M from the inside of the interferometer as $\delta_\alpha = 2t^2(U/c)\cos\alpha$. The factor 2 comes from the momentum inversion.

The light that is directed to C is a coherent superposition of the light that goes through paths A and B, either being reflected by BS_1 and transmitted by BS_2 via path A, or the other way around via path B. It can be shown that the light intensity in path C is $4r^2t^2U/c$, and thus the momentum that is transferred to the mirror M from this path is $\delta_\beta = 8r^2t^2(U/c)\cos\beta$.

The net momentum gained by the mirror is therefore $\delta_M = \delta_\alpha - \delta_\beta$. In a setting that r, t, α and β are chosen so that $\delta_\beta > \delta_\alpha$, the mirror is pushed towards the inside of the interferometer due to the fact that the radiation pressure in this direction is stronger than towards the outside. In Ref. [42], the authors choose $\cos\beta = \frac{1}{2}\cos\alpha$ and $r > t$, such

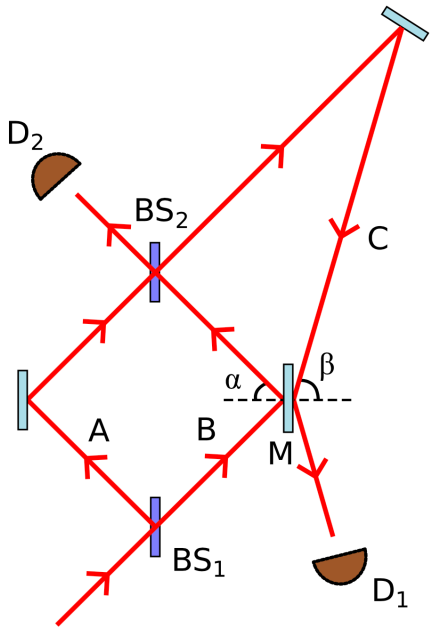

Figure 1 – A Mach-Zehnder interferometer in which the light that propagates in it hits the mirror M from the inside at an angle α and can exchange momentum with it. The light that goes to exit C hits the back of the mirror M at an angle β before it reaches detector D_1. (Content distributed under the terms of the Creative Commons Attribution 3.0 licence, authors and work title available at Ref. [42], DOI:10.1088/1367-2630/15/9/093006.)

that

$$\delta_M = -2t^2(U/c)(r^2 - t^2)\cos\alpha \quad < \quad 0, \tag{2.1}$$

which evidences that the mirror M is pushed to the inside of the interferometer.

Let us now consider the case that a single photon with energy $\hbar\omega$ is sent inside the interferometer. Following the same reasoning as in the classical case, the momentum kick given by the photon to the mirror M when it goes through path B is now $\delta_\alpha = 2(\hbar\omega/c)\cos\alpha$. After going through the first beam splitter, the quantum state of the propagation degree of freedom of the photon is in a superposition of the two paths $|A\rangle$ and $|B\rangle$, namely $|\Psi\rangle = ir|A\rangle + t|B\rangle$. If we write $\phi(p)$ for the momentum wave function of the mirror in the direction perpendicular to its surface, after the reflection the photon-mirror system ends up in the entangled state

$$ir|A\rangle\phi(p) + t|B\rangle\phi(p - \delta_\alpha), \tag{2.2}$$

where only the component of the photon propagating through path B gives the mirror a momentum kick of δ_α.

The authors of Ref. [42] now consider that the size of the kick $|\delta_\alpha|$ is much smaller than the width of $\phi(p)$, such that one can approximate $\phi(p - \delta_\alpha) \approx \phi(p) - \delta_\alpha \frac{\mathrm{d}\phi(p)}{\mathrm{d}p}$. This

approximation gives rise to the weak interaction regime, used in Ref. [42], and is used in the theory of weak values [44,45]. If one selects only the photons leaving the interferometer towards detector D_1, i.e. in state[1] $|\Phi_1\rangle = t|A\rangle - ir|B\rangle$, the momentum wave function of the mirror is projected into

$$\begin{aligned}\langle\Phi_1|\Big[ir|A\rangle\phi(p) + t|B\rangle\phi(p-\delta_\alpha)\Big] &= irt\Big[\phi(p) + \phi(p-\delta_\alpha)\Big] \\ &\approx irt\left[2\phi(p) - \delta_\alpha\frac{\mathrm{d}\phi(p)}{\mathrm{d}p}\right] \\ &\approx 2irt\ \phi\left(p - \frac{\delta_\alpha}{2}\right). \end{aligned} \tag{2.3}$$

Therefore the superposition of a momentum kick δ_α on the mirror from the photon component propagating on arm B with no kick from the component propagating on arm A results in a kick of $\delta_\alpha/2$ on the mirror from the photons that leave the interferometer towards D_1.

All of these photons, however, are redirected via path C to the back of the mirror and kick it once again with a momentum $\delta_\beta = 2(\hbar\omega/c)\cos\beta$. With the setting $\cos\beta = \frac{1}{2}\cos\alpha$, we get $\delta_\beta = \delta_\alpha/2$, but this is exactly the momentum gained by the mirror from when the photons were propagating inside the interferometer. Therefore the net radiation pressure $\delta_M = \delta_\alpha - \delta_\beta$ on the mirror is zero for the photons that are detected at D_1.

This leaves us with the photons that are detected at D_2, i.e. selected in state $|\Phi_2\rangle = -ir|A\rangle + t|B\rangle$. The momentum wave function of the mirror, in this case, is projected into

$$\begin{aligned}\langle\Phi_2|\Big[ir|A\rangle\phi(p) + t|B\rangle\phi(p-\delta_\alpha)\Big] &= -r^2\phi(p) + t^2\phi(p-\delta_\alpha) \\ &\approx -(r^2-t^2)\phi(p) - t^2\delta_\alpha\frac{\mathrm{d}\phi(p)}{\mathrm{d}p} \\ &\approx -(r^2-t^2)\ \phi\left(p + \frac{t^2}{(r^2-t^2)}\delta_\alpha\right), \end{aligned} \tag{2.4}$$

where in the last line it is assumed that $|\frac{t^2}{(r^2-t^2)}\delta_\alpha|$ is also much smaller than the width of $\phi(p)$ for the used approximation to be valid.

Note that, for $r > t$, the above expression means that the radiation pressure exerted on the mirror by the photons that are detected at D_2 is $-\frac{t^2}{(r^2-t^2)}\delta_\alpha$, i.e. in the opposite direction of the momentum δ_α. These photons, however, never kick the mirror M from the outside, and yet the momentum gained by M is directed towards the inside of the interferometer. The authors in [42] explain that the quantum superposition of no kick from the photon in arm A with a kick to the outside in arm B leads to a radiation pressure on the mirror that pulls it to the inside, and this is in strike contrast to the analysis made in

[1] The following state can be obtained by evolving the photon state backwards from detector D_1 through the beam splitter.

the classical case, in which the only way for the mirror to be pushed to the inside is for the light to push it harder from the back on path C than on path B.

In what follows, we will generalize the results of Ref. [42] by leaving the weak interaction regime and considering more general quantum systems. We give a more detailed explanation of the interference phenomenon that is behind this effect, which we name quantum interference of force, and the generalizations allow us to propose experiments to detect it in the lab.

2.2 A force that acts inside an interferometer

To discuss the effect in detail, let us consider a quantum particle propagating in a two-path Mach-Zehnder interferometer. In our experimental proposals, these paths can be either actually spatially separated paths, as in Fig. 2, or can represent two different internal states of the particle. Let us first consider the case of an electron propagating in a spatial Mach-Zehnder interferometer, as depicted in Fig. 2. Later we will discuss a proposal where the paths are the internal states of atoms from a Bose-Einstein condensate. During our discussion, only the z component of the particles wave function will be considered, since the plane of propagation is the x–y plane (see Fig. 2), while the force acts only in the z direction.

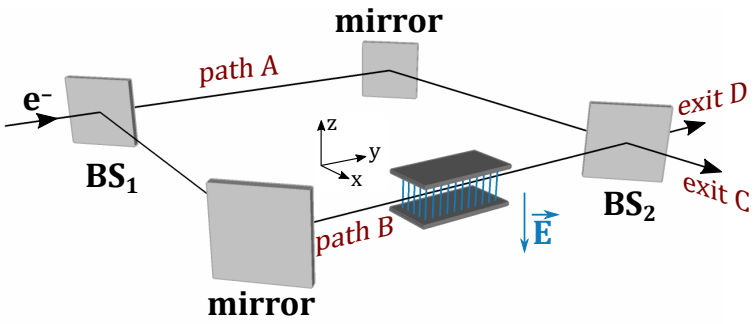

Figure 2 – Simplified scheme of an electron Mach-Zehnder interferometer. The first beam splitter (BS_1) splits the electron wave function into two path components A and B. Path B contains a capacitor with an uniform electric field $\mathbf{E}$ in the $-\hat{\boldsymbol{z}}$ direction, generating a force in the $\hat{\boldsymbol{z}}$ direction on a propagating electron. Mirrors re-join the wave function components and mix them at a second beam splitter (BS_2), whose exit ports are labeled C and D.

First, the electron propagation path is split by a beam splitter BS_1 into two paths A and B. Path A is free from the influence of any force, while on path B an external electric field generates a force in the $\hat{\boldsymbol{z}}$ direction. The paths are re-joined at a second beam splitter BS_2, where they are mixed towards exit ports C and D. We will consider that the first beam splitter has a reflection coefficient ir (with r real) and a transmission coefficient $t = \sqrt{1-r^2}$, while the second one has reflection and transmission coefficients equal to

$i/\sqrt{2}$ and $1/\sqrt{2}$ respectively. If $|\Phi\rangle$ is the prepared initial momentum state of the electron, then after the first beam splitter the state becomes

$$|\Phi_1\rangle = t|\Phi, A\rangle + ir|\Phi, B\rangle, \tag{2.5}$$

where $|\Phi, j\rangle$ stands for the electron propagating through path j with the state $|\Phi\rangle$ representing the quantum state of the z component of the electron wave function.

After BS_1 each component A and B will evolve differently, until they reach the second beam splitter BS_2. Due to the different propagation lengths and interactions associated with each path, the electron state inside the interferometer just before BS_2 is:

$$|\Phi_2\rangle = t|\Phi, A\rangle + ire^{i\beta}|\Phi', B\rangle. \tag{2.6}$$

where $|\Phi', B\rangle$ stands for the change in the momentum state of the component traveling through path B, and β is the phase difference between the arms due to propagation.

Finally, after BS_2 we will have on exit ports C and D the respective (non-normalized) states

$$|\Phi_C\rangle = \frac{t}{\sqrt{2}}|\Phi\rangle - \frac{re^{i\beta}}{\sqrt{2}}|\Phi'\rangle, \tag{2.7}$$

$$|\Phi_D\rangle = \frac{t}{\sqrt{2}}|\Phi\rangle + \frac{re^{i\beta}}{\sqrt{2}}|\Phi'\rangle. \tag{2.8}$$

We keep the $1/\sqrt{2}$ factors in the above expressions so that $\int |\langle p|\Phi_C\rangle|^2 dp + \int |\langle p|\Phi_D\rangle|^2 dp = 1$, where p is the component of the electron momentum in the z direction.

In our analysis, we consider that the external force $\mathbf{F}$ displaces the electron z momentum wave function by a positive quantity δ without changing its form. This can be achieved with an impulsive force, characterized by a potential acting during a very short period of time (see Appendix A). In this case, the evolved electron state after its propagation through path A is $\langle p|\Phi'\rangle \approx e^{i\gamma}\Phi(p-\delta)$, where $\Phi(p)$ is the initial electron wave function and γ represents a possible extra phase.

Finally, we can write the wave functions corresponding to the states of Eqs. (2.7) and (2.8), respectively, as

$$\Phi_C(p) = \langle p|\Phi_C\rangle = \frac{t}{\sqrt{2}}\Phi(p) - \frac{re^{i\alpha}}{\sqrt{2}}\Phi(p-\delta), \tag{2.9}$$

$$\Phi_D(p) = \langle p|\Phi_D\rangle = \frac{t}{\sqrt{2}}\Phi(p) + \frac{re^{i\alpha}}{\sqrt{2}}\Phi(p-\delta), \tag{2.10}$$

with $\alpha = \beta + \gamma$ and $r = \sqrt{1-t^2}$.

2.2.1 Quantum interference of force with a Gaussian initial wave function

We can now investigate how the average z momentum of the final wave functions associated with exit ports C and D relate to that of the initial wave function $\Phi(p)$. We

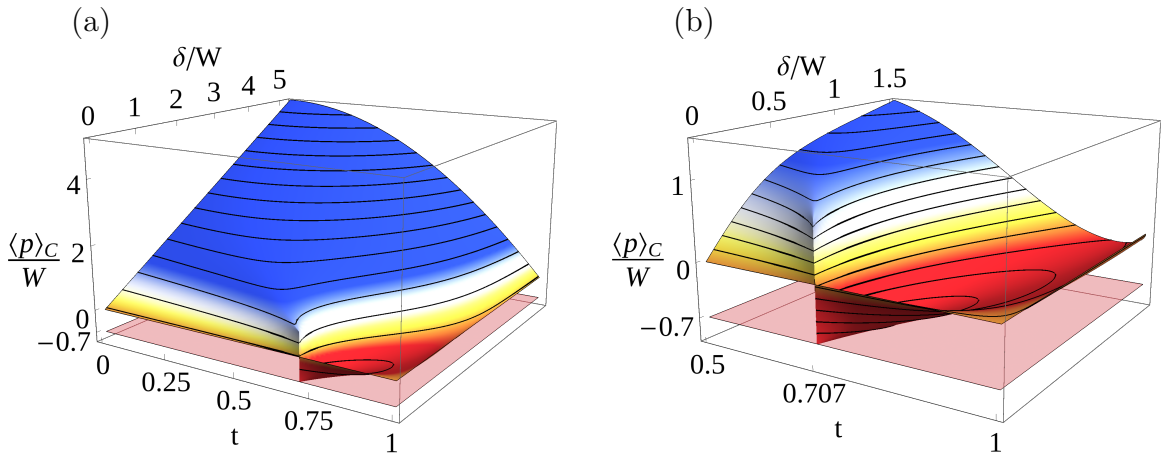

Figure 3 – Average momentum $\langle p\rangle_C$ of the electrons selected at port C in units of the Gaussian width W, as a function of the BS_1 transmission coefficient t and of the momentum kick δ, also in units of W. The electron wave function is given by Eq. (2.9) with $e^{i\alpha} = 1$ and $\Phi(p)$ from Eq. (2.11). The red region is where $\langle p\rangle_C < 0$. The transparent plane corresponds to $\langle p\rangle_C = -0.7W$. (a) Overall parameter view. (b) Zoom on the parameter region where $\langle p\rangle_C < 0$.

will specify $\Phi(p)$ as a Gaussian function with width W and zero mean value,

$$\Phi(p) = \frac{\pi^{-\frac{1}{4}}}{\sqrt{W}} \exp\left[-\frac{1}{2}\left(\frac{p}{W}\right)^2\right]. \tag{2.11}$$

To maximize the anomalous force effect, we will fix $\alpha = 2n\pi$ with integer n in Eqs. (2.9) and (2.10), which can be achieved by adjusting the relative A and B path lengths.

The average momentum of the wave function at a port j is

$$\langle p\rangle_j = \frac{1}{P_j}\int p\ |\Phi_j(p)|^2\ dp, \tag{2.12}$$

where $P_j = \int |\Phi_j(p)|^2 dp$ is the probability that the electron will exit through port j. In Fig. 3 we plot the average momentum $\langle p\rangle_C$ of the electrons selected at port C in units of the Gaussian width W, as a function of the BS_1 transmission coefficient t and of the momentum kick δ in arm B, which is also in units of W. It is clear that there is a range of parameters for which the average momentum is negative, and can attain values as negative as $-0.7W$. These values are clearly out of the weak interaction regime considered in Ref. [42] (see Sec. 2.1), since neither δ nor $|\langle p\rangle_C|$ have to be much smaller than W in order to get $\langle p\rangle_C < 0$.

So we see that, for an ensemble of quantum particles, the combination of a force in the positive z direction with a zero force may generate a displacement of the average momentum of these particles in the negative z direction, when the appropriate post-selection is made. In other words, the superposition of a positive force with a zero force may generate a "negative force" on quantum particles. This is a counter-intuitive behavior with no

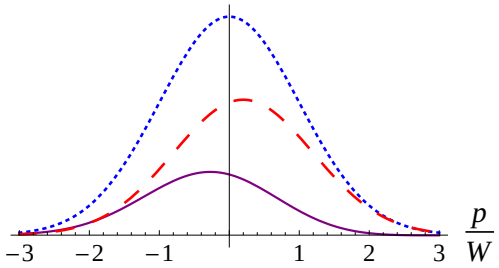

Figure 4 – Components of the wave function of Eq. (2.9) when $\Phi(p)$ is given by the Gaussian function of Eq. (2.11), with $t = 0.85$, $\delta = 0.2W$, and $e^{i\alpha} = 1$: $t\Phi(p)/\sqrt{2}$ (blue dotted curve), $r\Phi(p-\delta)/\sqrt{2}$ (red traced curve), and $\Phi_C(p)$ (continuous purple curve).

classical analogue. For classical particles, any momentum-independent post-selection must generate a positive or zero average momentum. This odd feature can be explained as an interference effect.

We plot in Fig 4 the components $t\Phi(p)/\sqrt{2}$ and $r\Phi(p-\delta)/\sqrt{2}$ of Eq. (2.9) when $\Phi(p)$ is given by Eq. (2.11), for $t = 0.85$ and $\delta = 0.2W$. The resulting wave function $\Phi_C(p)$ is the difference between these two components, as seen in Eq. (2.9) when $e^{i\alpha} = 1$. In Fig. 4, $\Phi_C(p)$ is also plotted, and has an average momentum around $-0.3W$. We can see that the positive momentum part of the displaced function $r\Phi(p-\delta)$ subtracts more from the positive than from the negative momentum part of $t\Phi(p)$, leaving an amplitude that is higher on the negative than on the positive momentum part of $\Phi_C(p)$. This is why the superposition of a positive-mean with a zero-mean function can result in a negative-mean one. It is a destructive interference effect on momentum wave functions, which is why we call it an *interference of force*.

As can be seen in Fig. 3, as the kick δ grows, only positive momentum expectation values can be achieved. This can be understood under the light of Fig. 5 (a), where a growing of δ means that the original $t\Phi(p)$ (blue dotted curve) and the displaced wave function $r\Phi(p-\delta)$ (red traced curve) get further and further apart. This leads to a very small overlapping region between the two (compare it with Fig. 4, where there is a practically full overlap), such that the interference becomes ever more negligible. When we write (see Eq. (2.9))

$$\langle p\rangle_C \propto \left[t^2 \int p|\Phi(p)|^2 dp\right] + \left[r^2 \int p|\Phi(p-\delta)|^2 dp\right] + \left[-2rt\cos\alpha \int p\ \Phi(p)\Phi(p-\delta)dp\right] \tag{2.13}$$

we can see that, as the overlap between $\Phi(p)$ and $\Phi(p-\delta)$ vanishes, the interference contribution to the expectation value (the third term in the sum) vanishes with it. It becomes thus clear that the average momentum of the particles approaches a statistical mixture of the events where they propagate through path A and no force is applied (first term), with those where they propagate via path B and the force is applied (second term).

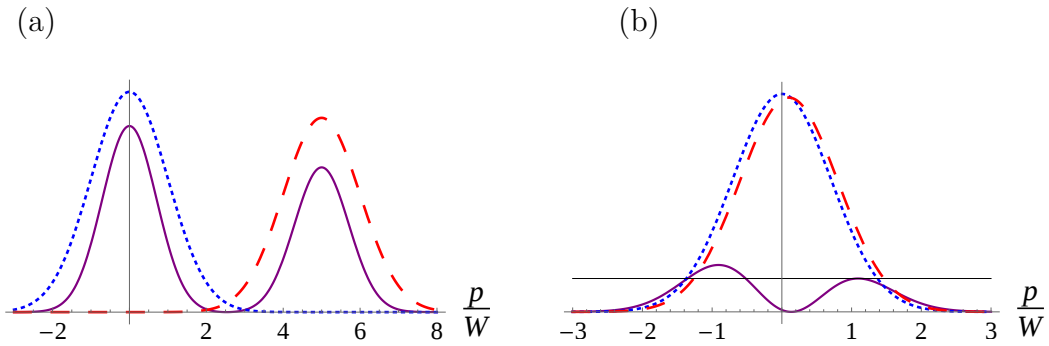

Figure 5 – Components of the wave function of Eq. (2.9) when $\Phi(p)$ is given by the Gaussian function of Eq. (2.11) and $e^{i\alpha} = 1$. (a) $t = 0.75$, $\delta = 5W$. When δ is large, $t\Phi(p)$ (blue dotted curve) and $r\Phi(p-\delta)$ (red traced curve) become too far apart and their overlap is small, such that the momentum distribution $|\Phi_C(p)|^2$ (continuous purple curve is $3 \times |\Phi_C(p)|^2$) approaches a statistical mixture of the distributions of each separate wave function without a significant interference contribution. (b) $t = (1/\sqrt{2}) + 0.003$, $\delta = 0.1W$. When $t \approx 1/\sqrt{2} \approx r$, $\Phi(p)$ (blue dotted curve) and $\Phi(p-\delta)$ (red traced curve) contribute with a nearly equal weight to $\Phi_C(p)$. Therefore, for small δ, any deviation from $t = r$ will significantly change whether the positive or negative part of the final momentum distribution $|\Phi_C(p)|^2$ (continuous purple curve is $100 \times |\Phi_C(p)|^2$) is the largest, and the sign of the average momentum is very sensitive to small variations of t. The thin horizontal line indicates that for the used parameters the negative part of the distribution is larger than the positive.

In Fig. 5 (a), this appears in the fact that the momentum distribution $|\Phi_C(p)|^2$ (continuous purple curve is $3 \times |\Phi_C(p)|^2$) consists basically of the two bumps correspondent to the contributions of $\Phi(p)$ and $\Phi(p-\delta)$ separately. The anomalous momentum transfer therefore cannot be observed for a displacement δ a few times larger than the wave function width W, but it is not necessary that $\delta \ll W$, as considered in Ref. [42] (see Sec. 2.1). When δ is smaller than W, but of the same order of magnitude, as in Fig. 4, the anomalous force is maximized while the final wave function keeps a considerable amplitude, which means this case should be easier to be observed in an experiment.

We would also like to comment on the spiky behavior of $\langle p \rangle_C$ that appears on the region around $t = 1/\sqrt{2} \approx 0.707$ and small δ shown in Fig 3. This value for t means that $r = \sqrt{1-t^2} = t$, and thus $\Phi(p)$ and $\Phi(p-\delta)$ will have equal weight on the composition of $\Phi_C(p)$. This behavior is illustrated in Fig. 5 (b), where we plot $\Phi(p)$ (blue dotted curve) and $\Phi(p-\delta)$ (red traced curve) with nearly equal amplitude, and the momentum distribution $|\Phi_C(p)|^2$ (continuous purple curve is $100 \times |\Phi_C(p)|^2$) resulting from their superposition. When δ is small and $r \approx t$, the two wave functions $\Phi(p)$ and $\Phi(p-\delta)$ will be very close to each other. Whether the positive or the negative part of the resulting momentum distribution is the largest will depend very sensitively on which of the two wave functions has a slightly larger amplitude. And if the positive part of the distribution is slightly larger

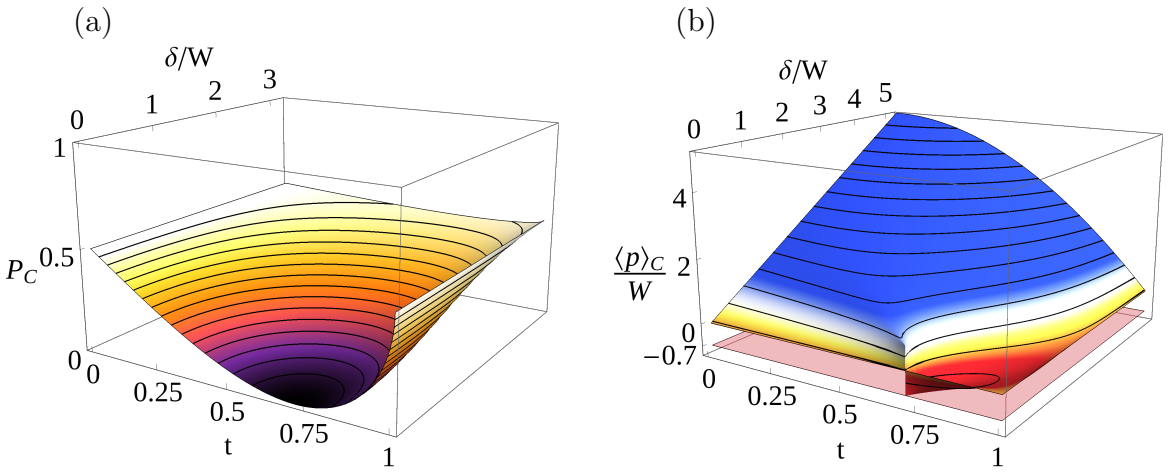

Figure 6 – (a) Probability P_C that an electron exits the interferometer of Fig. 2 at port C, as a function of the transmission coefficient t of BS_1 and of the kick δ in units of the Gaussian width W. The electron wave function is given by Eq. (2.9) with $e^{i\alpha} = 1$ and $\Phi(p)$ from Eq. (2.11). (b) Replica of Fig. 3 (a). The region with $\langle p\rangle_C < 0$ coincides with that of small detection probabilities.

than the negative one, the final average momentum is positive; when the opposite happens, the final average momentum is negative. This parameter sensitivity is the reason that there is this spike on the region around $t = 1/\sqrt{2} \approx 0.707$ and small δ shown in Fig 3.

2.3 Ehrenfest's theorem and momentum conservation

In general, quantum particles suffer diffraction through the interaction with energy potentials, exchanging momentum with the agent of that potential. However, when the gradient of the potential does not vary much in the region occupied by the particle wave function, Ehrenfest's theorem tells us that the average momentum gained by the particle should be the expected classical one, computed as the result of a classical force acting on the particle [46]. The component of the wave function that propagates through path B in the interferometer of Fig. 2 does receive an average momentum equal to the classically computed one. But when this component interferes with the component that propagates through path A with no momentum exchange, the average momentum received by the particle when it exits by port C can be in the opposite direction in relation to the classically expected one, as depicted in Figs. 3 and 4. This interference of different momentum exchanges, which may result in a momentum displacement that corresponds to a force applied in the opposite direction, is a genuinely quantum effect with no classical analogue.

One could then wonder if the described process suggests that momentum is not being conserved. Or, stated in another way, how could we get the electron with average momentum in a direction if it has only gained momentum in the opposite one? In order to

understand this we have to stress that, because the negative momentum transfer takes place with destructive interference, the successful selection of the electron at the interferometer port C must be unlikely. For instance, in the case illustrated in Fig. 4 the probability P_C that the electron comes out at port C is around 6%. To have a quantitative view of that, we plot in Fig. 6 (a) the probability P_C as a function of t and δ/W. By comparison with Fig. 3 (replicated in Fig. 6 (b)), clearly the region with most negative average momenta coincides with the lowest probabilities of successful selection.

Let us take a look at the discarded events. If we compute the momentum average $\langle p\rangle_D$ of the case that the electron is selected on port D of the interferometer, we see that the whole range of average momenta is positive (Fig. 7 (a)). When we sum both averages weighed by their respective probabilities, we see that

$$P_C\langle p\rangle_C + P_D\langle p\rangle_D = t^2\langle p\rangle_\Phi + r^2\langle p\rangle_{\Phi'}, \tag{2.14}$$

where $\langle p\rangle_\Phi$ and $\langle p\rangle_{\Phi'}$ are the momentum averages calculated with the corresponding states $|\Phi, A\rangle$ and $|\Phi', B\rangle$ of Eq. (2.6). This is exactly what we would expect from Ehrenfest's theorem and it implies conservation of momentum, since r^2 and t^2 are the respective probabilities that the electron has or has not interacted with the external field. What the post-selection allows us to do, then, is a re-arrangement of the probabilities of selecting the electron with certain transverse momentum eigenvalues. We correlate most of the amplitude for positive z momentum with the electron exiting through port D, and leave the negative values associated with the electron exiting at C. The impression that momentum is not conserved then comes from the fact that we are discarding many detection events. We stress that this is an effect that is intrinsically quantum in nature, and in fact it can have no classical analogue. This is because it requires particles interfering destructively, and we cannot associate negative probability amplitudes with "states" of classical particles.

2.4 Proposals for experimental implementation

Matter interferometry is an extensively developed field, with decades of research on electron, neutron and atom interferometers [47–50]. Mach-Zehnder interferometers with electrons in free space can be constructed with diffraction gratings acting as beam splitters and mirrors [51, 52], as shown in Fig. 8. It should not be difficult to place a capacitor in one of the arms of the interferometer, since this was already done with similar atomic interferometers [53–55]. A thin metallic foil should be placed between the interferometer arms near the capacitor to avoid the presence of the capacitor field on path A of Fig. 2.

The gratings with 100 nm periodicity used in Ref. [52], when illuminated by their 6 keV electron beam source, can generate a separation of 55 μm between the two paths at a distance of 35 cm from the grating. In Ref. [53], which performs the interferometer with atoms, this separation is enough to have control of different capacitor tensions for

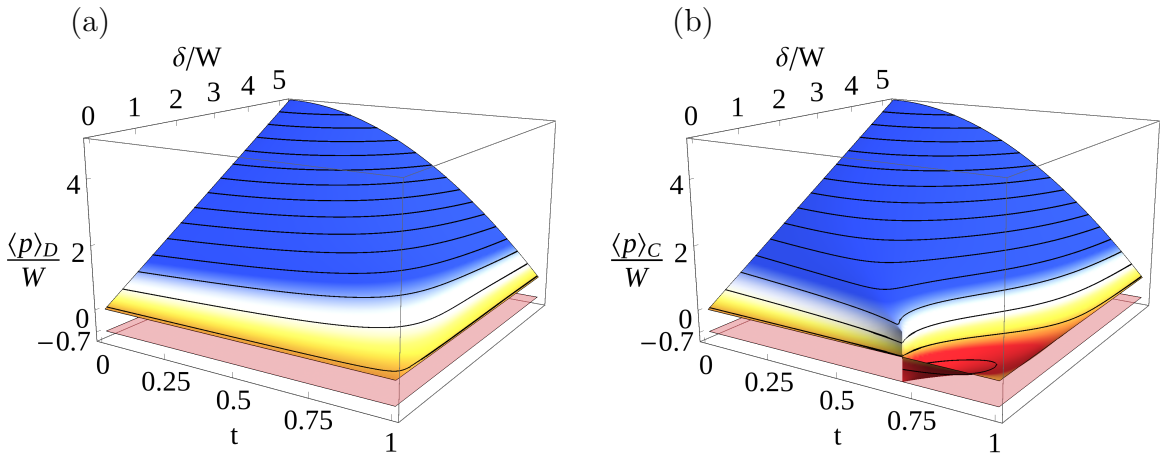

Figure 7 – (a) Average momentum $\langle p \rangle_D$ of the electrons selected at port D in units of the Gaussian width W, as a function of the BS_1 transmission coefficient t and of the momentum kick δ, also in units of W. The electron wave function is given by Eq. (2.10) with $e^{i\alpha} = 1$ and $\Phi(p)$ from Eq. (2.11). (b) Replica of Fig. 3 (a) showing $\langle p \rangle_C$.

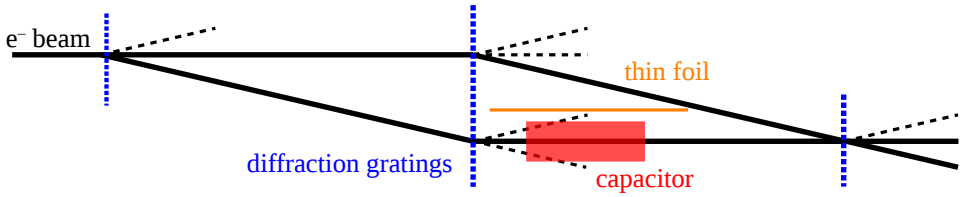

Figure 8 – Experimental implementation of an electron Mach-Zehnder for the detection of the quantum interference of force. Diffraction gratings play the role of beam splitters and mirrors, and a capacitor exerts a force on the electron in only one of the interferometric paths, while the other path is isolated by a thin metallic foil.

each beam path. By using the slit of 1.5 μm width of Ref. [52] for the initial electron spatial state preparation, we approximate it by a Gaussian profile and estimate the beam width after 1 m of propagation to be 1.7 μm, such that the wave function spreading is small. In this setup, for capacitor plates separated by 1 mm with a length of 1 cm in the beam propagation direction and with an applied tension of 0.2 mV, the displacement of the momentum wave function is around 10% of its width, compatible to the displacement needed to show the anomalous force effect. So the experimental verification of the effect should be feasible with current technology.

It should also be possible to perform the experimental verification of the quantum interference of force with neutron interferometers [56, 57]. Nowadays it is possible to apply different magnetic fields on each arm of a Mach-Zehnder neutron interferometer [58, 59]. If this setup is adapted to apply an inhomogeneous magnetic field in one of the interferometer arms, producing a Stern-Gerlach force, and no field on the other, it should be possible to

produce the superposition of a positive force with a null force on the neutrons resulting in an average negative momentum transfer to them with the appropriate post-selection.

Another possibility for the experimental verification of the quantum interference of force is in a setup with atoms from a Bose-Einstein condensate when the atomic trap is turned off. In this case, paths A and B of Fig. 2 can be associated to internal atomic states $|A\rangle$ and $|B\rangle$ with an energy difference on the microwave region and definite magnetic moments in the z direction. If the atoms are all initially in the state $\Phi(p)|A\rangle$, where $\Phi(p)$ represents the quantum state of the z component of the atoms wave function in momentum space, a microwave pulse resonant with the transition can create the superposition $t\Phi(p)|A\rangle + r\Phi(p)|B\rangle$, where $t = \sqrt{1-|r|^2}$ (assumed real) depends on the duration and amplitude of the microwave pulse [60, 61]. The subsequent application of an inhomogeneous magnetic field that generates a Stern-Gerlach force during a short period of time can create the state

$$t\Phi(p-\delta_a)|A\rangle + r\Phi(p-\delta_b)|B\rangle, \tag{2.15}$$

where δ_a and δ_b depend on the duration and spatial configuration of the inhomogeneous magnetic field and on the z component of the magnetic moments of the states $|A\rangle$ and $|B\rangle$ respectively. A microwave resonant $\pi/2$ pulse can then transform this state into

$$t\Phi(p-\delta_a)\frac{(|A\rangle + |B\rangle)}{\sqrt{2}} + r\Phi(p-\delta_b)\frac{(-|A\rangle + |B\rangle)}{\sqrt{2}}. \tag{2.16}$$

The application of a second inhomogeneous magnetic field, but now transmitting the opposite momentum in relation to the previous one, leads to

$$\frac{t\Phi(p) - r\Phi(p-\Delta_{ab})}{\sqrt{2}}|A\rangle + \frac{r\Phi(p) + t\Phi(p+\Delta_{ab})}{\sqrt{2}}|B\rangle, \tag{2.17}$$

where $\Delta_{ab} = \delta_b - \delta_a$. A selection of the atoms in the atomic state $|A\rangle$ therefore generates a momentum state analogous to the momentum wave function of Eq. (2.9) with $e^{i\alpha} = 1$ and $\delta = \Delta_{ab}$, and it can thus show the anomalous force effect. The combination of a total positive momentum transfer with a total zero momentum transfer to the atoms may result in a negative average momentum transfer.

2.5 Effective electrostatic attraction between electrons due to quantum interference

We turn ourselves now to the situation in which the force used to generate the quantum interference effect is caused by the interaction with another quantum particle. Namely, we propose an experiment in which two electrons propagate parallel to each other through the same Mach-Zehnder interferometer, and post-select the interferometer port

where each electron exits. We show that the quantum superposition of the situations where the electrons propagate in the same interferometer arm, repelling each other, with the situations where they propagate in opposite arms, with no interaction, may result in an effective attraction between them. This effective electrostatic attraction between the electrons manifests itself in the momentum distribution of each electron, that change its mean value in the direction of the other electron with the propagation through the interferometer.

This effect is connected to the anomalous weak values obtained by Aharonov *et al.* in their treatment of Hardy's paradox [62], that would be manifested as an effective repulsion between an electron and a positron inside the interferometer in the weak interaction regime [63]. Our treatment, besides avoiding some controversial interpretations of the weak values, is valid outside the weak interaction regime, which led us to a feasible experimental proposal for observing the effective attraction between electrons due to quantum interference.

2.5.1 Two electrons propagating in a Mach-Zehnder interferometer

In the proposed experiment we consider a two-paths Mach-Zehnder interferometer with two electrons e_1 and e_2 sent at the same time through the apparatus, as shown in Fig. 9. The electrons can be distinguished from one another by the z component of their position, with their separation d being much larger than the width of their wave functions. Apart from this displacement, the states of the electrons are essentially the same. Both paths are considered to be free from any external influence and isolated from each other so that only the electromagnetic interactions between electrons taking the same path are allowed to take place. We associate the orthogonal state vectors $|A_i\rangle$ and $|B_i\rangle$ with the distinguishable paths of propagation possible for the electrons during their travel through the system, and the vectors $|C_i\rangle$ and $|D_i\rangle$ with the possible exit ports of the Mach-Zehnder interferometer, matching the labeling given by Fig. 9. The index $i = \{1, 2\}$ labels each electron. The reflection and transmission coefficients for each beam-splitter BS_1 and BS_2 are the same, denoted respectively by ir and $t = \sqrt{1 - r^2}$, with real r and t. The initial quantum state of the z component of the electron i's momentum will be denoted by $|\Phi_i\rangle$.

We consider a post-selection of the totality of events where electron e_1 exits the interferometer by D_1 and e_2 exits by C_2, as indicated in Fig. 9. By considering this post-selection choice, the final joint state of the system that consists of the two electrons will be a coherent sum over the amplitudes associated with all the possible ways for this system to have evolved in time towards this final state. There are in total four possibilities of evolution for the described system: two where the electrons take different paths inside the interferometer and therefore do not interact, and two where they do travel by the same path and a Coulomb interaction between them exists during some time interval. In

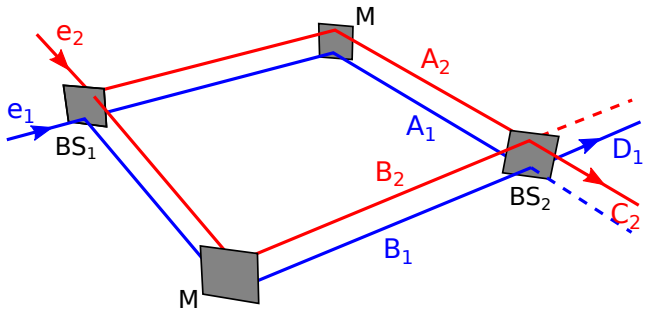

Figure 9 – Two electrons propagate parallel to each other in a Mach-Zehnder interferometer, entering by the indicated ports. Beam splitter BS_1 splits the incident wave functions and the mirrors M redirect the electrons to interfere at the second beam-splitter BS_2. The lines represent the center of the wave functions of the electrons e_1 (blue) and e_2 (red) while propagating in the interferometer. The distance d between the electrons paths is considered to be much larger than the width of their wave function, such that the electrons can be labeled as e_1 and e_2 due to their spatial distinguishability. If the electrons propagate in the same arm they repel each other, while if they propagate in opposite arms their interaction is negligible. We will post-select the events where electron e_1 exits by D_1 and electron e_2 exits by C_2.

the first two cases where the electrons do not interact, the two particles are either both reflected or both transmitted in each beam splitter, and the state of the system will evolve to the post-selected state as:

- e_1 goes through path A_1 and e_2 goes through B_2: $-r^2t^2e^{i\phi}|\Phi_1, D_1\rangle|\Phi_2, C_2\rangle$;
- e_1 goes through path B_1 and e_2 goes through A_2: $-r^2t^2e^{i\phi}|\Phi_1, D_1\rangle|\Phi_2, C_2\rangle$;

where the vector states associated to each electron individually are labeled accordingly, and ϕ represents an extra phase for an electron propagation through path A_i in relation to a propagation through path B_i.

In turn, if one of the electrons is reflected and the other transmitted in each beam splitter, they will take the same path and interact with each other. These two other possibilities that take to the the post-selection state, when we consider that the interaction will change the two electrons momentum states, will lead the quantum state to evolve as:

- e_1 goes through path A_1 and e_2 goes through A_2: $-r^2t^2e^{i(2\phi+\alpha)}|\Phi_1^-, D_1\rangle|\Phi_2^+, C_2\rangle$;
- e_1 goes through path B_1 and e_2 goes through B_2: $-r^2t^2e^{i\alpha}|\Phi_1^-, D_1\rangle|\Phi_2^+, C_2\rangle$;

where we have taken the vectors $|\Phi_i^{\mp}\rangle$ to represent the electrons momentum states that were disturbed by their electromagnetic interaction, and α represents a phase gained due

to the interaction. Considering the combination of these four probability amplitudes, the post-selected electrons momentum state is

$$|\Phi_{ps}\rangle \propto |\Phi_1\rangle|\Phi_2\rangle + e^{i\alpha}\cos\phi\ |\Phi_1^-\rangle|\Phi_2^+\rangle. \tag{2.18}$$

2.5.2 Effective attraction between electrons with Gaussian initial wave functions

To closely analyze these results, we shall once again specify the initial wave functions for the z component of the electrons momentum $\Phi_i(p) = \langle p|\Phi_i\rangle$ as Gaussian distributions with width W centered at zero,

$$\Phi_i(p) = \frac{\pi^{-\frac{1}{4}}}{\sqrt{W}}\ \exp\left[-\frac{1}{2}\left(\frac{p}{W}\right)^2\right], \tag{2.19}$$

where the origin of the z axis for each electron was defined at the corresponding center of its position wave function. If the electrons separation is much larger than the width of their wave functions, and if this width does not change appreciably during the electrons time travel along the interferometer, and also since each electron wave function is submitted to an approximately constant electric field, the electrons interaction results in shifts δ on their momentum wave functions without altering their Gaussian forms (see Appendix A). The exact magnitude of δ will depend on the electrons separation d and on the interaction time. In this case the wave functions for the z component of the electrons momentum altered by the interaction become

$$\Phi_1^-(p) \equiv \langle p|\Phi_1^-\rangle = \Phi_1(p+\delta), \tag{2.20}$$

$$\Phi_2^+(p) \equiv \langle p|\Phi_2^+\rangle = \Phi_2(p-\delta), \tag{2.21}$$

which correspond to momentum shifts of $\mp\delta$ in the wave functions. We note that electron e_1 gains a negative momentum while electron e_2 gains a positive momentum of the same amplitude.

It is possible to analyze the quantum states associated to each of the electrons separately by taking the partial traces over the post-selected state of Eq. (2.18). In this way, the state ρ_1 associated to electron e_1 is

$$\begin{aligned}\rho_1 &= \mathrm{Tr}_{(2)}(|\Phi_{ps}\rangle\langle\Phi_{ps}|) \\ &= |\Phi_1\rangle\langle\Phi_1| + \cos^2\phi\ |\Phi_1^-\rangle\langle\Phi_1^-| + Ie^{-i\alpha}\cos\phi\ |\Phi_1\rangle\langle\Phi_1^-| + Ie^{i\alpha}\cos\phi\ |\Phi_1^-\rangle\langle\Phi_1|\end{aligned} \tag{2.22}$$

apart from a normalization factor, with

$$I = \int \Phi_2(p)\Phi_2(p-\delta)\ dp = \exp\left(-\frac{\delta^2}{4W^2}\right). \tag{2.23}$$

In the same manner, and because $\int \Phi_1(p)\Phi_1(p \mp \delta)dp = \int \Phi_2(p)\Phi_2(p \mp \delta)dp = I$ for the Gaussian $\Phi_i(p)$ of Eq. (2.19), the state ρ_2 associated to the electron e_2 is

$$\rho_2 = |\Phi_2\rangle\langle\Phi_2| + \cos^2\phi\ |\Phi_2^+\rangle\langle\Phi_2^+| + Ie^{-i\alpha}\cos\phi\ |\Phi_2\rangle\langle\Phi_2^+| + Ie^{i\alpha}\cos\phi\ |\Phi_2^+\rangle\langle\Phi_2|, \quad (2.24)$$

apart from a normalization factor.

Both states ρ_1, from Eq. (2.22), and ρ_2, from Eq. (2.24), which were derived from the generally entangled pure state of Eq. (2.18), represent mixed states for the electrons e_1 and e_2 individually. We are able to obtain the probability distributions for the electrons momenta as $P_1(p) = \langle p|\rho_1|p\rangle$ and $P_2(p) = \langle p|\rho_2|p\rangle$, obtaining

$$P_1(p) = \Phi_1^2(p) + \cos^2\phi\ \Phi_1^2(p+\delta) + 2I\cos\phi\ \cos\alpha\ \Phi_1(p)\Phi_1(p+\delta), \quad (2.25)$$

$$P_2(p) = \Phi_2^2(p) + \cos^2\phi\ \Phi_2^2(p-\delta) + 2I\cos\phi\ \cos\alpha\ \Phi_2(p)\Phi_2(p-\delta), \quad (2.26)$$

apart from normalization factors. Both probability distributions have the same form except for a sign change in δ.

Fig. 10 shows the counter-intuitive result that we want to emphasize. Fig. 10(a) shows the initial distributions of the z component of the electrons momenta, given by the squared modulus of the momentum wave function of Eq. (2.11). Fig. 10(b) shows the momentum distributions for the situations where the electrons propagate through the same path in the interferometer, given by the squared modulus of the momentum wave functions of Eqs. (2.20) and (2.21) with $\delta = 0.3W$. The momentum distribution for electron e_1 is displaced for negative values and the distribution for electron e_2 is displaced for positive values, which indicates the repulsive character of the interaction. Fig. 10(c) shows the momentum distributions predicted by Eqs. (2.25) and (2.26) with the parameters $\delta = 0.3W$, $\phi = 3\pi/4$ and $e^{i\alpha} = 1$. The momentum distribution for electron e_1 is displaced for positive values and the distribution for electron e_2 is displaced for negative values, a result that indicates an effective attractive interaction during their propagation through the interferometer.

Again, as expected from the quantum interference of force, the strange behavior of an effective electrostatic attraction between electrons in the interferometer is the result of a quantum interference effect. In Fig. 11 we plot the terms of Eq. (2.25) that result in the post-selected momentum distribution for electron e_1 with the same parameters $\delta = 0.3W$, $\phi = 3\pi/4$ and $e^{i\alpha} = 1$. The term $T_a(p) \equiv \Phi_1^2(p) + \cos^2(\phi)\Phi_1^2(p+\delta)$ can be interpreted as a "classical" probability term, because it is a convex sum of two probability distributions. On the other hand, $T_b(p) \equiv 2I\cos(\phi)\cos(\alpha)\Phi_1(p)\Phi_1(p+\delta)$ comes from the crossed terms $|\Phi_1\rangle\langle\Phi_1^-|$ in Eq. (2.22), which arise from coherently adding probability amplitudes – i.e. it is a genuine interference term. It is precisely the interference term $T_b(p)$ who is responsible for the shift to a positive mean value of momentum, since it subtracts more from the classical term $T_a(p)$ for negative values of p than for positive values of p, resulting in a

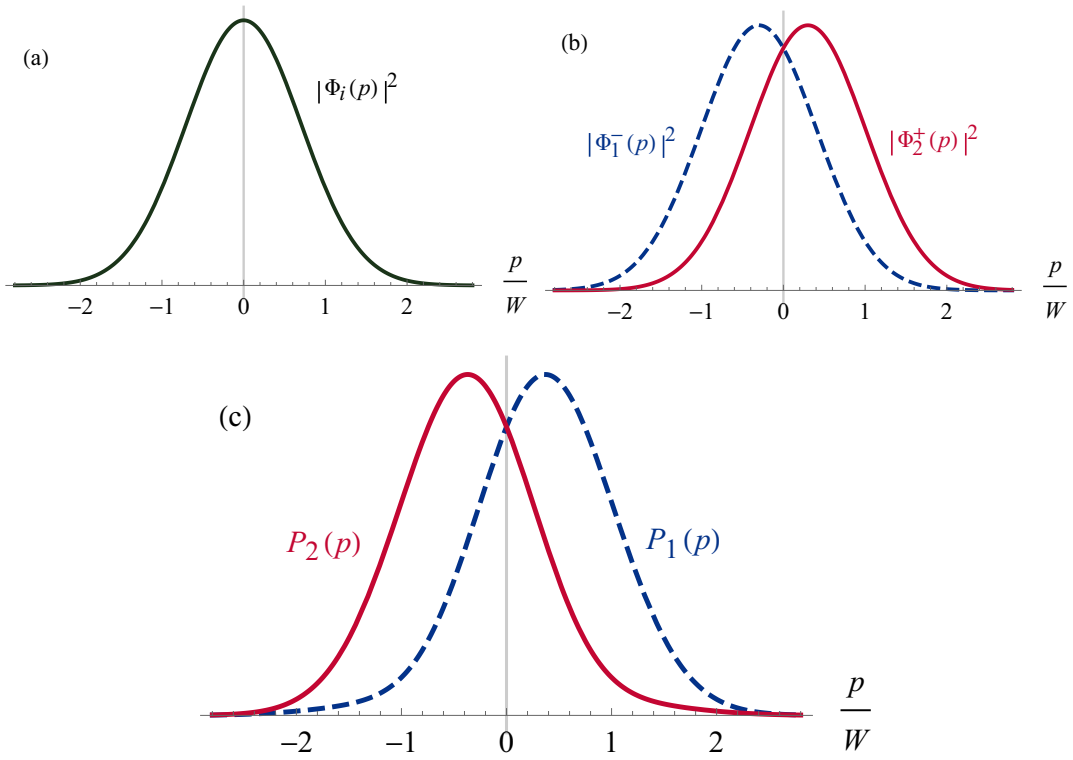

Figure 10 – Distributions for the z component of the electrons momentum wave functions. (a) Initial momentum distribution for each electron, given by $|\Phi_i(p)|^2$ with $\Phi_i(p)$ from Eq. (2.11). (b) Momentum distributions of the situations where the electrons propagate through the same path of the interferometer, given by $|\Phi_1^-(p)|^2$ and $|\Phi_2^+(p)|^2$, with $\Phi_1^-(p)$ and $\Phi_2^+(p)$ from Eqs. (2.20) and (2.21), for $\delta = 0.3W$. (c) Momentum distributions corresponding to the quantum superposition of the two situations, given by Eqs. (2.25) and (2.26) with the parameters $\delta = 0.3W$, $\phi = 3\pi/4$ and $e^{i\alpha} = 1$. We see that the quantum superposition of an electrostatic repulsion between the electrons with no interaction may result in an effective attraction between them.

positive average momentum for the distribution $P_1(p)$. This situation is analogous to the single-particle situation in Sec. 2.2.1 depicted in Fig. 4, only now the force is caused by another quantum particle instead of an external force, and we ought to look at the reduced density matrix distributions instead of the wave function amplitudes.

Also analogously to Sec. 2.2.1, we plot the average momentum of the particles as a function of the the momentum kick δ and phase factor ϕ, due to a path length difference in the interferometer. The momentum expectation value of e_1 at the post-selection condition when it leaves the interferometer is

$$\langle p_1 \rangle_{ps} = \frac{\int_{-\infty}^{\infty} p\ P_1(p)\ dp}{\int_{-\infty}^{\infty} P_1(p)\ dp} = \frac{-\delta\left[\cos^2\phi + \cos\phi\ \exp\left(\frac{-\delta^2}{4W^2}\right)\right]}{1 + \cos^2\phi + 2\cos\phi\ \exp\left(\frac{-\delta^2}{4W^2}\right)}, \tag{2.27}$$

with $P_1(p)$ given by Eq. (2.25) with $e^{i\alpha} = 1$. Since switching δ for $-\delta$ in $P_1(p)$ gives $P_2(p)$ (see Eqs. (2.25) and (2.26)), it is easy to see that the momentum expectation value of

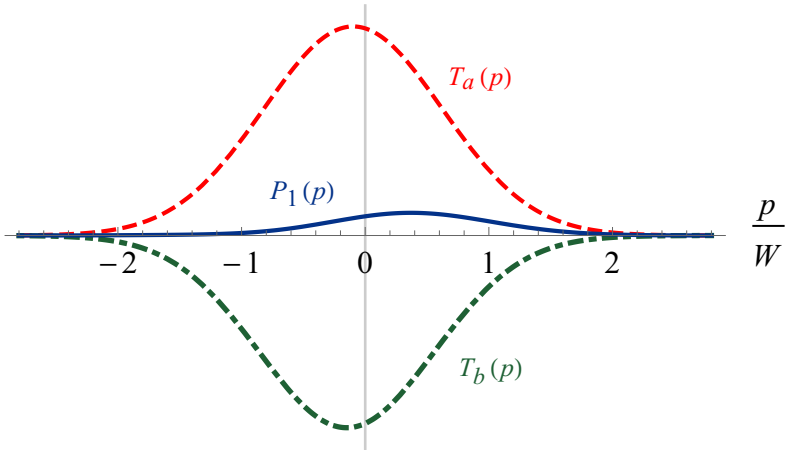

Figure 11 – Terms of Eq. (2.25) when $\delta = 0.3W$, $\phi = 3\pi/4$ and $e^{i\alpha} = 1$. The "classical" term $T_a(p) \equiv \Phi_1^2(p) + \cos^2(\phi)\Phi_1^2(p+\delta)$ (dashed red line), the interference term $T_b(p) \equiv 2I\cos(\phi)\cos(\alpha)\Phi_1(p)\Phi_1(p+\delta)$ (dot-dashed green line) and their sum $P_1(p) = T_a(p) + T_b(p)$ (continuous blue line).

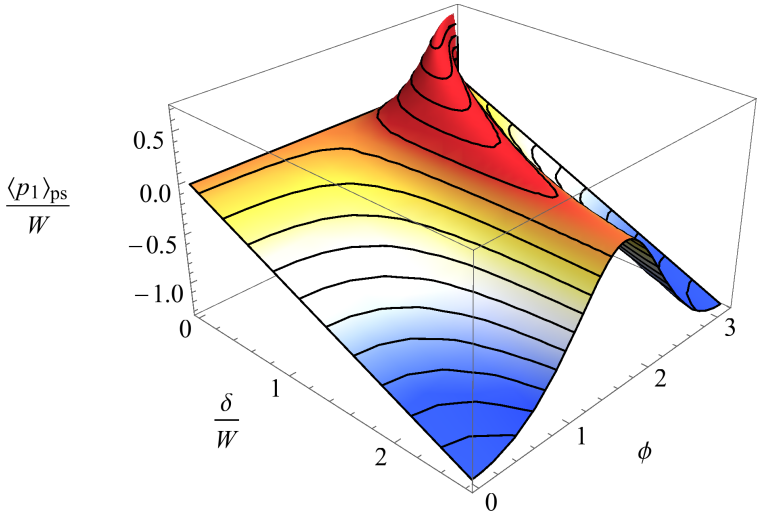

Figure 12 – Expectation value of the average momentum of electron e_1 normalized by the width of the distribution, $\langle p_1\rangle_{ps}/W$, as a function of δ/W and ϕ. Anomalous positive values, associated to an effective electrostatic attraction between the electrons, are shown in red.

e_2 is $\langle p_2\rangle_{ps} = -\langle p_1\rangle_{ps}$. The anomalous behavior of an effective attraction between the electrons depicted in Fig. 10 happens for many values of the interferometer parameters. In Fig. 12 we plot the value of $\langle p_1\rangle_{ps}/W$ as a function of the parameters δ/W and ϕ for $e^{i\alpha} = 1$. We note that anomalous positive values for $\langle p_1\rangle_{ps}/W$ occur in a large range of parameters, particularly out of the weak interaction regime explored in Ref. [63], which demands $\delta \ll W$ and $|\langle p_1\rangle_{ps}| \ll W$.

2.5.3 Ehrenfest's theorem in the two-particle setting

Analogously to what was pointed out in Sec. 2.3, it is important to mention that, independently of the parameters used in the interferometer, the average interaction between the electrons is always repulsive when we consider all possible events, without post-selection. This means that if the post-selection of electron e_1 exiting by D_1 and electron e_2 exiting by C_2 results in an effective attraction between them, as in the situation depicted in Fig. 10, the average interaction in the other situations (electron e_1 by D_1 and electron e_2 by D_2, electron e_1 by C_1 and electron e_2 by C_2, electron e_1 by C_1 and electron e_2 by D_2) is necessarily repulsive, such that the average total interaction is repulsive. We proceed to demonstrate that the average of the momentum gained by each electron agrees with what is expected classically, which is a way to show the validity of Ehrenfest's theorem.

First we note that there are in total 4 possibilities of paths for the two particles jointly inside the apparatus, and 4 possible ways that they can leave the system at the end of the experiment, making up for a total of 16 evolution possibilities for the system. This means that we have in principle a 16 term superposition for our complete two-electron state after they leave the apparatus. The four-term superposition for the joint state inside the interferometer, just before the action of BS_2, can be written as

$$\begin{aligned} &irte^{2i\phi}e^{i\alpha}|\Phi_1^-, A_1\rangle|\Phi_2^+, A_2\rangle + irte^{i\alpha}|\Phi_1^-, B_1\rangle|\Phi_2^+, B_2\rangle \\ &+ t^2e^{i\phi}|\Phi_1, A_1\rangle|\Phi_2, B_2\rangle - r^2e^{i\phi}|\Phi_1, B_1\rangle|\Phi_2, A_2\rangle. \end{aligned} \tag{2.28}$$

The effect of BS_2 over each of the terms of this state can be written as

$$\begin{aligned} |A_1\rangle|A_2\rangle &\Rightarrow t^2|C_1\rangle|C_2\rangle - r^2|D_1\rangle|D_2\rangle + irt(|C_1\rangle|D_2\rangle + |D_1\rangle|C_2\rangle), \\ |B_1\rangle|B_2\rangle &\Rightarrow -r^2|C_1\rangle|C_2\rangle + t^2|D_1\rangle|D_2\rangle + irt(|C_1\rangle|D_2\rangle + |D_1\rangle|C_2\rangle), \\ |A_1\rangle|B_2\rangle &\Rightarrow irt(|C_1\rangle|C_2\rangle + |D_1\rangle|D_2\rangle) + t^2|C_1\rangle|D_2\rangle - r^2|D_1\rangle|C_2\rangle, \\ |B_1\rangle|A_2\rangle &\Rightarrow irt(|C_1\rangle|C_2\rangle + |D_1\rangle|D_2\rangle) - r^2|C_1\rangle|D_2\rangle + t^2|D_1\rangle|C_2\rangle. \end{aligned} \tag{2.29}$$

By plugging Eqs. (2.29) into Eq. (2.28), we reach the final joint state for the two electrons leaving the system,

$$\begin{aligned} &irt\Big[e^{i\alpha}(t^2e^{i\phi} - r^2e^{-i\phi})|\Phi_1^-\rangle|\Phi_2^+\rangle + (t^2 - r^2)|\Phi_1\rangle|\Phi_2\rangle\Big]|C_1\rangle|C_2\rangle + \\ &+ irt\Big[e^{i\alpha}(t^2e^{-i\phi} - r^2e^{i\phi})|\Phi_1^-\rangle|\Phi_2^+\rangle + (t^2 - r^2)|\Phi_1\rangle|\Phi_2\rangle\Big]|D_1\rangle|D_2\rangle + \\ &+ \Big[-r^2t^2e^{i\alpha}(e^{i\phi} + e^{-i\phi})|\Phi_1^-\rangle|\Phi_2^+\rangle + (t^4 + r^4)|\Phi_1\rangle|\Phi_2\rangle\Big]|C_1\rangle|D_2\rangle + \\ &- r^2t^2\Big[e^{i\alpha}(e^{i\phi} + e^{-i\phi})|\Phi_1^-\rangle|\Phi_2^+\rangle + 2|\Phi_1\rangle|\Phi_2\rangle\Big]|D_1\rangle|C_2\rangle. \end{aligned} \tag{2.30}$$

The post-selection of exit ports made previously in our discussion meant projecting the above state superposition in the vector state $|D_1\rangle|C_2\rangle$, and by doing this we get the wave function of Eq. (2.18) used to derive our results, as it should be.

To show that the average interaction is always repulsive when no post-selection is made, we can focus on what happens to electron e_1 (for e_2 it is analogous). Its momentum expectation value is

$$\langle p_1 \rangle = \langle p_1 \rangle_{CC} P_{CC} + \langle p_1 \rangle_{DD} P_{DD} + \langle p_1 \rangle_{CD} P_{CD} + \langle p_1 \rangle_{DC} P_{DC}, \tag{2.31}$$

where P_{jk} is the probability of detecting electron e_1 at exit j and e_2 at k, and $\langle p_1 \rangle_{jk}$ is the respective average momentum for this detection. This quantity can be derived by repeating the process done in Eqs. (2.22), (2.25) and (2.27) for each of the four exit ports possibilities, $|C_1\rangle|C_2\rangle$, $|D_1\rangle|D_2\rangle$, $|C_1\rangle|D_2\rangle$ and $|D_1\rangle|C_2\rangle$. Some straightforward algebra shows us that the total average momentum gained by electron e_1 is

$$\langle p_1 \rangle = (t^4 + r^4)\langle \Phi_1 | p_1 | \Phi_1 \rangle + 2t^2 r^2 \langle \Phi_1^- | p_1 | \Phi_1^- \rangle = -2t^2 r^2 \delta. \tag{2.32}$$

This perfectly agrees with our classical intuition, as the term term calculated with $|\Phi_1\rangle$ is accompanied by the probability that the electrons are either both transmitted or both reflected by BS_1 (they do not interact), and the term calculated with $|\Phi_1^-\rangle$ is weighted by the probability that one of the electrons is transmitted and the other is reflected at BS_1 (they do interact). The above expression is thus analogous to the result for a single particle in Eq. (2.14), both expressing the agreement with the classical intuition when the full average is taken. The final average momentum is simply the momentum gained when they do interact $\langle \Phi_1^- | p_1 | \Phi_1^- \rangle = -\delta$, which comes from a repulsive interaction, times the probability of interacting $2t^2 r^2$. Therefore the average interaction is repulsive, in agreement with momentum conservation and Ehrenfest's theorem.

2.5.4 Notes on the feasibility of such an experiment

As described in Sec. 2.4, electronic Mach-Zehnder interferometers in free space can be implemented using diffraction gratings acting as mirrors and beam splitters [51, 52]. Highly coherent ultrashort electron beams can be generated by laser-triggered emissions from metal tips [64–66], and it is possible to have the emission of at most one electron per laser pulse [67]. The optimal coherence properties of such electron beams, as well as the precise control of the emission time with the incidence of a femtosecond laser pulse in the metal tips, could be used to implement the incidence of two electrons at the same time in a Mach-Zehnder interferometer coming from two tips illuminated by the same laser beam.

Consider that the produced electron beams have width $\Delta x_0 \approx 10$ μm at the entrance of the interferometer, corresponding to a transversal momentum spread $2W \approx \hbar/\Delta x_0 \approx 10^{-29}$kg m/s, and a kinetic energy around 10 eV, corresponding to a longitudinal velocity $v \approx 2 \times 10^6$ m/s. The width of a Gaussian beam as a function of time can be written as $\Delta x(t) = \Delta x_0 \sqrt{1 + \hbar^2 t^2/(m^2 \Delta x_0^4)}$ [46], such that with the considered parameters and the propagation through an interferometer with a typical length $L \approx 5$ cm, the change

on the beams width is of the order of 0.1% and thus negligible. Moreover, if the parallel electron beams are separated by a distance $d \approx 2$ mm, the total momentum exchange between the electrons $\delta = [q^2/(4\pi\epsilon_0 d^2)] \times [L/v]$ would be around 10% of W, ideal for an observation of the effect. For electron emissions that last 100 fs, the longitudinal width of the electron wave functions is around 200 nm for $v \approx 2 \times 10^6$ m/s, much smaller than the considered separation d between the electrons. So the components of the forces that act on the electrons on their propagation direction are negligible compared to the transversal forces, which justifies our 1D analysis of the dynamics. A thin metallic foil can be placed between the interferometer arms to avoid the interaction between the electrons when they propagate through opposite paths. Though an optimal technical implementation may be challenging, these considered parameters are within the scope of what could be experimentally achieved with existing techniques [51, 52, 64–66].

2.6 Chapter remarks

In this chapter, we have presented the phenomenon of *quantum interference of force*. We have shown how the quantum superposition of a positive force with no force on a quantum particle may result in a "negative force" on that particle.

In the first part of the chapter, we have explored the situation in which the force is caused by an external device, for instance a capacitor in one of the arms of an electron Mach-Zehnder interferometer. We also presented proposals for feasible experiments that could verify this anomalous momentum transfer on electrons, neutrons and atoms from a Bose-Einstein condensate.

In the last section, we investigated a setup in which the force that the quantum particle feels is caused by another quantum particle. We show the intriguing phenomenon of two electrons effectively attracting each other, when they propagate through the same Mach-Zehnder interferometer and a suitable post-selection is made. So, in this scenario, the common sense that two charges of equal sign always repel each other is violated due to a quantum interference effect. As we have discussed, an experimental observation of this effect is, in principle, feasible.

In all cases we show that, when we do not post-select the results and consider all the particles possible final states, momentum is always conserved and Ehrenfest's theorem holds.

3 Fermionic Hanbury Brown and Twiss interference in free space with two independent electron sources

In the 1950s Hanbury Brown and Twiss (HBT) introduced intensity interferometry [3–6] as a way to determine the angular diameter of stars in the absence of first-order coherence. Based on their discovery of intensity correlations of light, the HBT experiment initiated a paradigm shift towards a quantum statistical description of light and is nowadays regarded as one of the founding pillars for the development of modern quantum optics [68]. In particular it was recognized that, beyond single-photon interference, two-photon [69–72] and multi-photon [73–77] interference is possible, even if the photons originate from independent incoherent emitters. The crucial ingredient, however, is the need for indistinguishability of the photons, such that the detectors that measure the photons are not, even in principle, provided with any which-way information, e.g. via different frequencies, polarizations or arrival times of the photons.

The use of second- and higher-order correlations for far-field imaging of incoherent light sources, which can be regarded as an extension of the landmark HBT experiment, is an active field of research due to the potential for superresolving imaging in fields other than astronomy [74, 77, 78]. Taking up these ideas and transferring them to incoherent electron sources will thus open new paths in electronic imaging.

The bunching behavior of indistinguishable photons is revealed by light intensity correlations and can be attributed to their bosonic nature. An electronic HBT-like experiment, however, would exhibit anti-bunching, i.e. a vanishing intensity correlation function if two detectors measure on the same spatial and temporal mode. This is derived from the fermionic nature of electrons and the Pauli exclusion principle, which prohibits simultaneous detection of electrons in the same spin state at the same position in space and time [79]. This two-electron interference effect has been demonstrated with electrons propagating in the controlled environment of semiconductor chip devices [7, 8, 80], but there has been controversy on whether HBT anti-correlations have been observed with electrons propagating in free space [9–11, 67]. One of the reasons is that the continuously driven nanotip source used in the experiment creates an electron beam with very small degeneracy, that is, an extremely low number of particles per phase space volume of the quantum state emitted. The small degeneracy means that two-particle effects are extremely rare due to the low probability of having two detections with some coherence with each other – that is, events in which the joint probability of detecting two particles is

different from the probability of detecting two particles independently. Another reason for controversy is the fact that for two-electron events both electrons have to be created within the same nanotip, i.e. in close vicinity to each other. By this, there is a strong Coulomb repulsion between the two electrons that masks the fermionic anti-bunching effects, since the repulsion leads to a decrease in the coincidence of detections and it can thus be mistaken by the HBT anti-correlations interference dip [10, 11, 67].

In this chapter, in order to detect the HBT effect in free space with electrons, we propose an experimental setup with two separate pulsed electron nanotip sources, in the spirit of previously realized photonic experiments [74,77,78]. By this, the period of the HBT oscillations can be adjusted in order to unambiguously distinguish a decrease in coincidence detections due to interference from the effects of Coulomb repulsion. In addition, strong Coulomb repulsion effects do not arise since electrons are not required to be created in close vicinity to each other, i.e. within the same nanotip. We argue that laser-triggered tungsten nanotips [64–66] are extremely well suited as the electron sources for such experiments, since they provide the high degeneracies needed [81]. An implementation of the setup with currently available technology can thus be readily achieved. This also constitutes an important first step for using electron-electron correlations in HBT-like far-field imaging, in the spirit of the recently developed technique of using high-order photon correlations to build image from incoherently scattered light [77, 78].

We first present in Sec. 3.1 a brief review of the Hanbury Brown and Twiss interference for light emitted by two independent sources, from a classical optics point of view. Then in Sec. 3.2 we present the quantization of the electromagnetic field, so we can later discuss detection correlations for quantum fields. In Sec. 3.3 we take some time to discuss the bunching and anti-bunching effect on photodetection. We compare the semi-classical and fully quantum description of the bunching effect, while the anti-bunching effect is only possible with a quantum field. We finally proceed in Sec. 3.4 to the discussion of the fermionic HBT, and show how this effect could be unambiguously detected with the use of two pulsed electron sources.

The work presented in this chapter was developed during the Sandwich PhD period of April 2017 to March 2018 at the University of Erlangen-Nuremberg (Germany), under the supervision of Prof. Joachim von Zanthier. The financial support was provided by Coordenação de Aperfeiçoamento de Pessoal de Nível Superior (CAPES), under the program Programa de Doutorado Sanduíche no Exterior (PDSE), process number 88881.134204/2016-01.

3.1 Hanbury Brown and Twiss interference with classical light

3.1.1 Single intensity measurement from independent light sources

Let us consider the optical field at point P emitted by two point-like independent light sources, separated by a distance d, as pictured in Fig. 13. One of the sources emits a field U_1, and the other a field U_2, both independently from each other.

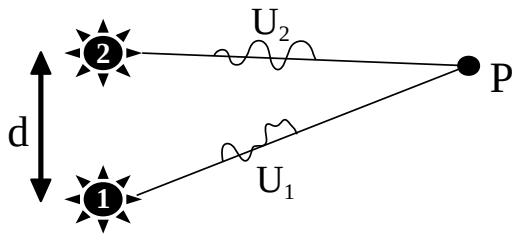

Figure 13 – Two independent light sources separated by a distance d. At point P, the optical fields emitted by each separate source 1 and 2 are labelled U_1 and U_2.

The average[1] intensity $\langle I_P \rangle$ of the field at point P is given by the modulus square of the sum of both fields,

$$\begin{aligned} \langle I_P \rangle &= \langle (U_1^* + U_2^*) \cdot (U_1 + U_2) \rangle \\ &= \langle U_1^* \cdot U_1 \rangle + \langle U_2^* \cdot U_2 \rangle + \langle U_1^* \cdot U_2 \rangle + \langle U_2^* \cdot U_1 \rangle. \end{aligned} \tag{3.1}$$

The first two terms are the separate intensities of each source, $\langle U_1^* \cdot U_1 \rangle \equiv \langle I_1 \rangle$ and $\langle U_2^* \cdot U_2 \rangle \equiv \langle I_2 \rangle$, which are not dependent on phase, while the last two terms depend on the phase difference between the fields emitted by the two sources. The two sources being statistically independent, the phase difference may vary significantly over times larger than the coherence time of the sources, and these terms should vanish. Alternatively, one could assume that there should be no correlation between the two independent fields in the first place, meaning that $\langle U_1^* \cdot U_2 \rangle = \langle U_1^* \rangle \cdot \langle U_2 \rangle$. The independence of the sources thus requires that the absolute phase of each independent source should also be averaged out, otherwise there would be phase correlation between them. In any case,

$$\langle I_P \rangle = \langle I_1 \rangle + \langle I_2 \rangle. \tag{3.2}$$

This means that the only information that can be extracted from the independent sources in a one-point intensity average are the intensities of each separate source, meaning that no spatial information about the sources distribution (contained in phase differences) can be obtained.

[1] From here on we admit the ergodic hypothesis for all the averages, i.e. we consider that the average over a long (infinite) time of a single realization of the statistical process tends to the average over a large (infinite) ensemble of different realizations of that process [82]. We may thus interchangeably use these two concepts, that of an ensemble average and that of a time average, in the same framework.

3.1.2 Intensity correlation measurement from independent light sources

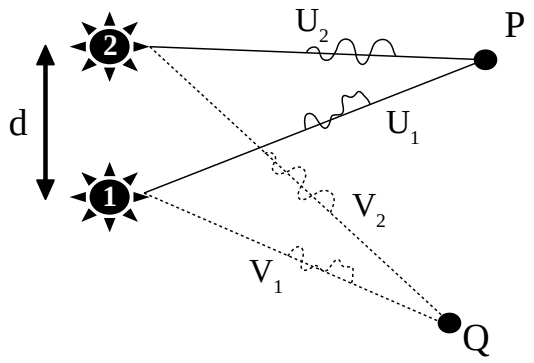

Figure 14 – Two independent light sources separated by a distance d. At point P, the optical fields emitted by each source i are labelled U_i, with $i = 1, 2$. At point Q, the fields are V_i.

The above discussion justifies why simple direct field measurements $\langle U_1 + U_2 \rangle$ may present difficulties when one wants to extract spatial information from independent sources. Furthermore, in the context of visible light optics, no direct field measurements can be made, the detectors only being able to directly resolve intensities. Luckily, single intensity averages are not the only thing that can be measured. The correlation of intensities at different points in space or in time can also be extremely useful. Let us thus look at the fields emitted by the two independent sources at two different points P and Q, as depicted in Fig. 14. The fields from source i at point P are labeled U_i, and at point Q are V_i.

The correlation of the intensities at points P and Q is given by

$$\begin{aligned}\langle I_P I_Q \rangle &= \langle (U_1^* + U_2^*) \cdot (U_1 + U_2) \times (V_1^* + V_2^*) \cdot (V_1 + V_2) \rangle \\ &= \langle I_{U1} I_{V1} \rangle + \langle I_{U2} I_{V2} \rangle + \langle I_{U1} \rangle \langle I_{V2} \rangle + \langle I_{U2} \rangle \langle I_{V1} \rangle \\ &\quad + \langle U_1^* \cdot U_2 \times V_1 \cdot V_2^* \rangle + \langle U_1 \cdot U_2^* \times V_1^* \cdot V_2 \rangle, \end{aligned} \tag{3.3}$$

where $I_{Ui} \equiv U_i^* \cdot U_i$ and $I_{Vi} \equiv V_i^* \cdot V_i$, and $\times$ is a simple algebraic multiplication. The first two terms are intensity correlations of the same source at different points, and therefore it will carry information about the emitted field statistics from each source, and no spatial information between the sources. The third and fourth terms, for which we already considered the independence of sources, are just the product of the intensities of each field at P_1 and P_2, and will not carry spatial information either.

The last two terms of Eq. (3.3) can be written in the following manner for scalar fields from independent sources,

$$\langle U_i^* \cdot U_j \times V_i \cdot V_j^* \rangle = \langle U_i^* \times V_i \rangle \langle U_j \times V_j^* \rangle, \tag{3.4}$$

with $j \neq i$. These terms are correlations between the field amplitudes of each individual source, and therefore may carry phase information due to the field propagation to two

different spatial points. They are proportional to single-source phase differences, which depend on the sources and detectors positions. Because they are single-source terms, they are *not washed out by the average*. Even more interestingly, because the two points P_1 and P_2 are shared by the field correlation functions of both sources, their product *will carry information about the spatial distribution of the sources* [83], e.g. the distance d in Fig. 14. The intensity terms in Eq. (3.3) are constant offsets in the intensity correlation measurement $\langle I_P I_Q \rangle$, while the field amplitude correlation terms detailed in Eq. (3.4) may give rise to oscillations in the intensity correlation, when the detector positions are varied. The shape of this variation was the information explored by Hanbury Brown and Twiss in their stellar interferometry series of experiments [3–6].

3.1.3 The Hanbury Brown and Twiss experiments

In a 1952 paper [3], Hanbury Brown, Jennison and Das Gupta published an experimental paper in which they describe the use of two antennas to make intensity measurements at radio frequency from extra-terrestrial radiation. A series of different separation distances between the two antennas was used, and for each of the distances the field amplitude correlation between the two antenna positions was extracted from the intensity correlation measurements, in a similar fashion to what was described in Subsec. 3.1.2 (see Eqs. (3.3) and (3.4)). A crucial difference is that, instead of a discrete number of independent light sources, the authors were looking at individual stars that were considered as one continuous planar source, such that each point in the source emits radiation independently from the other points. The authors then show that the field correlation is smaller for some antenna distances than for others, following an oscillatory pattern with respect to this distance.

An explicit formula with the spatial oscillation frequency is provided, and carefully derived by Hanbury Brown and Twiss in a 1954 paper [4], which is dependent only on the relative distance between the antennas, on the angular size of the source and on the emitted radiation frequency. This angular size is analogous to the distance d between the sources in Figs. 13 and 14, it playing the part of the spatial information about the continuum of independent radiation sources retrieved with the intensity correlation measurements. By knowing the distance from the Earth to the measured stars, the angular size determined by the spatial oscillation frequency of the intensity correlation measurements reveals the size of the stars. This kind of measurement was a huge breakthrough in interferometry, providing a technique much more resistant to phase fluctuations that are for instance strongly present in the Earth's atmosphere, which can pose a big problem for simple intensity measurements, similarly to the example given in our Eqs. (3.2) and (3.1).

Finally, in 1956, two papers were published with the use of visible radiation in the intensity correlation measurements [5, 6], instead of radio frequency. In [5], a tabletop

experiment was carried out with lasers by Hanbury Brown and Twiss to show that the two-intensity correlations observed in the radio frequency regime are still present in the visible light regime, and that the photo-electric emission process in the detectors preserves these correlations (see also [82]). Subsequently, in [6], the authors measured the diameter of a visible star with the two-intensity correlation technique, which is now known as *Hanbury Brown and Twiss interference*.

3.2 Quantization of the free electromagnetic field

We now make a detour from the Hanbury Brown and Twiss interference in order to briefly present the quantum description of an electromagnetic field in free space.

3.2.1 Plane wave expansion of the electromagnetic field

Maxwell's equations in free space, presented below, famously give rise to wave equations both for the electric and for the magnetic field.

$$\nabla \times \mathbf{E}(\mathbf{r}, t) = -\frac{\partial}{\partial t}\mathbf{B}(\mathbf{r}, t), \tag{3.5}$$

$$\nabla \times \mathbf{B}(\mathbf{r}, t) = \frac{1}{c^2}\frac{\partial}{\partial t}\mathbf{E}(\mathbf{r}, t), \tag{3.6}$$

$$\nabla \cdot \mathbf{E}(\mathbf{r}, t) = 0, \tag{3.7}$$

$$\nabla \cdot \mathbf{B}(\mathbf{r}, t) = 0, \tag{3.8}$$

where $\mathbf{E}(\mathbf{r}, t)$ and $\mathbf{B}(\mathbf{r}, t)$ are respectively the electric and magnetic fields as functions of position $\mathbf{r}$ and time instant t, and c is the speed of light in the vacuum. Taking the curl of Eqs. (3.5) and (3.6) and working out the equations gives us the wave equation for the electric field

$$\nabla^2\mathbf{E}(\mathbf{r}, t) - \frac{1}{c^2}\frac{\partial^2}{\partial t^2}\mathbf{E}(\mathbf{r}, t) = 0, \tag{3.9}$$

and an analogous one to the magnetic field.

Instead of working with the fields themselves, we will conveniently use the vector potential in the Coulomb gauge, defined by the condition $\nabla \cdot \mathbf{A}(\mathbf{r}, t) = 0$. This gauge choice is convenient because it separates the fields into an "instantaneous" part given by the Coulomb potential[2], and purely a radiative part given by the vector potential [84]. In the absence of charge sources, then, the Coulomb potential is zero and fields are given only by the vector potential as

$$\mathbf{E}(\mathbf{r}, t) = -\frac{\partial}{\partial t}\mathbf{A}(\mathbf{r}, t), \tag{3.10}$$

$$\mathbf{B}(\mathbf{r}, t) = \nabla \times \mathbf{A}(\mathbf{r}, t). \tag{3.11}$$

[2] Despite the potential being instantaneous the fields themselves are not, and thus there is no instantaneous transfer of information between different points in space.

When we write Ampère's law in the absence of currents (Eq. (3.6)) with the vector potential, we get a homogeneous wave equation for $\mathbf{A}$,

$$\nabla^2 \mathbf{A}(\mathbf{r},t) - \frac{1}{c^2}\frac{\partial^2}{\partial t^2}\mathbf{A}(\mathbf{r},t) = 0, \tag{3.12}$$

which can be used to fully describe the dynamics of a radiation field in the Coulomb gauge.

Any vector $\mathbf{A}(\mathbf{r},t)$ can thus be written as a linear combination of independent solutions of Eq. (3.12), and we choose a plane wave expansion to write [82]

$$\mathbf{A}(\mathbf{r},t) = \frac{1}{\epsilon_0^{1/2} L^{3/2}} \sum_{\mathbf{k}} \sum_{s} [c_{\mathbf{k}s} \boldsymbol{\epsilon}_{\mathbf{k}s} e^{i(\mathbf{k}\cdot\mathbf{r}-\omega t)} + \text{c.c.}], \tag{3.13}$$

where the space is a cube[3] of side L, ϵ_0 is the electric permittivity of free space and c.c. denotes the complex conjugate of the previous term. It is easy to check that each term of the above expansion is a solution of Eq. (3.12) with $\omega = c|\mathbf{k}|$. The vector $\mathbf{k}$ is a wave vector allowed in that space when we consider periodic boundary conditions. These vectors thus must have components $k_j = 2\pi n_j / L$, with integer n_j for each component $j = x, y, z$. The vector $\boldsymbol{\epsilon}_{\mathbf{k}s}$ is a unit polarization vector allowed for a plane wave propagating in the direction defined by $\mathbf{k}$ with polarization s. The coefficients $c_{\mathbf{k}s}$ provide the amplitude of each linearly independent plane wave solution $\boldsymbol{\epsilon}_{\mathbf{k}s} e^{i(\mathbf{k}\cdot\mathbf{r}-\omega t)}$.

For convenience, the coefficients can be redefined as time dependent, $u_{\mathbf{k}s}(t) \equiv c_{\mathbf{k}s} e^{-i\omega t}$. In this way the vector potential and the fields derived from it by Eqs. (3.10) and (3.11) can be written as

$$\mathbf{A}(\mathbf{r},t) = \frac{1}{\epsilon_0^{1/2} L^{3/2}} \sum_{\mathbf{k}} \sum_{s} [u_{\mathbf{k}s}(t) \boldsymbol{\epsilon}_{\mathbf{k}s} e^{i\mathbf{k}\cdot\mathbf{r}} + \text{c.c.}], \tag{3.14}$$

$$\mathbf{E}(\mathbf{r},t) = \frac{i}{\epsilon_0^{1/2} L^{3/2}} \sum_{\mathbf{k}} \sum_{s} \omega [u_{\mathbf{k}s}(t) \boldsymbol{\epsilon}_{\mathbf{k}s} e^{i\mathbf{k}\cdot\mathbf{r}} - \text{c.c.}], \tag{3.15}$$

$$\mathbf{B}(\mathbf{r},t) = \frac{i}{\epsilon_0^{1/2} L^{3/2}} \sum_{\mathbf{k}} \sum_{s} [u_{\mathbf{k}s}(t) (\mathbf{k} \times \boldsymbol{\epsilon}_{\mathbf{k}s}) e^{i\mathbf{k}\cdot\mathbf{r}} + \text{c.c.}]. \tag{3.16}$$

3.2.2 The Hamiltonian of the electromagnetic field

In order to proceed with the quantization process, we need to write a Hamiltonian for the electromagnetic field in terms of canonical variables. The energy of the electromagnetic field is [84]

$$H = \frac{1}{2} \int_{L^3} \left[\epsilon_0 |\mathbf{E}(\mathbf{r},t)|^2 + \frac{1}{\mu_0} |\mathbf{B}(\mathbf{r},t)|^2 \right] d^3 r, \tag{3.17}$$

where L^3 is the whole space of the cube with side L that we are considering.

[3] An extension of this cube to an infinite space is possible, and it leads to a continuous base instead of a discrete one. For details, see Sec. 10.8 of Ref. [82].

Now that we have a basis to write the electromagnetic field, let us write the energy of the field in terms of the coefficients $u_{\mathbf{k}s}(t)$. After substitution and integration, one gets the very neat expression [82]

$$H = 2\sum_{\mathbf{k}}\sum_{s}\omega^2|u_{\mathbf{k}s}(t)|^2, \tag{3.18}$$

which is a sum of the energy of each mode in the expansion. Note that $|u_{\mathbf{k}s}(t)|$ is time-independent, and consequently the total field energy H is time-independent for constant coefficients $c_{\mathbf{k}s}$.

We now define a pair of variables $q_{\mathbf{k}s}(t)$ and $p_{\mathbf{k}s}(t)$,

$$q_{\mathbf{k}s}(t) = [u_{\mathbf{k}s}(t) + u^*_{\mathbf{k}s}(t)], \tag{3.19}$$
$$p_{\mathbf{k}s}(t) = -i\omega[u_{\mathbf{k}s}(t) - u^*_{\mathbf{k}s}(t)], \tag{3.20}$$

which respect the relations

$$\frac{\partial}{\partial t}q_{\mathbf{k}s}(t) = p_{\mathbf{k}s}(t), \tag{3.21}$$
$$\frac{\partial}{\partial t}p_{\mathbf{k}s}(t) = -\omega^2 q_{\mathbf{k}s}(t). \tag{3.22}$$

With these variables, the energy of the field is written as [82]

$$H = \frac{1}{2}\sum_{\mathbf{k}}\sum_{s}[p^2_{\mathbf{k}s}(t) + \omega^2 q^2_{\mathbf{k}s}(t)], \tag{3.23}$$

from which it is easy to see that

$$\frac{\partial H}{\partial p_{\mathbf{k}s}} = p_{\mathbf{k}s}(t) = \frac{\partial}{\partial t}q_{\mathbf{k}s}(t), \tag{3.24}$$
$$\frac{\partial H}{\partial q_{\mathbf{k}s}} = \omega^2 q_{\mathbf{k}s}(t) = \frac{\partial}{\partial t}p_{\mathbf{k}s}(t). \tag{3.25}$$

The above equations are the canonical relations that show that $q_{\mathbf{k}s}$ and $p_{\mathbf{k}s}$ defined at Eqs. (3.19) and (3.20) form a pair of canonical variables. We can thus conclude that Eq. (3.23) is the Hamiltonian of the electromagnetic field, which has the same form as that of a system of independent harmonic oscillators with unit mass [85], one oscillator for each mode defined by $\mathbf{k}$ and s.

With the classical Hamiltonian in hand, we can now use a quantum version of the canonical variables, that is, we promote them to Hermitian operators $Q_{\mathbf{k}s}(t)$ and $P_{\mathbf{k}s}(t)$ respecting the quantum canonical commutation relations

$$\begin{aligned}[Q_{\mathbf{k}s}(t), P_{\mathbf{k}'s'}(t)] &= i\hbar\delta^3_{\mathbf{k},\mathbf{k}'}\delta_{s,s'},\\ [Q_{\mathbf{k}s}(t), Q_{\mathbf{k}'s'}(t)] &= 0,\\ [P_{\mathbf{k}s}(t), P_{\mathbf{k}'s'}(t)] &= 0.\end{aligned} \tag{3.26}$$

In the same fashion of what is done for the quantum harmonic oscillator [46], a non-Hermitian operator called the annihilation operator (for reasons that will become apparent later) is defined as

$$a_{\mathbf{k}s}(t) = \frac{1}{\sqrt{2\hbar\omega}}[\omega Q_{\mathbf{k}s}(t) + iP_{\mathbf{k}s}(t)], \tag{3.27}$$

and its Hermitian conjugate is called the creation operator. With them, the canonical operators can be written as [82]

$$Q_{\mathbf{k}s}(t) = \sqrt{\frac{\hbar}{2\omega}}\,[a_{\mathbf{k}s}(t) + a^{\dagger}_{\mathbf{k}s}(t)], \tag{3.28}$$

$$P_{\mathbf{k}s}(t) = -i\sqrt{\frac{\hbar\omega}{2}}\,[a_{\mathbf{k}s}(t) - a^{\dagger}_{\mathbf{k}s}(t)], \tag{3.29}$$

and their commutation relations follow from those of $Q_{\mathbf{k}s}$ and $P_{\mathbf{k}s}$,

$$\begin{aligned}
&[a_{\mathbf{k}s}(t), a^{\dagger}_{\mathbf{k}'s'}(t)] = \delta^3_{\mathbf{k},\mathbf{k}'}\delta_{s,s'},\\
&[a_{\mathbf{k}s}(t), a_{\mathbf{k}'s'}(t)] = 0,\\
&[a^{\dagger}_{\mathbf{k}s}(t), a^{\dagger}_{\mathbf{k}'s'}(t)] = 0.
\end{aligned} \tag{3.30}$$

When we compare the operators in Eqs. (3.28) and (3.29) with the respective classical variables in Eqs. (3.19) and (3.20), we see that apart from a dimensionality factor the operators $a_{\mathbf{k}s}(t)$ and $a^{\dagger}_{\mathbf{k}s}(t)$ correspond to the complex amplitudes $u_{\mathbf{k}s}(t)$ and $u^{*}_{\mathbf{k}s}(t)$. When one works their time evolution, one sees that they even have the same time dependence, namely [82]

$$\begin{aligned}
a_{\mathbf{k}s}(t) &= a_{\mathbf{k}s}(0)e^{-i\omega t},\\
a^{\dagger}_{\mathbf{k}s}(t) &= a^{\dagger}_{\mathbf{k}s}(0)e^{i\omega t}.
\end{aligned} \tag{3.31}$$

The Hamiltonian written in terms of the annihilation and creation operators can be worked out from plugging $Q_{\mathbf{k}s}$ and $P_{\mathbf{k}s}$ respectively in place of $q_{\mathbf{k}s}$ and $p_{\mathbf{k}s}$ in Eq. (3.23), and it is

$$H = \frac{1}{2}\sum_{\mathbf{k}}\sum_{s}\hbar\omega[a_{\mathbf{k}s}(t)a^{\dagger}_{\mathbf{k}s}(t) + a^{\dagger}_{\mathbf{k}s}(t)a_{\mathbf{k}s}(t)]. \tag{3.32}$$

Analogously to $|u_{\mathbf{k}s}(t)|^2$, the operator product $a_{\mathbf{k}s}(t)a^{\dagger}_{\mathbf{k}s}(t)$ and its Hermitian conjugate are time-independent, since their composing operators have a complex harmonic time dependence. We have thus a time-independent Hamiltonian for the quantum electromagnetic field. From the first commutation relation of Eq. (3.30), we finally arrive at the quantum Hamiltonian for the electromagnetic field in its most known form

$$H = \sum_{\mathbf{k}}\sum_{s}\hbar\omega\left[a^{\dagger}_{\mathbf{k}s}(t)a_{\mathbf{k}s}(t) + \frac{1}{2}\right], \tag{3.33}$$

where the famous zero-point energy contribution $\hbar\omega/2$ of each field mode (see discussion in Sec. 3.2.3) is explicit.

3.2.3 Number states

Despite the creation and annihilation operators being non-Hermitian, their product $a^\dagger_{\mathbf{k}s}a_{\mathbf{k}s}$ that appears in the Hamiltonian of Eq. (3.33) is a Hermitian operator, which can be readily verified. The spectrum of this operator defined as $N_{\mathbf{k}s} \equiv a^\dagger_{\mathbf{k}s}a_{\mathbf{k}s}$ is discrete and infinite, composed of all non-negative integers [46, 82], such that

$$N_{\mathbf{k}s}|n_{\mathbf{k}s}\rangle = n_{\mathbf{k}s}|n_{\mathbf{k}s}\rangle, \qquad n_{\mathbf{k}s} = 0,\ 1,\ 2, \dots \tag{3.34}$$

with $n_{\mathbf{k}s}$ being the eigenvalue correspondent to the eigenstate $|n_{\mathbf{k}s}\rangle$. Since these are eigenstates of a Hermitian operator, they are all orthonormal to each other and form a basis on the Hilbert space of that mode. We will see that the eigenvalues $n_{\mathbf{k}s}$ correspond to the number of excitations in the harmonic oscillator mode defined by the pair $(\mathbf{k}, s)$, and for this reason the operator $N_{\mathbf{k}s}$ is called the *number operator*, its eigenstates being called *number states*.

The action of the creation and annihilation operators on the eigenvectors of $N_{\mathbf{k}s}$ is [46, 82]

$$a^\dagger_{\mathbf{k}s}|n_{\mathbf{k}s}\rangle = \sqrt{n_{\mathbf{k}s}+1}|n_{\mathbf{k}s}+1\rangle, \tag{3.35}$$

$$a_{\mathbf{k}s}|n_{\mathbf{k}s}\rangle = \sqrt{n_{\mathbf{k}s}}|n_{\mathbf{k}s}-1\rangle. \tag{3.36}$$

The creation operator thus transforms an eigenstate $|n_{\mathbf{k}s}\rangle$ into another eigenstate with an eigenvalue increased by 1. The annihilation takes that same eigenstate $|n_{\mathbf{k}s}\rangle$ into one with an eigenvalue decreased by 1. Because the eigenvalues are bounded from below, the annihilation operator into the eigenstate with eigenvalue 0 gives the null vector, $a_{\mathbf{k}s}|0_{\mathbf{k}s}\rangle = 0$.

We can now define a state that contains all modes and is still an eigenstate of $N_{\mathbf{k}s}$. This state will be a direct product of eigenstates of all modes, namely $|\{n\}\rangle \equiv \prod_{\mathbf{k},s}|n_{\mathbf{k}s}\rangle$, such that

$$N_{\mathbf{k}s}|\{n\}\rangle = n_{\mathbf{k}s}|\{n\}\rangle. \tag{3.37}$$

The state $|\{n\}\rangle$ is called a Fock state, after the Soviet physicist Vladimir Fock. The annihilation and creation operators, when acting on this multi-mode Fock state, also have an effect only on the mode that the operator is correspondent to.

The Hamiltonian of the free electromagnetic field, written in Eq. (3.33), can be written as a function of number operators only, such that the Fock states are also eigenvectors of the electromagnetic field Hamiltonian,

$$H|\{n\}\rangle = \left[\sum_{\mathbf{k},s}\hbar\omega\left(N_{\mathbf{k}s}+\frac{1}{2}\right)\right]|\{n\}\rangle = \left[\sum_{\mathbf{k},s}\hbar\omega\left(n_{\mathbf{k}s}+\frac{1}{2}\right)\right]|\{n\}\rangle. \tag{3.38}$$

Just like the single-mode number states, the Fock states are orthonormal among themselves and diagonalize the field Hamiltonian, thus they form an important basis to describe quantum states of the electromagnetic field.

As can be seen in Eq. (3.38), the number operator for a mode of the electromagnetic field counts how many excitations there are in that mode, which contributes to the energy of the state. The Hamiltonian counts those excitations and, weighted by the $\hbar\omega$ energy of each excitation of that mode, gives the energy of the multi-mode Fock state $|\{n\}\rangle$. Finally this justifies all the names given to the operators: the number operator counts the number of excitations in a mode, the creation operator creates an excitation, and the annihilation operator destroys one of them, in the given mode. Note that even in the absence of excitations, i.e. in the vacuum of the field, the zero-point energy of $\hbar\omega/2$ for each mode is still counted, thus justifying its name. This gives an infinite energy as a background to all eigenstates of that Hamiltonian, and it has dramatic consequences for the quantum field theories with open questions until these days [86]. However, since we will only be worried about energy differences, we will overlook these problems. The state with zero excitations is, for obvious reasons, called the vacuum state, and is denoted by $|\text{vac}\rangle$, sometimes $|\{0\}\rangle$ or even simply $|0\rangle$.

3.2.4 Coherent states

Another crucially important class of states of quantum optics is that of the so-called *coherent states*. These states are the eigenvectors of the annihilation operator,

$$a_{\mathbf{k}s}|\alpha_{\mathbf{k}s}\rangle = \alpha_{\mathbf{k}s}|\alpha_{\mathbf{k}s}\rangle. \tag{3.39}$$

Since this is a non-Hermitian operator, its eigenvelues $\alpha_{\mathbf{k}s}$ are in general complex numbers. In the number state basis, these states are written as [82]

$$|\alpha_{\mathbf{k}s}\rangle = e^{-|\alpha_{\mathbf{k}s}|^2/2}\sum_{n=0}^{\infty}\frac{(\alpha_{\mathbf{k}s})^n}{n!}|n\rangle, \tag{3.40}$$

where the mode subscripts $\mathbf{k}s$ were dropped from $n_{\mathbf{k}s}$ for simplicity, but are implied. As a generalization, just like for the number states, a multi-mode coherent state can be defined as $|\{\alpha\}\rangle = \prod_{\mathbf{k},s}|\alpha_{\mathbf{k}s}\rangle$.

There are many reasons for the importance of such states, but a crucial one is that the operators for the quantum fields are functions of the annihilation and creation operators. For instance, the expression for the electric field operator is

$$\mathbf{E}(\mathbf{r},t) = \frac{1}{L^{3/2}}\sum_{\mathbf{k}}\sum_{s} i\sqrt{\frac{\hbar\omega}{2\epsilon_0}}\left[a_{\mathbf{k}s}(t)\boldsymbol{\epsilon}_{\mathbf{k}s}e^{i\mathbf{k}\cdot\mathbf{r}} - a^{\dagger}_{\mathbf{k}s}(t)\boldsymbol{\epsilon}^{*}_{\mathbf{k}s}e^{-i\mathbf{k}\cdot\mathbf{r}}\right], \tag{3.41}$$

which can be compared to the expression for the classical field on Eq. (3.15). Because the Fock states change on the application of the annihilation and creation operators, and

are transformed into an orthonormal state, the expectation value of any annihilation or creation operator is zero for these states, $\langle\{n\}|a_{\mathbf{k}s}(t)|\{n\}\rangle = \langle\{n\}|a^\dagger_{\mathbf{k}s}(t)|\{n\}\rangle = 0$. Therefore the expectation value for the field operators will also always be zero for Fock states.

The coherent states, on the other hand, will always give off a non-zero complex number as the expectation value for the annihilation operator[4], $\langle\{\alpha\}|a_{\mathbf{k}s}(t)|\{\alpha\}\rangle = \alpha_{\mathbf{k}s}(t)$, and despite them not being eigenvectors of the creation operator, the expectation values for states with large $|\alpha_{\mathbf{k}s}(t)|$ do give off approximately $\langle\{\alpha\}|a^\dagger_{\mathbf{k}s}(t)|\{\alpha\}\rangle \approx \alpha^*_{\mathbf{k}s}(t)$. Given the explicit time dependence of the annihilation and creation operators from Eq. (3.31), the expectation value of the field operators will therefore evolve just like the classical values, when one changes $u_{\mathbf{k}s}$ by $\sqrt{\frac{\hbar}{2\omega}}\alpha_{\mathbf{k}s}$ in Eq. (3.15),

$$\langle\{\alpha\}|\mathbf{E}(\mathbf{r},t)|\{\alpha\}\rangle \approx \frac{1}{L^{3/2}}\sum_{\mathbf{k}}\sum_{s} i\sqrt{\frac{\hbar\omega}{2\epsilon_0}}\left[\alpha_{\mathbf{k}s}(t)\boldsymbol{\epsilon}_{\mathbf{k}s}e^{i\mathbf{k}\cdot\mathbf{r}} - \alpha^*_{\mathbf{k}s}(t)\boldsymbol{\epsilon}^*_{\mathbf{k}s}e^{-i\mathbf{k}\cdot\mathbf{r}}\right]. \tag{3.42}$$

The coherent states thus provide a classical limit to electromagnetic fields, whenever the field is composed of states with large $|\alpha_{\mathbf{k}s}(t)|$.

Importantly, the coherent states also form a basis to write general quantum states of the electromagnetic field. However, differently from the Fock states, they form an over-complete basis, and thus there is in general more than one possible representation of a field state in terms of coherent states [82]. We will not go into more details here, but this basis gives rise to the so-called Glauber–Sudarshan representation of quantum optical states [87, 88], which gives us many insights on what novelties quantum mechanics brings into optics. In Sec. 3.3.3 we will discuss one of such novelties without recurring to this representation.

Another important feature of the coherent states is related to the optical correlation functions [82,89]. As will be mentioned later in Sec. 3.3.2, correlation functions of amplitudes and intensities of electromagnetic fields are related to photo-detections in that field. These functions will be proportional to annihilation and creation operators in such a way that the coherent states will provide correlation functions that are in a sense equivalent to correlation functions of classical electromagnetic fields. More precisely, the factorization of correlation functions is the property that defines the so-called degree of coherence of a classical field [82]. Because the $|\{\alpha\}\rangle$ state gives the maximum allowed value for the degree of coherence, indicating perfect factorization of the correlation functions in the quantum optical coherence theory [89], it receives the name of coherent state.

[4] Except for the vacuum state, naturally, which can be interpreted as a coherent state with zero amplitude.

3.3 Intensity correlation measurement and its relation to photodetection statistics

In this section, we will investigate how the intensity correlation measurement established by Hanbury Brown and Twiss relates to the photodetection statistics of the light emitted by certain sources. In a semi-classical picture, this will be related to the detection probabilities of a quantum detector that interacts with the classical field, while in the quantum picture, it will be related to the photon number statistics of the sources. The way we approach the subject will be by discussing the phenomenon called photon bunching, first from a semi-classical (classical light and quantum detectors) and then from a fully quantum point of view (light is also quantized), and subsequently we will discuss the exclusively non-classical phenomenon of anti-bunching.

3.3.1 Photon bunching: semi-classical description

Consider a quasi-monochromatic classical light source that emits a statistical mixture of classical electromagnetic fields. This mixture can contain both a mixture of random phases of the emitted fields and a mixture of many field amplitudes. In this sense we say that the field fluctuates, i.e. it does not have well defined values for its amplitude modulus or phase. For instance, each mode of a thermal light source, which is a source in thermal equilibrium at a certain temperature T, exhibits a Gaussian distribution of the modulus of the field amplitude U [82], the phase distribution being completely random and independent from the modulus,

$$\rho_{\text{amp}}(U) \propto e^{-|U|^2/W}. \tag{3.43}$$

Since the intensity is given by the square modulus of the field amplitude, $I = |U|^2$, the field intensity distribution is a decreasing exponential

$$\rho_{\text{int}}(I) \propto e^{-I/W}. \tag{3.44}$$

The width W of the distribution is given by the average intensity of the field, which in turn depends on the temperature T and on the frequency ω of that mode following the expression

$$W = \langle I \rangle_{\text{thermal}} \propto \frac{\hbar\omega}{e^{\hbar\omega/k_B T} - 1}, \tag{3.45}$$

where k_B is Boltzmann's constant and $\hbar$ is Planck's reduced constant[5]. One notes that W approaches zero as $T \to 0$, meaning that the intensity distribution concentrates on low intensity values in this limit. For large temperatures, on the other hand, the distribution grows approximately linearly with T, meaning that larger values of I contribute ever more as T grows.

In order to obtain the intensity correlation function via photodetections, we consider that two quantum detectors will be used. For quantum detectors we mean quantum systems that interact with light and perform a transition, specifically a material that ejects an electron, with a given probability P. When this probability P is sufficiently small, the interaction of the material with the field can be treated using perturbation theory. It can be shown [82] that, for a well defined[6] electromagnetic field with amplitude $U(\mathbf{r}, t)$ and intensity $I(\mathbf{r}, t) = |U(\mathbf{r}, t)|^2$, the photodetection probability at point $\mathbf{r}$ and at time t within a short time interval[7] Δt is proportional to the field intensity $I(\mathbf{r}, t)$ at this point and time,

$$P(\mathbf{r}, t) \propto \eta I(\mathbf{r}, t)\Delta t, \tag{3.46}$$

where η is a detection efficiency, dependent for instance on the coupling between the material and the field, on the light polarization and on the detector spatial orientation. When two detectors are used, one at $(\mathbf{r_1}, t_1)$ and the other at $(\mathbf{r_2}, t_2)$, the photodetection probabilities of each one does not influence the other, meaning that the joint detection probability is just the product of the two probabilities,

$$P(\mathbf{r_1}, t_1; \mathbf{r_2}, t_2) \propto \eta_1\eta_2 I(\mathbf{r_1}, t_1)I(\mathbf{r_2}, t_2)\Delta t_1 \Delta t_2, \tag{3.47}$$

where η_1 and η_2 are the detection efficiencies of each of the two detectors, and Δt_1 and Δt_2 are the short time intervals in each detection. This is easily generalized for an arbitrary number of detections.

We are however interested in fluctuating fields, which are not fixed for every realization of a statistical ensemble. Therefore, Eqs. (3.46) and (3.47) have to be generalized for a statistical mixture of classically well defined fields. By assuming that the fields are stationary, i.e. that their averages do not change in time, the detection probabilities are

[5] Note that $\hbar$ appears in the expression of Eq. (3.45), as it can only be correctly derived with the use of Planck's quantization hypothesis [82, 90]. When divided by $\hbar\omega$ the given expression is, not by coincidence, equal to the Bose-Einstein distribution for the average number of particles in an ensemble of bosons each with energy $\hbar\omega$ and zero chemical potential [91]. Each mode of the thermal optical field may thus be interpreted as composed of identical non-interacting bosonic particles each with energy $\hbar\omega$. The average intensity of the field, in this view, is proportional to the average number of particles in the field [82].

[6] "Well defined", here and later in the text, means that the field is described by a single amplitude $U(\mathbf{r}, t)$, and not a statistical ensemble of them.

[7] "Short" here means that the perturbation expansion is still valid and in this time interval the probability that two or more electrons are ejected in the same process is negligible.

generalized to

$$P(\mathbf{r},t) \propto \eta\langle I(\mathbf{r},t)\rangle_\rho \, \Delta t, \tag{3.48}$$

$$P_2(\mathbf{r_1},t_1;\mathbf{r_2},t_2) \propto \eta_1\eta_2\langle I(\mathbf{r_1},t_1)I(\mathbf{r_2},t_2)\rangle_\rho \, \Delta t_1\Delta t_2, \tag{3.49}$$

where the brackets denote averages over a statistical ensemble given by a probability distribution ρ. The term in brackets in Eq. (3.49) is a two-intensity correlation function, and therefore *the joint probability of two photodetections of a fluctuating light field is proportional to its two-intensity correlation function at the detector positions.*

Instead of having two detectors, Eq. (3.49) can refer to two detections in the same detector, within an interval τ. We drop the spatial point and probability distribution specification and write

$$P_2(t,t+\tau) \propto \eta^2\langle I(t)I(t+\tau)\rangle\Delta t_1\Delta t_2. \tag{3.50}$$

A Schwarz inequality can be constructed for the intensity correlation, and together with the fact that the field is stationary we are allowed to say that [82]

$$\langle I(t)I(t+\tau)\rangle \leq \langle I^2(t)\rangle, \tag{3.51}$$

meaning that

$$P_2(t,t+\tau) \leq P_2(t,t). \tag{3.52}$$

The above equation means that, for a fluctuating classical field, having two detections at the same time is either equally or more probable than having two detections at different times. This effect is termed *photon bunching*, alluding to the idea that the photodetections are bunched together at close times. It is directly connected to the fact that the field fluctuates. It is important to note that we have assumed statistical independence between the two correlations *for a well defined field* (see footnote 6 on page 47). It thus must be clear that the correlations should only appear when an ensemble of amplitudes is gathered.

One can have a rough intuitive view of the bunching effect by realizing that, for long time intervals τ, the intensity correlations should vanish, that is,

$$\lim_{\tau\to\infty}\langle I(t)I(t+\tau)\rangle = \langle I(t)\rangle\langle I(t+\tau)\rangle = \langle I(t)\rangle^2, \tag{3.53}$$

where in the last equality field stationarity, i.e. the constancy of its statistical properties in time, was invoked. For a classical field, which can be described as a mixture of fields with well defined intensities, the field intensity fluctuations must be positive by definition. The field intensity fluctuations at time t are measured by the variance

$$\langle(\Delta I)^2\rangle(t) \equiv \langle[I(t)-\langle I(t)\rangle]^2\rangle = \langle I^2(t)\rangle - \langle I(t)\rangle^2, \tag{3.54}$$

and therefore its positivity is connected to the fact that $\langle I(t)I(t)\rangle$ can be larger than $\langle I(t)I(t+\tau)\rangle$, but not smaller. Because the joint photodetection probability is proportional to the two-intensity correlation function, which is just the product of two independent intensity averages for well defined fields, we can thus not only say that in the semi-classical description the photon bunching effect is explained by the field fluctuations, but that it is caused by them.

We would like to note that the positivity of the fluctuations (see Eq. (3.54)) will be reflected in larger values of the first two terms of the two-intensity correlation expression in Eq. (3.3), namely $\langle I_{U1}I_{V1}\rangle$ and $\langle I_{U2}I_{V2}\rangle$. That is why, in our context, we will say that these terms reveal properties of the source statistics in the visibility of the two-intensity interference pattern. Large fluctuations means a greater constant offset in the two-intensity correlation and thus a spatial interference pattern with less visibility. This influence will appear explicitly in Sec. 3.4.4.

3.3.2 Photon bunching: fully quantum description

When we go to a fully quantum description, i.e. the electromagnetic field is also quantized, the picture changes. The probability of having a transition in the detector is proportional to the probability of subtracting one excitation—a photon—from the quantum field. That is to say that now the photodetection causes the field to be described by a different state than before the detection, since a photon was subtracted from it, something that is not present in the semi-classical description.

The positive-frequency optical field operator, i.e. the part of the field operator (see Eq. (3.41)) that oscillates with dependence $e^{-i\omega t}$, can be written as

$$\mathbf{E}^{(+)}(\mathbf{r},t) = \sum_s E_s^{(+)}(\mathbf{r},t)\ \boldsymbol{\epsilon}_s, \tag{3.55}$$

which is composed of fields $E_s^{(+)}(\mathbf{r},t)$ with polarization vector $\boldsymbol{\epsilon}_s$, such that $\boldsymbol{\epsilon}_s\cdot\boldsymbol{\epsilon}_{s'}^* = \delta_{s,s'}$. We define $\mathbf{E}^{(-)}(\mathbf{r},t) \equiv [\mathbf{E}^{(+)}(\mathbf{r},t)]^\dagger$ and $E_s^{(-)}(\mathbf{r},t) \equiv [E_s^{(+)}(\mathbf{r},t)]^\dagger$ to be the negative-frequency field operators. As can be seen from Eqs. (3.31) and (3.41), the positive- and negative-frequency fields of each polarization are functions respectively of annihilation and creation operators, and we can write

$$E_s^{(+)}(\mathbf{r},t) = \sum_\kappa f_\kappa(\mathbf{r},t)\ a_{\kappa,s}, \tag{3.56}$$

$$E_s^{(-)}(\mathbf{r},t) = \sum_\kappa f_\kappa^*(\mathbf{r},t)\ a_{\kappa,s}^\dagger, \tag{3.57}$$

where $a_{\kappa,s}$ is the annihilation operator for a photon in spatial mode κ of the field with polarization vector $\boldsymbol{\epsilon}_s$, $a_{\kappa,s}^\dagger$ is the corresponding creation operator, while $f_\kappa(\mathbf{r},t)$ contains the mode spatial dependence and its time evolution. The bosonic commutation relations for these operators are $[a_{\kappa,s}, a_{\kappa',s'}] = 0$ and $[a_{\kappa,s}, a_{\kappa',s'}^\dagger] = \delta_{\kappa,\kappa'}\delta_{s,s'}$ (see Eq. (3.30)). The

intensity average at point $\mathbf{r}$ and time t of a field characterized by the quantum state ρ is given by [82, 89]

$$\langle : I(\mathbf{r},t) : \rangle_\rho = \langle \mathbf{E}^{(-)}(\mathbf{r},t) \cdot \mathbf{E}^{(+)}(\mathbf{r},t) \rangle_\rho = \mathrm{Tr}[\rho\ \mathbf{E}^{(-)}(\mathbf{r},t) \cdot \mathbf{E}^{(+)}(\mathbf{r},t)], \tag{3.58}$$

where the colons indicate a normal ordering of the field operators. Normal ordering means that negative-frequency operators always act on the state ρ on the right, and positive-frequency on the left, which is seen from the cyclic property of the trace,

$$\langle : I(\mathbf{r},t) : \rangle_\rho = \sum_s \mathrm{Tr}[E_s^{(+)}(\mathbf{r},t)\ \rho\ E_s^{(-)}(\mathbf{r},t)]. \tag{3.59}$$

This is connected to the fact that the intensity measurement is the subtraction of a photon, which can be realized from the fact that $\mathbf{E}^{(+)}(\mathbf{r},t)$ only contains annihilation operators (see Eq. (3.56)). Also, just like in the classical case, the probability of detection of one photon when the field is in state ρ can be shown to be proportional to the field intensity average over that state, with an expression identical to the one in Eq. (3.48) given for a fluctuating field [82]. The difference is that in the quantum picture of the field the fluctuations are characterized by a quantum operator ρ instead of a classical statistical mixture, following Eq. (3.59),

$$P_\rho(\mathbf{r},t) \propto \eta \langle : I(\mathbf{r},t) : \rangle_\rho\ \Delta t. \tag{3.60}$$

Higher-order field correlation measurements can be shown to respect the same normal ordering [82, 89], and the two-intensity measurement is a particular case. Namely,

$$\begin{aligned} \langle : I(\mathbf{r},t) I(\mathbf{r}',t') : \rangle_\rho =& \langle : [\mathbf{E}^{(-)}(\mathbf{r},t) \cdot \mathbf{E}^{(+)}(\mathbf{r},t)]\ [\mathbf{E}^{(-)}(\mathbf{r}',t') \cdot \mathbf{E}^{(+)}(\mathbf{r}',t')] : \rangle_\rho \\ =& \sum_{s,s'} \mathrm{Tr}[E_{s'}^{(+)}(\mathbf{r}',t') E_s^{(+)}(\mathbf{r},t)\ \rho\ E_s^{(-)}(\mathbf{r},t) E_{s'}^{(-)}(\mathbf{r}',t')], \end{aligned} \tag{3.61}$$

only now we have to respect also time ordering of the operators, such that photons at a time t are subtracted from ρ before the ones at a later time $t' > t$.

Interestingly, we can define a photon-subtracted state $\tilde{\rho}$ [75, 76], which is obtained by subtracting a photon from ρ at position $\mathbf{r}$ at time t,

$$\tilde{\rho} \equiv \frac{\sum_s E_s^{(+)}(\mathbf{r},t)\ \rho\ E_s^{(-)}(\mathbf{r},t)}{\sum_s \mathrm{Tr}[E_s^{(+)}(\mathbf{r},t)\ \rho\ E_s^{(-)}(\mathbf{r},t)]}. \tag{3.62}$$

Therefore, the two-intensity correlation measurement on state ρ can be interpreted as an intensity average over the state $\tilde{\rho}$, conditioned on the probability of the first detection,

$$\begin{aligned} \langle : I(\mathbf{r},t) I(\mathbf{r}',t') : \rangle_\rho =& \sum_{s'} \mathrm{Tr}[E_{s'}^{(+)}(\mathbf{r}',t')\ \tilde{\rho}\ E_{s'}^{(-)}(\mathbf{r}',t')] \times \sum_s \mathrm{Tr}[E_s^{(+)}(\mathbf{r},t)\ \rho\ E_s^{(-)}(\mathbf{r},t)] \\ =& \langle : I(\mathbf{r}',t') : \rangle_{\tilde{\rho}} \times \langle : I(\mathbf{r},t) : \rangle_\rho \\ \propto& \langle : I(\mathbf{r}',t') : \rangle_{\tilde{\rho}} \times\ P_\rho(\mathbf{r},t). \end{aligned} \tag{3.63}$$

In other words, $\langle: I(\mathbf{r},t)I(\mathbf{r}',t') :\rangle_\rho$ is a two-step photon subtraction, and contrarily to the classical framework, the quantum description may be interpreted as the first subtraction changing the quantum state of the light field from ρ to $\tilde{\rho}$ before the second detection.

An important property of coherent fields (see Sec. 3.2.4) is that they have a well defined field intensity, i.e. there are no intensity fluctuations[8]. This is in accordance to the classical notion of optical coherence, which was admitted in our discussion of the previous section, and this is one of the many reasons for why these states are the quantum analogues to well defined classical fields. We have argued in Sec. 3.3.1 that a classical fluctuating field can be constructed from statistical mixtures of fields with a well defined amplitude and, consequently, a well defined intensity. This is connected to the fact that for all optically coherent quantum fields $|\alpha\rangle$ the intensity correlations factor in a product of intensity averages,

$$\langle: I(\mathbf{r},t)I(\mathbf{r}',t') :\rangle_{|\alpha\rangle} = \langle: I(\mathbf{r},t) :\rangle_{|\alpha\rangle} \ \langle: I(\mathbf{r}',t') :\rangle_{|\alpha\rangle}, \tag{3.64}$$

which leads to zero fluctuations when $\mathbf{r}' = \mathbf{r}$ and $t' = t$. From this fact, all the discussion from the previous section follows for a classical field whose state ρ_{cl} can be written as a statistical mixture of coherent states $|\alpha\rangle$. This includes the positivity of the fluctuations

$$\langle(\Delta I)^2\rangle_{\rho_{cl}}(t) \equiv \langle: [I(t) - \langle: I(t) :\rangle]^2 :\rangle_{\rho_{cl}} = \langle: I^2(t) :\rangle_{\rho_{cl}} - \langle: I(t) :\rangle^2_{\rho_{cl}} \geq 0, \tag{3.65}$$

and the validity of the Schwarz inequality of Eq. (3.51)

$$\langle: I(t)I(t+\tau) :\rangle_{\rho_{cl}} \leq \langle: I^2(t) :\rangle_{\rho_{cl}}. \tag{3.66}$$

We can finally interpret the photon bunching effect from a quantum point of view, having in mind that the two-intensity correlation is proportional to the probability of subtracting two photons from the quantum optical field. Because of this, the above Schwarz inequality of Eq. (3.66) tells us that, *after the detection of a photon at a given time instant, the probability of detecting a second photon from the field is higher the closer the second detection is to the first, whenever the field is composed of a statistical mixture of coherent fields*. That is why, in the quantum picture, the photon bunching effect is upgraded from a bunching of detection events, which do not concern any modification of the field, to a *bunching of the particles of the field*, translated in their joint subtraction probability. This

[8] This does not mean that there are no fluctuations in the clicks when performing photodetections on coherent states. Despite the photodetection probabilities being proportional to intensity averages and intensity correlations, photodetection fluctuations will have a different dependence. Classically, this difference appears as the shot noise, an effect of temporally random counts arising from the quantum nature of the detector [82]. When the field is also quantum, the difference will have to do with the relation between the photon number operator and normally-ordered intensity correlations. Intensity fluctuations $\langle(\Delta I)^2\rangle$ are proportional to $\langle: I^2 :\rangle = \langle(a^\dagger)^2(a)^2\rangle$, while photon number fluctuations $\langle(\Delta N)^2\rangle$, which are those that appear in photodetections, are proportional to $\langle N^2\rangle = \langle(a^\dagger a)^2\rangle$. The operators a and $a^\dagger$ do not commute, and this causes a difference between the two fluctuations, namely $\langle(\Delta N)^2\rangle = \langle N\rangle + \langle(\Delta I)^2\rangle$, which corresponds to the shot noise calculated with the classical field [82].

allows a promotion of the interpretation of the field fluctuations from the statistics of field intensity to its photon number statistics. For this reason, the photon bunching effect is often associated to the bosonic character of the electromagnetic field, with the idea that bosons "like to bunch together". Oppositely, fermionic particles are forbidden to be in the same quantum state, and therefore cannot be detected together at the same position and time instant if they have the same internal state.

3.3.3 Photon anti-bunching

Interestingly enough, quantum theory opens new possibilities for the statistics of electromagnetic fields. In particular, there are quantum states of these fields which cannot be written as a statistical mixture of coherent states, and this may lead to an odd behavior of the field fluctuations.

Let us take a look, for instance, to the case that the field is composed by a single photon in a well defined mode and polarization, i.e. in the Fock basis we can write $\rho = |1\rangle\langle 1|$. For this field, obviously, the photon-subtracted state $\tilde{\rho}$ is the vacuum, because we are subtracting the only available field excitation, and therefore following Eq. (3.63)

$$\langle : I(\mathbf{r},t)I(\mathbf{r}',t') : \rangle_{|1\rangle} = \langle : I(\mathbf{r}',t') : \rangle_{|\mathrm{vac}\rangle} \times \langle : I(\mathbf{r},t) : \rangle_{|1\rangle} = 0. \tag{3.67}$$

This is intuitive because, since the two-intensity correlation is proportional to the probability of subtracting two photons from the field, a field with only one photon has a null probability of having two photons subtracted from it. However, the probability of detecting a single photon from the field is non-zero, and therefore we get

$$\langle : I^2(\mathbf{r},t) : \rangle_{|1\rangle} < \langle : I(\mathbf{r},t) : \rangle^2_{|1\rangle}. \tag{3.68}$$

The above equation means that this field presents *negative intensity fluctuations*, $\langle(\Delta I)^2\rangle_{|1\rangle} < 0$, which is an entirely quantum feature. More generally, one can define *non-classical fields* as those that violate the intensity Schwarz inequality of Eq. (3.66), which immediately leads to the negative fluctuations. The term "sub-Poissonian statistics" is also applied to these states, alluding to the idea that their photon number variance, which is related to the intensity variance, is less than the photon number average [92]. More specifically, the photon number variance is composed by a shot noise term, given by the photon number average, plus the intensity variance [82], i.e. $\langle(\Delta N)^2\rangle = \langle N\rangle + \langle(\Delta I)^2\rangle$ (see footnote 8 on page 51). Since a Poissonian distribution has the variance equal to the mean, and this is the case for coherent states which have $\langle(\Delta I)^2\rangle = 0$, whenever $\langle(\Delta I)^2\rangle < 0$ the state will have a sub-Poissonian photon number distribution.

In opposition to the Schwarz inequality of Eq. (3.66), when we write

$$\langle : I(t)I(t+\tau) : \rangle_{\rho_{nc}} > \langle I^2(t)\rangle_{\rho_{nc}} \tag{3.69}$$

it becomes clear that, for a non-classical state ρ_{nc} which violates the inequality, after the detection of one photon at a given time instant the probability of detection of a second photon is larger as time passes. That is why this effect is termed *photon anti-bunching*, alluding to the idea that it is more probable to detect photons separated than together, for these states. It is important to stress that *only genuinely quantum states, i.e. those that have negative intensity fluctuations and therefore cannot be written as a mixture of coherent states, will be able to show anti-bunching.*

In comparison to our discussion in the last paragraph of Sec. 3.3.1, when we discussed the role of the sources statistics in the visibility of the interference pattern, we note that now, with negative fluctuations, these terms will be responsible for a higher visibility of the interference pattern! The offset terms $\langle I_{U1} I_{V1} \rangle$ and $\langle I_{U2} I_{V2} \rangle$ in Eq. (3.3) being less than the minimum allowed by classical sources, $\langle I_{U1} \rangle \langle I_{V1} \rangle$ and $\langle I_{U2} \rangle \langle I_{V2} \rangle$, means that the oscillation caused by the phase terms will be able to achieve lower values with the use of sources that exhibit sub-Poissonian statistics [93]. This will be explicit when we discuss the specific interference pattern generated by the two-intensity correlation measurements with the use of electron sources in Sec. 3.4.4. We note that the influence of source statistics in interference pattern visibilities can be generalized to higher-order intensity correlation measurements [74–76, 94].

3.3.4 The Hong–Ou–Mandel effect: a different perspective on particle bunching

Let us consider the following setup. Two independent sources emit identical single-particle fields that propagate toward different input ports of a 50:50 beam splitter, as depicted in Fig. 15, and we are interested in the field at the output ports. The initial state

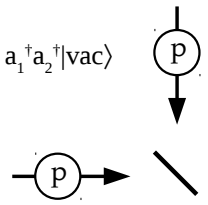

Figure 15 – Two identical particles p enter a 50:50 beam splitter through different input ports.

is therefore

$$|1\rangle_1 |1\rangle_2 = a_1^\dagger a_2^\dagger |\text{vac}\rangle, \tag{3.70}$$

where $a_j^\dagger$ is the creation operator of a particle in the input port j of the beam splitter, and $|\text{vac}\rangle$ is the vacuum state. The beam splitter either transmits or reflects the particles with equal probability, while the reflection gives the particle a $\pi/2$ phase, and therefore the

evolution of the operators is given by

$$a_j^\dagger \to (b_j^\dagger + ib_k^\dagger)/\sqrt{2}, \tag{3.71}$$

with $b_j^\dagger$ the creation operator of a particle in the output port j of the beam splitter, and $k \neq j$.

The evolution of the two-particle creation operator is therefore given by

$$\begin{aligned} a_1^\dagger a_2^\dagger &\to (b_1^\dagger + ib_2^\dagger)(b_2^\dagger + ib_1^\dagger)/2 \\ &= [b_1^\dagger b_2^\dagger - b_2^\dagger b_1^\dagger + i(b_1^\dagger)^2 + i(b_2^\dagger)^2]/2. \end{aligned} \tag{3.72}$$

There are four possible situations: one in which both are transmitted, one in which both are reflected, and two possibilities in which one particle is reflected and the other transmitted, as depicted in Fig. 16.

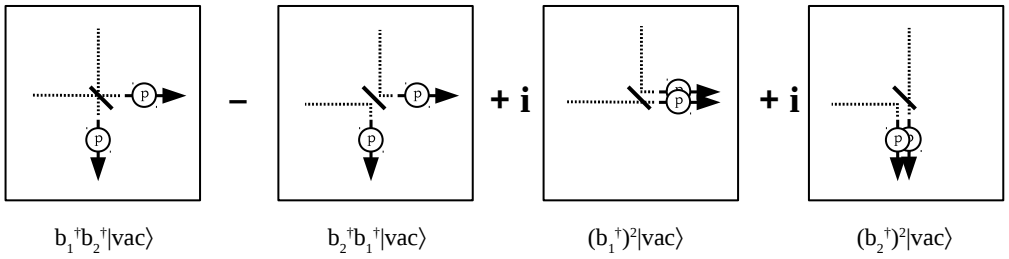

Figure 16 – The four possibilities of the two identical p particles to leave the beam splitter and its respective phases.

Due to the particles indistinguishability, the first two possibilities interfere with each other. In the case that the two particles are bosons, the creation operators between different modes commute, i.e. $b_1^\dagger b_2^\dagger = b_2^\dagger b_1^\dagger$, and this causes the first two terms in Eq. (3.72) to interfere destructively and cancel each other. That is, if the two identical particles are bosons they always come out of the beam splitter through the same output port. This is known as the Hong–Ou–Mandel effect, which was measured with photons in 1987 by the three authors that give the effect its name [72]. It has become known as a situation in which the *bunching* behavior of bosons shows up, as it is precisely the commutation relation for bosonic operators that causes the destructive interference of the particles leaving at different ports, and favors the situation in which they leave together.

In a coincidence detection setup, the Hong–Ou–Mandel bunching causes coincidence detections to be absent between the two output ports of the beam splitter. These detection correlation measurements are related to the Hanbury Brown and Twiss interference effect, but in HBT the $\pi/2$ phase gained in the reflection is instead a phase given by the free propagation. It thus varies continuously with the relative position of the detectors, which provides the oscillations in the intensity correlation measurements. In this sense, the HBT

has within it a Hong–Ou–Mandel-type of interference, but in a more generalized way [95]. This will show clearly in Section 3.4.2, when we discuss the HBT interference in more detail, from a quantum point of view.

If the particles incident in the beam splitter were fermions, then its creation operators respect an anti-commutation rule $b_1^\dagger b_2^\dagger = -b_2^\dagger b_1^\dagger$ [90], and the first two terms in Eq. (3.72) would instead interfere constructively. The last two terms are the ones that would be zero, since the square of fermionic creation operators is zero by the anti-commutation rule [90]. In this case, then, the two particles always come out of the beam splitter through different ports, and this situation is identified with an *anti-bunching* behavior. This is in agreement with the Pauli exclusion principle, that forbids two identical fermions of existing in the same quantum state. In a coincidence detection scenario, this means 100% chance of coincidence detection, in contrast to the null bosonic chance, and in the HBT continuous generalization, it will be revealed that the fermionic intensity correlation interference fringes are complementary to the bosonic ones.

We must stress that the (anti-)bunching discussed here is a substantially different effect from that discussed in the previous sections. What mattered there was the sign of the amplitude fluctuations of one mode of the photon field, where the anti-bunching reveals non-classical features of the field. In the Hong–Ou–Mandel effect with the incident field composed of single particles, this field is non-classical and therefore sub-Poissonian, displaying anti-bunching of temporal detections[9]. The (anti-)bunching behavior discussed in this section, on the other hand, is probing some kind of exchange symmetry between the particles in different modes of the field, and is related to what happens when two bosonic or fermionic particles interfere with each other. It is nonetheless important to note that the fermionic anti-commutation rule restricts the particle number statistics of fermionic fields, and therefore a single-mode bunching behavior of temporal detections due to field amplitude fluctuations, analogous to the photon bunching effect, can never be obtained.

3.4 Fermionic Hanbury Brown and Twiss interference

We proceed to the main goal of this chapter, that is to describe an experimental proposal in which the Hanbury Brown and Twiss interference effect can be reliably measured for a fermionic field in free space.

[9] A generalized version of the Hong–Ou–Mandel effect with classical fields also shows a decrease in coincident detections of the two output ports of the beam splitter, when compared to independent detections. There is however a limit to how low this decrease can be for classical input fields, and the signature of non-classicality lies in a larger suppression of coincidences than is allowed classically [93,96].

3.4.1 Definition of the experimental setup and correlation functions

Let us consider the setup depicted in Fig. 17, analogously to the classical HBT effect of Fig. 14 in Sec. 3.1.2. Two independent pulsed electron sources are placed at positions $\mathbf{R}_l$ $(l = 1, 2)$ in relation to an origin $\mathbf{O}$. Each source emits an electron field in a quantum state ρ_l. The sources are of equal intensity and possess equal spatial mode profiles. In the far field of the sources, electrons are jointly detected at positions $\mathbf{r}_j$ $(j = 1, 2)$ and at the same time instant, e.g. by use of a pixelated camera where each pixel acts as an individual detector. The sources are assumed to emit nearly-monochromatic fields at wavelength λ.

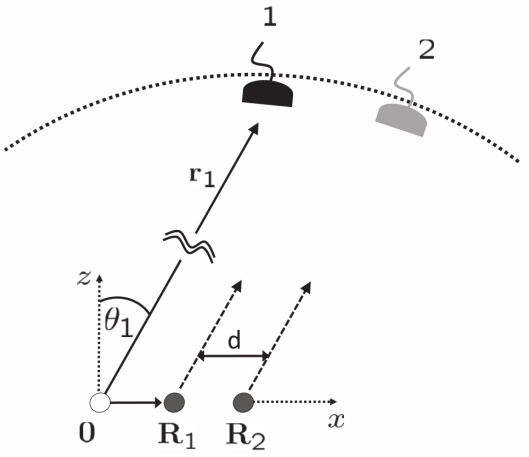

Figure 17 – Two independent electron sources at positions $\mathbf{R}_1$ and $\mathbf{R}_2$ in relation to an origin $\mathbf{O}$ each emit electrons to be detected in the far field of the sources by detectors at positions $\mathbf{r}_1$ and $\mathbf{r}_2$.

This assumption is based on the fact that a pulsed tungsten nanotip can emit electron wave packets with an energy uncertainty of around 1% [66].

Under all these conditions, the vector field operator for electrons at position $\mathbf{r}$ in the non-relativistic regime (in which spin is decoupled from spatial degrees of freedom) may be written in a form analogous to the the electromagnetic field operator of Eq. (3.56), with an explicit spatial[10] function [95, 97, 98] as

$$\mathbf{\Psi}(\mathbf{r}) = \sum_{s=1}^{2}\sum_{l=1}^{2} \exp\left[i\left(\frac{2\pi}{\lambda}\right)\frac{\mathbf{r}\cdot\mathbf{R}_l}{||\mathbf{r}||}\right] a_{l,s,\mathbf{n}}\ \boldsymbol{\epsilon}_s, \tag{3.73}$$

where $a_{l,s,\mathbf{n}}$ is the annihilation operator of a particle of source l, with spin s, propagating in a plane wave mode with direction $\mathbf{n} = \mathbf{r}/||\mathbf{r}||$ and wavelength λ. These operators respect the fermionic anti-commutation relations $\{a_{l,s,\mathbf{n}}, a_{l',s',\mathbf{n}'}\} = 0$ and $\{a_{l,s,\mathbf{n}}, a^{\dagger}_{l',s',\mathbf{n}'}\} = \delta_{l,l'}\delta_{s,s'}\delta(\mathbf{n}-\mathbf{n}')$, where $\delta_{i,j}$ is the Kronecker delta and $\delta(\mathbf{n}-\mathbf{n}')$ is the so-called Dirac delta function. The vectors $\boldsymbol{\epsilon}_s$ are again unitary vectors such that $\boldsymbol{\epsilon}_s \cdot \boldsymbol{\epsilon}^*_{s'} = \delta_{s,s'}$, completely analogous to the photon polarization vector.

[10] Since we are dealing with simultaneous detections, the field operator does not depend explicitly on time.

We define $\Psi_s(\mathbf{r}) \equiv \sum_{l=1}^{2} \exp\left[i\left(\frac{2\pi}{\lambda}\right)\frac{\mathbf{r}\cdot\mathbf{R}_l}{||\mathbf{r}||}\right] a_{l,s,\mathbf{n}}$, such that $\mathbf{\Psi}(\mathbf{r}) = \sum_{s=1}^{2} \Psi_s(\mathbf{r})\boldsymbol{\epsilon}_s$, and the two-electron correlation function analogous to the photonic version of Eq. (3.61) is given by

$$\begin{aligned} G^{(2)}(\mathbf{r}_1,\mathbf{r}_2) &\equiv \left\langle : \left[\mathbf{\Psi}^\dagger(\mathbf{r}_1)\cdot\mathbf{\Psi}(\mathbf{r}_1)\right] \left[\mathbf{\Psi}^\dagger(\mathbf{r}_2)\cdot\mathbf{\Psi}(\mathbf{r}_2)\right] : \right\rangle \\ &= \sum_{s=1}^{2}\sum_{s'=1}^{2} \left\langle \Psi_s^\dagger(\mathbf{r}_1)\Psi_{s'}^\dagger(\mathbf{r}_2)\Psi_{s'}(\mathbf{r}_2)\Psi_s(\mathbf{r}_1)\right\rangle, \end{aligned} \tag{3.74}$$

where the colons indicate normal ordering of the creation and annihilation operators, and the brackets indicate the expectation value to be calculated according to the sources product state $\rho_1 \otimes \rho_2$. We define

$$G^{(2)}_{s,s'}(\mathbf{r}_1,\mathbf{r}_2) \equiv \left\langle \Psi_s^\dagger(\mathbf{r}_1)\Psi_{s'}^\dagger(\mathbf{r}_2)\Psi_{s'}(\mathbf{r}_2)\Psi_s(\mathbf{r}_1)\right\rangle, \tag{3.75}$$

such that $G^{(2)}(\mathbf{r}_1,\mathbf{r}_2) = \sum_{s=1}^{2}\sum_{s'=1}^{2} G^{(2)}_{s,s'}(\mathbf{r}_1,\mathbf{r}_2)$ is the sum over the contributions with equal and different spin polarizations.

3.4.2 Quantum description of the Hanbury Brown and Twiss interference

When we insert the field expression of Eq. (3.73) into the correlation function of Eq. (3.75) and assume statistically independent sources[11], we get

$$\begin{aligned} &\langle \Psi_s^\dagger(\mathbf{r}_1)\Psi_{s'}^\dagger(\mathbf{r}_2)\Psi_{s'}(\mathbf{r}_2)\Psi_s(\mathbf{r}_1)\rangle = \\ &\quad \langle a^\dagger_{1,s,\mathbf{n}_1} a^\dagger_{1,s',\mathbf{n}_2} a_{1,s',\mathbf{n}_2} a_{1,s,\mathbf{n}_1}\rangle + \langle a^\dagger_{2,s,\mathbf{n}_1} a^\dagger_{2,s',\mathbf{n}_2} a_{2,s',\mathbf{n}_2} a_{2,s,\mathbf{n}_1}\rangle \\ &\quad + \langle a^\dagger_{1,s,\mathbf{n}_1} a^\dagger_{2,s',\mathbf{n}_2} a_{2,s',\mathbf{n}_2} a_{1,s,\mathbf{n}_1}\rangle + \langle a^\dagger_{2,s,\mathbf{n}_1} a^\dagger_{1,s',\mathbf{n}_2} a_{1,s',\mathbf{n}_2} a_{2,s,\mathbf{n}_1}\rangle \\ &\quad + e^{-if(\theta_2)}\langle a^\dagger_{2,s,\mathbf{n}_1} a^\dagger_{1,s',\mathbf{n}_2} a_{2,s',\mathbf{n}_2} a_{1,s,\mathbf{n}_1}\rangle + e^{if(\theta_2)}\langle a^\dagger_{1,s,\mathbf{n}_1} a^\dagger_{2,s',\mathbf{n}_2} a_{1,s',\mathbf{n}_2} a_{2,s,\mathbf{n}_1}\rangle, \end{aligned} \tag{3.76}$$

where the expectation values are calculated with respect to a two-source state ρ, and we recapitulate that $a_{l,s,\mathbf{n}_j}$ is the annihilation operator correspondent to a particle from source l, with spin s, that propagates on a plane wave mode towards direction $\mathbf{n}_j = \frac{\mathbf{r}_j}{||\mathbf{r}_j||}$ and thus is absorbed by detector j in Fig. 17. We use the definition $f(\theta_2) \equiv \left(\frac{2\pi}{\lambda}\right) d\sin\theta_2$, with $\frac{\mathbf{r}_j\cdot\mathbf{R}_l}{||\mathbf{r}_j||} = ld\sin\theta_j$ according to Fig. 17, and we assume $\theta_1 = 0$ without loss of generality.

We reproduce below the expression for the two-intensity correlation of Eq. (3.3), so that we can make an easier comparison:

$$\begin{aligned} \langle I_P I_Q\rangle &= \langle I_{U1} I_{V1}\rangle + \langle I_{U2} I_{V2}\rangle + \langle I_{U1}\rangle\langle I_{V2}\rangle + \langle I_{U2}\rangle\langle I_{V1}\rangle \\ &\quad + \langle U_1^*\cdot U_2 \times V_1\cdot V_2^*\rangle + \langle U_1\cdot U_2^*\times V_1^*\cdot V_2\rangle. \end{aligned} \tag{3.3}$$

[11] We refer back to the discussion in Sec. 3.1 justifying why field amplitude averages have to be zero when assuming statistical independence between the two sources. By extending the argument to field operator averages, it follows that the only terms which will survive are those that contain either single-source intensity correlations, intensity averages, or single-source field correlations that carry phase differences.

The first two terms in Eq. (3.76) follow the discussions in Sec. 3.3, being analogous to the first two terms of the two-intensity correlation expression in Eq. (3.3), namely $\langle I_{U1} I_{V1} \rangle$ and $\langle I_{U2} I_{V2} \rangle$. These terms are thus respectively related to the individual statistics of sources 1 and 2, since each term contains two particle subtractions from the same source. Whenever the respective source emits less than two particles the term yields zero, since there is a zero probability of extracting two particles from a field that has less than two of them. The term can also be larger or smaller than the product of two independent subtractions in the same state. This effect, based on the source statistics, is the particle bunching effect when the two-detection probability is larger than the product of two independent detections, and the anti-bunching when it is smaller [69, 71, 82] (see Sec. 3.3). In our setting these two-particle terms do not show any oscillating pattern in the far field, and will merely be responsible for an offset in the correlation function $G^{(2)}_{s,s'}(\mathbf{r}_1, \mathbf{r}_2)$ when two or more particles from the same source are available.

The remaining four summands in Eq. (3.76) represent the two-particle interference terms between the different electron sources, i.e. when one particle is subtracted from each source. Terms 3 and 4 can be written as $\langle a^\dagger_{i,s,\mathbf{n}_1} a_{i,s,\mathbf{n}_1} \rangle \langle a^\dagger_{j,s',\mathbf{n}_2} a_{j,s',\mathbf{n}_2} \rangle$ and are analogous to the intensity product terms $\langle I_{Ui} \rangle \langle I_{Vj} \rangle$ in Eq. (3.3). Terms 5 and 6 can be written as $e^{\mp i f(\theta_2)} \langle a^\dagger_{i,s,\mathbf{n}_1} a_{j,s,\mathbf{n}_1} a^\dagger_{j,s',\mathbf{n}_2} a_{i,s',\mathbf{n}_2} \rangle$ and are analogous to the terms that carry phase information, $\langle U_i^* \cdot U_j \times V_i \cdot V_j^* \rangle$. Because of the propagation phase difference $f(\theta_2)$, these added terms will be responsible for an oscillation pattern in the joint detection. Note that, if the particles were bosons, the operators of different sources commute resulting in an interference pattern of the kind $|1 + e^{i f(\theta_2)}|^2$, while the fermionic operators anti-commute, leading to the complementary pattern $|1 - e^{i f(\theta_2)}|^2$ (see Sec. 3.3.4).

Following the discussion in Sec. 3.3.4, these last terms in Eq. (3.76) are also the ones responsible for the Hong–Ou–Mandel effect [72, 95], where the interference is due to a fundamental indistinguishability of the two particles, and a fixed phase shift of $f(\theta_2) = \pi$ acquired through a reflection at the beam splitter. The particles being indistinguishable means that an event in which particle 1 is absorbed by detector 1 and particle 2 by detector 2 cannot be distinguished from an event in which particle 1 is absorbed by detector 2 and particle 2 by detector 1. The different phases accumulated by these two events must then be added coherently in the intensity correlation, which leads to the observed interference pattern. The terms have the signature of the type of particles involved, since for bosons the particles will have a higher chance of being detected at the same point in space and time, and zero chance when the phase difference between the two-particle quantum paths is π. Fermions exhibit the opposite behavior since an extra π phase is introduced due to the anti-commutation relation, which is a face of the Pauli exclusion principle.

In the first two terms of Eq. (3.76) that involve detecting two particles from the same source, it is the particle number statistics that is generated by the sources that

matters, while for the last four terms, for the same sources statistics, it is the propagation of the two particles towards two distinct positions in the far field that develops the particle distribution into bunching or anti-bunching. We note that, as an extension to the Hong–Ou–Mandel effect [95], the free space setup provides an extra degree of freedom: the detector position θ_2. Varying θ_2 presents an increase or a decrease in the joint detection probability when compared to products of individual detections, due to the different phases acquired during propagation.

The dependence of the last four terms of Eq. (3.76) on the type of particle motivates us to separate this contribution from the first two terms. We will say that, from the point of view of our setup, the first two terms are the ones that survey the sources statistics, in the style of the temporal photon bunching effect (see Secs. 3.3.1 to 3.3.3), while the last four terms are related to a Hong–Ou–Mandel type of interference (see Sec. 3.3.4). In this sense, the Hanbury Brown and Twiss effect can be seen as a sum of a free space Hong–Ou–Mandel effect and a source statistics offset term.

3.4.3 The quantum state of the electron sources

We now make the assumption that the electron field state is generated at both sources simultaneously by a pulsed laser, and that the inability to control the relative phases between pulses will destroy any coherence between different electron number states [67]. We consider that the probability of each single source emitting three electrons is negligible, and therefore the state emitted by each source is

$$\rho_l = p_0|0_l\rangle\langle 0_l| + p_1 \sum_{s=1}^{2} |1_{\mathrm{el},l,s}\rangle\langle 1_{\mathrm{el},l,s}| + p_2 \sum_{s=1}^{2}\sum_{s'=1}^{2} |2_{\mathrm{el},l,s,s'}\rangle\langle 2_{\mathrm{el},l,s,s'}|, \tag{3.77}$$

where the ket $|0_l\rangle$ represents no particles being created at source l and $|1_{\mathrm{el},l,s}\rangle$ corresponds to one particle from source l in an arbitrary nearly-monochromatic mode

$$|1_{\mathrm{el},l,s}\rangle = \int d\boldsymbol{\kappa}\; C(\boldsymbol{\kappa})\; a^\dagger_{l,s,\boldsymbol{\kappa}}|0_l\rangle, \tag{3.78}$$

and $|2_{\mathrm{el},l,s,s'}\rangle$ is a two-electron state in which the two particles are created at the same source l in two possibly different spatial modes,

$$|2_{\mathrm{el},l,s,s'}\rangle = \int d\boldsymbol{\kappa}_1 \int d\boldsymbol{\kappa}_2\; C_A(\boldsymbol{\kappa}_1)C_B(\boldsymbol{\kappa}_2)\; a^\dagger_{l,s,\boldsymbol{\kappa}_1} a^\dagger_{l,s',\boldsymbol{\kappa}_2}|0_l\rangle. \tag{3.79}$$

The factors $C(\boldsymbol{\kappa})$, $C_A(\boldsymbol{\kappa})$ and $C_B(\boldsymbol{\kappa})$ are the emission modes in transverse momentum space, and they are complex functions of the unitary direction of propagation $\boldsymbol{\kappa}$, which will be responsible for the envelope in the far-field detection pattern. Note that in Eq. (3.77) we have made the assumption that different spin states are generated with equal probability.

The joint state of the two sources will contain terms in which no electron is emitted, one electron is emitted by one source and zero from the other, one electron is emitted by

each source, and so on, as seen below:

$$\begin{aligned}\rho_1 \otimes \rho_2 = p_0^2\ &|0_1\rangle\langle 0_1| \otimes |0_2\rangle\langle 0_2| \\ &+ p_0 p_1 \sum_{s=1}^{2} \Big(|1_{\mathrm{el},1,s}\rangle\langle 1_{\mathrm{el},1,s}| \otimes |0_2\rangle\langle 0_2| + |0_1\rangle\langle 0_1| \otimes |1_{\mathrm{el},2,s}\rangle\langle 1_{\mathrm{el},2,s}| \Big) \\ &+ p_1^2 \sum_{s=1}^{2}\sum_{s'=1}^{2} |1_{\mathrm{el},1,s}\rangle\langle 1_{\mathrm{el},1,s}| \otimes |1_{\mathrm{el},2,s'}\rangle\langle 1_{\mathrm{el},2,s'}| \\ &+ p_0 p_2 \sum_{s=1}^{2}\sum_{s'=1}^{2} \Big(|2_{\mathrm{el},1,s,s'}\rangle\langle 2_{\mathrm{el},1,s,s'}| \otimes |0_2\rangle\langle 0_2| + |0_1\rangle\langle 0_1| \otimes |2_{\mathrm{el},2,s,s'}\rangle\langle 2_{\mathrm{el},2,s,s'}| \Big) + \dots \end{aligned} \tag{3.80}$$

The terms which contain less than two particles in total will not contribute to $G^{(2)}_{s,s'}(\mathbf{r}_1, \mathbf{r}_2)$, because there must be at least two particles available for a joint detection event. Therefore, we can write for this state

$$\begin{aligned} G^{(2)}_{s,s'}(\mathbf{r}_1, \mathbf{r}_2) = p_1^2 &\sum_{w=1}^{2}\sum_{w'=1}^{2} \langle 1_{\mathrm{el},1,w}, 1_{\mathrm{el},2,w'}| \Psi_s^\dagger(\mathbf{r}_1)\Psi_{s'}^\dagger(\mathbf{r}_2)\Psi_{s'}(\mathbf{r}_2)\Psi_s(\mathbf{r}_1) |1_{\mathrm{el},1,w}, 1_{\mathrm{el},2,w'}\rangle \\ &+ p_0 p_2 \sum_{w=1}^{2}\sum_{w'=1}^{2} \langle 2_{\mathrm{el},1,w,w'}, 0_2| \Psi_s^\dagger(\mathbf{r}_1)\Psi_{s'}^\dagger(\mathbf{r}_2)\Psi_{s'}(\mathbf{r}_2)\Psi_s(\mathbf{r}_1) |2_{\mathrm{el},1,w,w'}, 0_2\rangle \\ &+ p_0 p_2 \sum_{w=1}^{2}\sum_{w'=1}^{2} \langle 0_1, 2_{\mathrm{el},2,w,w'}| \Psi_s^\dagger(\mathbf{r}_1)\Psi_{s'}^\dagger(\mathbf{r}_2)\Psi_{s'}(\mathbf{r}_2)\Psi_s(\mathbf{r}_1) |0_1, 2_{\mathrm{el},2,w,w'}\rangle, \end{aligned} \tag{3.81}$$

where we have considered that $p_0 \gg p_1 \gg p_2$, and the terms of order $p_1 p_2$ and p_2^2 were neglected. The last two double sums, which contain two electrons from each source, will be equal because we admit that the two sources emit the modes identically, as seen from Eq. (3.79). Therefore, the expression above can be simplified to

$$G^{(2)}_{s,s'}(\mathbf{r}_1, \mathbf{r}_2) = \sum_{w=1}^{2}\sum_{w'=1}^{2} \Big[p_1^2\ G^{(2)}_{s,s'}(\mathbf{r}_1, \mathbf{r}_2)|_{|1_{\mathrm{el},1,w}, 1_{\mathrm{el},2,w'}\rangle} + 2 p_0 p_2 G^{(2)}_{s,s'}(\mathbf{r}_1, \mathbf{r}_2)|_{|2_{\mathrm{el},1,w,w'}, 0_2\rangle} \Big], \tag{3.82}$$

where $G^{(2)}_{s,s'}(\mathbf{r}_1, \mathbf{r}_2)|_{|\psi\rangle}$ is the correlation function defined in Eq. (3.75) calculated with the two-particle pure state $\rho = |\psi\rangle\langle\psi|$.

Note that, if the sources particle number distribution is of the kind $p_n \sim c^n$ (e.g. thermal or weak Poissonian distribution), then $p_0 p_2 \sim p_1^2$, and we cannot neglect the contribution of two electrons coming from the same source, which already indicates the role of source statistics in the two-detection interference pattern commented in previous sections.

3.4.4 The specific form of the HBT two-detection correlation measurement

We now proceed to incorporate the spatial setting into the the correlation function of Eq. (3.82). For each (w, w') pair the expression contains two terms: a two-source one proportional to a two-intensity correlation function calculated with state $|1_{\mathrm{el},1,w}, 1_{\mathrm{el},2,w'}\rangle$,

and single-source one proportional to the same correlation function calculated with state $|2_{\mathrm{el},1,w,w'}, 0_2\rangle$. We thus calculate each of these correlation functions for the respective states, with the spatial features of our setup (see Fig. 17) given by Eq. (3.76).

Because the state $|1_{\mathrm{el},1,w}, 1_{\mathrm{el},2,w'}\rangle$ has at most one electron coming from each source, the first two terms in Eq. (3.76), which contain two subtractions from a single source, will be zero for this state. We get, by using the one-particle state from Eq. (3.78),

$$G^{(2)}_{s,s'}(\mathbf{r}_1,\mathbf{r}_2)|_{|1_{\mathrm{el},1,w},1_{\mathrm{el},2,w'}\rangle} = |C(\mathbf{n}_1)|^2|C(\mathbf{n}_2)|^2\Big\{\delta_{w,s}\delta_{w',s'} + \delta_{w,s'}\delta_{w',s} - 2\delta_{w,s}\delta_{w,s'}\delta_{w',s}\delta_{w',s'}\cos[f(\theta_2)]\Big\}. \tag{3.83}$$

The last term between the curly brackets in the above equation, which corresponds to the last two terms of Eq. (3.76), will be non-zero only if $s = s' = w = w'$. This fulfills the expectation that no oscillation can appear if the detected particles have orthogonal spins (i.e. are distinguishable), since the term appears due to the interference effect caused by the indistinguishability of the particles in their propagation. Following the discussion of Sec. 3.4.2, the terms in the state $\rho_1 \otimes \rho_2$ (see Eq. (3.80)) that have one particle coming from each source, both of them with the same spin, contribute to the Hong–Ou–Mandel type of interference in $G^{(2)}(\mathbf{r}_1,\mathbf{r}_2)$. Terms with different spins contribute with a constant factor.

If we calculate Eq. (3.76) for the state $|2_{\mathrm{el},1,w,w'}, 0_2\rangle$ in which both electrons originate at the same source, the four last terms will be zero. This is because in this state one of the sources emits no particles, and the four last terms in Eq. (3.76) are proportional to the product of the number of particles in each of the two sources. Therefore, only the first two terms in Eq. (3.76) will be non-zero, oppositely to the behavior of the state $|1_{\mathrm{el},1,w}, 1_{\mathrm{el},2,w'}\rangle$. We obtain, by using the two-particle state from Eq. (3.79),

$$G^{(2)}_{s,s'}(\mathbf{r}_1,\mathbf{r}_2)|_{|2_{\mathrm{el},1,w,w'},0_2\rangle} = \delta_{w,s}\delta_{w',s'}|C_A(\mathbf{n}_1)|^2|C_B(\mathbf{n}_2)|^2 + \delta_{w,s'}\delta_{w',s}|C_A(\mathbf{n}_2)|^2|C_B(\mathbf{n}_1)|^2 - 2\delta_{w,s}\delta_{w,s'}\delta_{w',s}\delta_{w',s'}\mathrm{Re}\Big[C_A(\mathbf{n}_1)C^*_A(\mathbf{n}_2)C_B(\mathbf{n}_2)C^*_B(\mathbf{n}_1)\Big]. \tag{3.84}$$

The last term in the above equation will only be non-zero if $s = s' = w = w'$. This can be understood by realizing that equal spins force the anti-symmetrization of the emitted two-particle mode, while different spins do not. One could stretch the argument and see this term as an "interference" effect coming from the anti-symmetrization of the identical particles. In this sense, the detected pattern will show this "interference" only for the cases where the spins are equal, and this will put a constraint in the possible source statistics. We note that, under the light of our differentiation between the statistics and the Hong–Ou–Mandel terms (see Sec. 3.4.2), the terms in the state $\rho_1 \otimes \rho_2$ (see Eq. (3.80)) that have two particles coming from the same source are surveying their respective statistics. Under this view we will say that the anti-symmetrization is an statistical effect taking place at the source, while the Hong–Ou–Mandel is a genuine interference effect arising due to the propagation.

It is now left to check the specific shape of this interference with the state $|2_{\mathrm{el},1,w,w'}, 0_2\rangle$. We consider that all the modes emitted are the same, whether the sources emit one or two electrons each. This means that we can use $C_A(\boldsymbol{\kappa}) = C_B(\boldsymbol{\kappa}) = C(\boldsymbol{\kappa})$ in Eqs. (3.78) and (3.79). Looking at Eq. (3.84) shows us that this consideration leads to total destructive interference in the case that $s = s'$. This is a consequence of the absolutely expected fact that each source cannot emit two identical electrons, i.e. two monochromatic electrons with the same wavelength, in the same spatial mode, and with the same spin. This is an example of the anti-symmetrization restriction on the sources statistics, which forces them to be close to single-particle sources. We note that Lougovski *et al.* [67] have modeled the two modes of the two-electron process as two equally shaped momentum distributions which are displaced from each other in the propagation direction, therefore not resulting in total destructive interference. Note though, that the 1% energy uncertainty reported for tungsten nanotips [66] allows for the nearly-monochromatic sources approximation, and the non-zero frequency width only adds a small number of detection counts which can be neglected.

Thus, for $C_A(\boldsymbol{\kappa}) = C_B(\boldsymbol{\kappa}) = C(\boldsymbol{\kappa})$, and summing the contributions of one- and two-electron emissions per tip from Eqs. (3.83) and (3.84), we obtain for Eq. (3.82)

$$G^{(2)}_{s,s'}(\mathbf{r}_1, \mathbf{r}_2) = |C(\mathbf{n}_1)|^2 |C(\mathbf{n}_2)|^2 \sum_{w=1}^{2} \sum_{w'=1}^{2} \Big\{ \Big(\delta_{w,s}\delta_{w',s'} + \delta_{w,s'}\delta_{w',s} \Big) \Big[p_1^2 + 2p_0 p_2 \Big] - 2\delta_{w,s}\delta_{w,s'}\delta_{w',s}\delta_{w',s'} \Big[p_1^2 \cos[f(\theta_2)] + 2p_0 p_2 \Big] \Big\}. \tag{3.85}$$

When $s = s'$, all the Kronecker delta factors will be 1 for $w = w' = s = s'$ and zero otherwise, such that only one term in the sum survives,

$$G^{(2)}_{s=s'}(\mathbf{r}_1, \mathbf{r}_2) = 2|C(\mathbf{n}_1)|^2 |C(\mathbf{n}_2)|^2 \; p_1^2 \Big\{ 1 - \cos[f(\theta_2)] \Big\}, \tag{3.86}$$

where the Hong–Ou–Mandel type of interference can be seen from the presence of the cosine term, and the fermionic statistical effect is evident by the suppression of the term proportional to $p_0 p_2$ – i.e. the probability of emitting two electrons in the same quantum state is zero.

When $s \neq s'$, two terms in the sum will have non-zero elements, one for which $w = s$ and $w' = s'$, and the term with the inverse association $w' = s$ and $w = s'$. In each of these terms, just one Kronecker delta product survives, such that

$$G^{(2)}_{s\neq s'}(\mathbf{r}_1, \mathbf{r}_2) = 2|C(\mathbf{n}_1)|^2 |C(\mathbf{n}_2)|^2 \; \Big(p_1^2 + 2p_0 p_2 \Big). \tag{3.87}$$

If one can select the spins such that $s = s'$, the interference pattern exhibits 100% visibility, just like in the photonic case [93], but with complementary fringes due to the fermionic anti-commutation relation. Without spin selection, the resulting far-field second-order correlation function is a sum of the two expressions of Eqs. (3.86) and (3.87),

each multiplied by 2 to account for the spin combination possibilities ((s, s') equal to $(1, 1)$ and $(2, 2)$ for Eq. (3.86), and $(1, 2)$ and $(2, 1)$ for Eq. (3.87)). Therefore the worked out form of the correlation function of state $\rho_1 \otimes \rho_2$ from Eq. (3.80) reads

$$G^{(2)}(\mathbf{r}_1, \mathbf{r}_2) = 8|C(\mathbf{n}_1)|^2|C(\mathbf{n}_2)|^2 \ (p_1^2 + p_0 p_2) \left\{1 - \frac{p_1^2}{2(p_1^2 + p_0 p_2)} \cos[f(\theta_2)]\right\}, \qquad (3.88)$$

for which the visibility is given by $\mathcal{V} = 1/\left(2 + \frac{p_0 p_2}{p_1^2}\right)$. For ideal single-electron emitters ($p_2 = 0$) the visibility yields the maximum value of 50%, while for $p_2 > 0$ there is a reduced visibility. This means that the visibility of the detected pattern could be used to estimate the statistics of the laser-driven tungsten nanotip sources. Towards this goal the slight blur in the oscillation pattern caused by the 1% energy uncertainty should also be considered as a source of a reduced visibility.

3.4.5 Considerations on the experimental implementation

Another effect that needs to be taken into account is the Coulomb interaction, since the repulsion of two electrons can lead to a pattern that mimics the effect of the Pauli exclusion principle (PEP). The effect is especially crucial for a single nanotip setup where two particles are created in close vicinity, within the same source. In a two tip experiment the influence of Coulomb repulsion is strongly mitigated, due to much larger spatial separation of the particle creation locations.

As pointed out in the introduction, the experiment by Kiesel *et al.* [9] investigated far field correlations between electrons emitted by a continuously driven tungsten nanotip source. There were first hints for a reduced coincidence rate due to the PEP, yet the statistics and signature of the derived correlations did not allow for a clear discrimination of the effect from Coulomb repulsion [10, 11]. The two obstacles were the relatively small source degeneracy[12] of 10^{-4} and similarity between the expected signatures from the PEP and Coumlomb repulsion. In the theoretical considerations by Lougovski *et al.* [67], for a pulsed electron source the degeneracy during the pulse may exceed this value by far, reaching up to 10^{-1}. In this regime, they showed that the PEP should lead to a measurable weakly pronounced degeneracy at one detector, and to a clearly measurable interference dip in a spatial HBT setup with two detectors measuring coincident counts. More recently, Keramati *et al.* have discussed in detail that ultrashort pulsed electron sources (shorter pulses meaning higher degeneracies) are within the necessary reach for measuring the HBT interference with electrons along the pulse propagation direction [81]. This highlights the importance of using pulsed sources with a high degeneracy, as low degeneracy implies that too few detected particles are overlapping and causing two-particle

[12] The degeneracy is defined as the average number of particles in a phase-space-cell volume of the field [67]. This volume can be defined as the minimum position-momentum uncertainty volume in the phase space. The minimum uncertainty relation $\Delta\mathbf{x}\Delta\mathbf{k} = 1$ then leads to a phase-space-cell volume in position space of $\Delta V = 1/\Delta\mathbf{k}$.

interference detection events. Such electron sources are presently available [64–66] and provide enough spatial coherence [66] in the emitted wave packets so that our descriptions of the one- and two-electron states in Eqs. (3.78) and (3.79) are valid.

Even with the large degeneracy, the proposal of Lougovski *et al.* [67] relies on two electrons being generated at the same tip. Note that the detected pattern of Eq. (3.88) oscillates with the cossine of $f(\theta_2) = \left(\frac{2\pi}{\lambda}\right) d \sin\theta_2$, where θ_2 is related to the detector position (see Fig. 17). In the far field, where the angles are small, $\sin\theta_2 \approx \theta_2$ and thus the interference pattern along the "position" θ_2 has a spatial period of oscillation λ/d, which is inversely proportional to the distance d between the points where the electrons are generated. Electrons generated in the same tip are emitted with a very short distance d, and thus their oscillation pattern has a very large period (see Fig. 18 (a)). This pattern can be mimicked by the decrease in coincident counts caused by Coulomb repulsion. Our proposal solves this problem with the addition of a second nanotip as a second electron source. A large distance between the tips means a large distance d between the points where the electrons are generated. Thus one gets a shorter period of oscillation in the interference pattern, with lots of crests and valleys in the detection window (see Fig. 18 (b)). In this case, the detected pattern is qualitatively distinguishable from the Coulomb dip, as the latter can never give rise to oscillations. Also, Coulomb repulsion is much weaker in a setting with two tips, since the strongest repulsion happens close to the tips, where the electrons are closest [11].

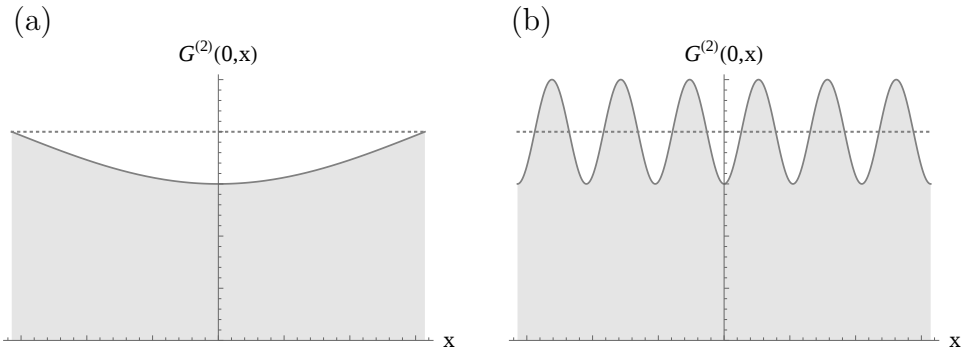

Figure 18 – A sketch of the generated coincidence interference pattern $G^{(2)}(0,x)$ (see Eq. (3.88)), conditioned on the detection of one electron at the origin and the other at point x. The dotted line corresponds to two independent detections. (a) The pattern generated when the electrons are emitted very closely to each other has a very large period, and can be mimicked by a Coulomb repulsion dip. (b) The oscillatory pattern generated when the electrons are emitted from distant independent tips is qualitatively different from the Coulomb repulsion dip.

The influence of Coulomb repulsion in the detected pattern can be estimated by calculating the distance that the centers of mass of the two electrons' wave packets will be separated, and then comparing it to the spread of the free wave packets propagating

from each source [67]. We assume that the electrons are created at an approximately equal time instant, by means of excitaton with an ultrashort laser pulse that hits both tips simultaneously. Their initial separation thus reads $s_i = \sqrt{\Delta x^2 + (v_i \Delta t)^2} \approx \Delta x = d$ [11], where v_i is their initial propagation velocity, and Δt the time difference in the creation of the particles. For our estimation, we use the experimental parameters of the nanotips from Ref. [66]. If the tips are considered to emit spatially limited wave packets separated by a distance $d = 1000$ nm, with wavelength $\lambda = 1.8$ Å, and if the screen is located $z_{\mathrm{det}} = 8$ cm away from the sources, the Coulomb separation is estimated to be $x_C = 0.31$ mm. For the wave packet width, Ehberger *et al.* [66] report a full coherence length of $\xi_\perp = 5.9$ mm, while the intensity distribution's full-width at half maximum is about 1.4 mm $\approx 4.5 x_C$. Meanwhile, the second-order interference pattern of Eq. (3.88) leads to a fringe spacing with spatial period $x_P = 14.4$ μm. In total, the wave packets should have significant superposition, in a way that oscillations in the second-order interference (due to the PEP and generalized Hong–Ou–Mandel interference) in the center of the detected pattern would be clearly distinguishable from the Coulomb dip. By contrast, for the single-tip setup Lougovski *et al.* [67] conclude that "Coulomb repulsion will, indeed, dominate quantum effects by roughly one order of magnitude".

3.5 Chapter remarks

In this chapter we proposed an experiment that, for the first time, would allow for a clear and unique identification of Hanbury Brown and Twiss anti-correlations in a two-electron interference experiment in free space, by use of two independent laser-driven tungsten nanotip electron sources. We provided arguments that show that in this scenario Coulomb repulsion effects play only a minor role. With this setup, the oscillation pattern with a dense fringe spacing in the two-point correlation function that arises due to the Pauli exclusion principle for indistinguishable electrons cannot be mistaken by a Coulomb repulsion dip. Our results might also lead to new techniques for electron imaging, where incoherent electrons sources themselves or incoherently scattered electrons in combination with correlation measurements would reveal the sought-after information. Further, the control of the higher-order interference effects will certainly open new additional horizons for electronic imaging techniques with incoherent sources.

An experimental implementation of this proposal is on the way, in collaboration with Prof. Peter Hommelhoff of the University of Erlangen-Nuremberg. Prof. Hommelhoff's group has the expertise to build and control the nanotips [64, 66], and new electron detectors bought by the group provide the necessary platform to perform the experiment. A preliminary theoretical paper with the results presented here has been written, but we are waiting in order to have a joint publication with the experimental implementation.

4 Photon reflection by a quantum mirror: a wave function approach

The advances in nanofabrication techniques have allowed extensive research on mechanical systems whose masses are small enough so that they can significantly exchange momentum with electromagnetic fields – these are called optomechanical systems. An important class of those systems are optomechanical cavities, in which the mechanical system is described by a harmonic oscillator that couples with the light [99]. In some cases the cavity is composed of mirrors, and since the mid 1990s there were proposals of studying quantum properties of such mirrors, for instance quantum fluctuations [100] and the construction of superposition states [101–105]. Also, recently there have been many theoretical discussions on entanglement between vibration modes of mirrors in a quantum regime and light [106–108]. The detection of entanglement between a mechanical system and light has been reported for mechanical systems other than mirrors [109, 110], and even a Bell inequality has been violated with this kind of system [111].

The quantum mechanical treatment for a cavity quantum mirror interacting with photons can be based on a Hamiltonian formulation [112], with a second quantization approach for light and for the motion degrees of freedom of the mirror. But here we take a different path, by using a photon wave function approach to treat the reflection of a single photon by a quantum mirror. Our treatment is constructed from first principles and can be used to describe a photon interacting with quantum mirrors in a cavity as well as a single photon reflection by a quantum mirror.

We first present the photon wave function formalism in Sec. 4.1, which will help us to construct the quantum solution of the problem based on its classically known version. Then in Sec. 4.2 we show that the mirror imposes boundary conditions for the photon wave function at its surface and this naturally leads to the photon radiation pressure on the mirror. We discuss the mirror-photon entanglement and its dependence on the relation between the photon average momentum and the mirror momentum uncertainty, and evaluate that this kind of entanglement cannot be significantly generated with current technology. In Sec. 4.3, we briefly present the historical Abraham-Minkowski debate, which concerns the momentum of light when it is propagating through a material medium [20, 21]. When the quantum mirror is immersed in a medium with refractive index n, we show that the radiation pressure that the light exerts on it is proportional to n, which agrees with experiments performed with classical mirrors [22, 23]. We analyze this effect based on the association of the Minkowski momentum (which is proportional to n) with the canonical momentum of light [113], thus contributing to the long-standing Abraham-Minkowski

debate.

The results presented in this chapter are published in Ref. [24].

4.1 A wave function for the photon

In order to address our problem of the reflection of a single photon by a quantum mirror, we will make use of the photon wave function formalism developed independently by Bialynicki-Birula [12] and Sipe [13] during the 1990s. It is notoriously difficult to provide a quantum description of the electromagnetic field operator in the presence of a material medium [16–19] due to dispersion and absorption of light, and also due to boundary conditions imposed by the interfaces of different media. The photon wave function, which is a function of position and time, will allow us to circumvent this problem when describing the interaction of the photon with a reflective surface. Despite the non-existence of position operators for photons[1] [114, 115], Bialynicki-Birula and Sipe were able to construct a wave function for the photon without the need for position eigenvectors, while maintaining its consistency as a function of positions in space. As we will see later, this will be mirrored in the fact that this wave function does not directly provide the probability of finding the photon in a certain position in space, but rather its energy density in that position.

The Bialynicki-Birula–Sipe photon wave function [12–15] is a complex vector function of space and time coordinates that completely describes the quantum state of a single photon field. It can be decomposed into the $\mathbf{\Psi}_\pm$ eigenstates of the helicity operator $\hat{\sigma}$ in the following way:

$$\mathbf{\Psi}(\mathbf{r},t) = \mathbf{\Psi}_+(\mathbf{r},t) + \mathbf{\Psi}_-(\mathbf{r},t), \tag{4.1}$$

where

$$\mathbf{\Psi}_\pm(\mathbf{r},t) = \sqrt{\frac{\epsilon_0}{2}}\mathbf{E}_\pm(\mathbf{r},t) \pm i\sqrt{\frac{1}{2\mu_0}}\mathbf{B}_\pm(\mathbf{r},t). \tag{4.2}$$

In the above expression ε_0 represents the electric permittivity and μ_0 is the magnetic permeability of free space. We have $\hat{\sigma}\mathbf{\Psi}_\pm = \pm\mathbf{\Psi}_\pm$ and the condition $\nabla\cdot\mathbf{\Psi} = 0$ is imposed. The helicity eigenstates are associated with photons with circular polarizations, and the photon electric and magnetic fields are given by $\mathbf{E} = \mathrm{Re}[\sqrt{2/\varepsilon_0}\mathbf{\Psi}(\mathbf{r},t)] = \mathbf{E}_+ + \mathbf{E}_-$ and $\mathbf{B} = \mathrm{Im}[\sqrt{2\mu_0}\hat{\sigma}\mathbf{\Psi}(\mathbf{r},t)] = \mathbf{B}_+ + \mathbf{B}_-$. By introducing the term $\mathbf{J}(\mathbf{r},t)$ accounting for the induced current in the medium due to the presence of the photon field, Maxwell's equations for the electromagnetic field in a medium can be recovered with the use of the photon

[1] In 1949, Newton and Wigner used group theoretical considerations to construct position operators for quantum particles [114]. In their paper, they show that it is impossible to construct such an operator for massless particles with a spin higher than 1/2. This has a consequence for the photon, which is a massless particle with spin 1, meaning that it is impossible to have such an operator for the photon.

wave equation [15]

$$i\frac{\partial \mathbf{\Psi}(\mathbf{r},t)}{\partial t} = c\hat{\sigma}\nabla \times \mathbf{\Psi}(\mathbf{r},t) - i\frac{\mathbf{J}(\mathbf{r},t)}{\sqrt{2\epsilon_0}}. \tag{4.3}$$

In order to extract Maxwell's equations from the above wave equation, we write it for each helicity component $\mathbf{\Psi}_\pm$ of Eq. (4.1) in terms of the electric and magnetic fields according to Eq. (4.2),

$$i\sqrt{\frac{\epsilon_0}{2}}\frac{\partial \mathbf{E}_\pm}{\partial t} \mp \sqrt{\frac{1}{2\mu_0}}\frac{\partial \mathbf{B}_\pm}{\partial t} = \pm c\sqrt{\frac{\epsilon_0}{2}}\nabla \times \mathbf{E}_\pm + ic\sqrt{\frac{1}{2\mu_0}}\nabla \times \mathbf{B}_\pm - i\frac{\mathbf{J}_\pm}{\sqrt{2\epsilon_0}}, \tag{4.4}$$

where we have separated $\mathbf{J}$ into two helicity components, such that $\mathbf{J} = \mathbf{J}_+ + \mathbf{J}_-$ in the same fashion as all the fields. We can rewrite the above equation as

$$\pm\left[\nabla \times \mathbf{E}_\pm + \frac{\partial \mathbf{B}_\pm}{\partial t}\right] + ic\left[\nabla \times \mathbf{B}_\pm - \frac{1}{c^2}\frac{\partial \mathbf{E}_\pm}{\partial t} - \mu_0 \mathbf{J}_\pm\right] = 0. \tag{4.5}$$

In order to get Ampère's law with Maxwell's correction term, we sum the positive and the negative helicity equations and take the imaginary part of the result. In order to get Faraday's law, we subtract instead of summing them and take the real part. Gauss' law with zero charge for electricity and magnetism are trivially given by the condition $\nabla \cdot \mathbf{\Psi} = 0$.

The current term $\mathbf{J}(\mathbf{r},t)$ in Eq. (4.3) accounts for the total current in the medium, i.e. both the free current and the bound current (caused by the magnetization and electric polarization of the medium), in response to the presence of the photon. This Maxwell wave equation determines the photon evolution, just like the Schrödinger equation does for a quantum massive particle. A crucial difference, though, is that the squared modulus of $\mathbf{\Psi}(\mathbf{r},t)$ is an energy density, and not a probability density like for the Schrödinger wave function[2].

A neat picture of this forms when we construct a continuity equation for $|\mathbf{\Psi}(\mathbf{r},t)|^2$ [15]. We first multiply the wave equation of Eq. (4.3) by $-i\mathbf{\Psi}^*$, such that when we sum the resulting equation with its complex conjugate, and note that $(\partial_t \mathbf{\Psi})\cdot\mathbf{\Psi}^* + (\partial_t \mathbf{\Psi}^*)\cdot\mathbf{\Psi} = \partial_t(\mathbf{\Psi}\cdot\mathbf{\Psi}^*)$, we get

$$\frac{\partial}{\partial t}|\mathbf{\Psi}|^2 = -ic\Big\{[\hat{\sigma}(\nabla \times \mathbf{\Psi})]\cdot\mathbf{\Psi}^* - [\hat{\sigma}(\nabla \times \mathbf{\Psi})]^*\cdot\mathbf{\Psi}]\Big\} - \frac{1}{\sqrt{2\epsilon_0}}(\mathbf{\Psi}+\mathbf{\Psi}^*)\cdot\mathbf{J}. \tag{4.6}$$

The term between curly brackets can be worked out if we use the relation $[\hat{\sigma}(\nabla\times\mathbf{\Psi})]^*\cdot\mathbf{\Psi}] = (\nabla\times\mathbf{\Psi}^*)\cdot(\hat{\sigma}\mathbf{\Psi})$, and then realize that the vectorial identity $[\nabla\times(\hat{\sigma}\mathbf{\Psi})]\cdot\mathbf{\Psi}^* - (\nabla\times\mathbf{\Psi}^*)\cdot(\hat{\sigma}\mathbf{\Psi}) =$

[2] Given $\langle E\rangle$ as the average energy of the photon, it is possible to interpret the quantity $P_R(t) = \int_R |\mathbf{\Psi}(\mathbf{r},t)|^2 \mathrm{d}^3 r/\langle E\rangle$ as the probability of detecting a photon in a region R of space, provided that this region is much larger than the relevant wavelengths that form the photon wavelength distribution [116].

$\nabla \cdot [(\sigma\mathbf{\Psi}) \times \mathbf{\Psi}^*]$ applies. The resulting continuity equation reads

$$\begin{aligned}\frac{\partial}{\partial t}|\mathbf{\Psi}|^2 &= ic\nabla \cdot [\mathbf{\Psi}^* \times (\hat{\sigma}\mathbf{\Psi})] - \frac{1}{\sqrt{2\epsilon_0}}(\mathbf{\Psi} + \mathbf{\Psi}^*) \cdot \mathbf{J} \\ &= -\nabla \cdot \mathbf{S} - \mathbf{E} \cdot \mathbf{J}. \end{aligned} \tag{4.7}$$

In the above equation, $\mathbf{S} \equiv -ic\mathbf{\Psi}^* \times (\hat{\sigma}\mathbf{\Psi})$ plays the role of the current density for the photon characterized by the wave function $\mathbf{\Psi}$. If a time average is taken of $\mathbf{S}$ over one period of oscillation of the photon field, then $\langle \mathbf{S} \rangle = \langle \mathbf{E} \times \mathbf{B} \rangle / \mu_0$ is analogous to the classical electromagnetic energy flux, given by the average of the Poynting vector[3]. This average $\langle \mathbf{S} \rangle$ is proportional to the momentum density carried by the light described by fields $\mathbf{E}$ and $\mathbf{B}$. Therefore, the term $\nabla \cdot \mathbf{S}$ in Eq. 4.7 can be seen as representing the change in the energy density caused by the energy flux $\mathbf{S}$ in the form of momentum carried by the photon. The term $\mathbf{E} \cdot \mathbf{J}$ in turn represents the amount of energy density that is converted into work needed for the generation of currents (free and bound) induced by the photon in the material.

The way that Eq. 4.7 is written contains implicitly the assumption of a certain division between electromagnetic and material parts of the energy of the photon when it enters a medium. This can be done differently, for instance Bialynicki-Birula [12, 116] includes the bound currents in the fields that characterize the photon wave function. For a medium with electric permittivity ϵ and magnetic permeability μ, and thus electric displacement field $\mathbf{D} = \epsilon\mathbf{E}$, the photon wave function is defined in Refs. [12, 116] as $\mathbf{F}_\pm = \mathbf{D}/\sqrt{2\epsilon} \pm i\mathbf{B}/\sqrt{2\mu}$, therefore including the energy due to material bound currents in the photon energy density. There is no unique form of dividing the energy of an electromagnetic field, when it propagates through a material medium, between the electromagnetic and material parts – this division is arbitrary and can be done according to different physical principles. This discussion comes a long way shaped as the question "what is the momentum carried by an electromagnetic field when it propagates through a material medium?". The beginning of this debate dates from the early 20th century [117–120] and it is known as the Abraham–Minkowski debate [20]. We will briefly refer to this discussion in the upcoming Sec. 4.3.

We stress once again that to apply the second quantization procedure to the electromagnetic field in the presence of matter is an extremely difficult task [16–19]. The boundary conditions imposed by the interface between different media and the field dispersion and absorption that are caused by the medium make the quantization process very complicated. In this sense, the use of the Maxwell wave equation greatly simplifies the treatment in relation to the second quantization method when there is no absorption or

[3] The averaging process is needed in the vectorial treatment of Ref. [15], which is the one we follow, in order to identify the current density with the Poynting vector. In the spinorial form used by Bialynicki-Birula [12, 116], however, the two functions can be identified even without the average.

emission of photons in the problem to be treated[4]. This is the case in the present problem of the photon reflection by a quantum mirror. Since the photon equation is equivalent to Maxwell's equations, a boundary conditions problem for a photon interacting with different media has the same solution as the one for a classical electromagnetic field.

4.2 The quantum state of the photon-mirror system after reflection

We consider one photon in a paraxial beam state with arbitrary polarization that reaches a perfectly conducting plane surface (the mirror) and interacts with it during a finite time. The mirror surface is considered to be larger than the photon beam diameter and its description is quantized in the z direction, which corresponds to the direction orthogonal to the surface plane. We consider the mirror initially in an arbitrary quantum state. We want to know the state of the system after the photon is completely reflected, while considering that the photon-mirror interaction occurs in a time scale much smaller than the one by the quantum mirror free evolution – in such case the mirror wave function can be considered stationary during the reflection process. Our strategy to solve the problem is to make use of the linearity of both Schrödinger's and Maxwell's equations, meaning that we can construct an arbitrary solution from superpositions of the simpler problem of a monochromatic classical electromagnetic field being reflected by a fixed infinite plane mirror. In order to do this, we are going to describe both the mirror and the photon with wave functions.

The mirror wave function is the traditional quantum mechanical wave function whose time evolution is described by the Schrödinger equation. For a perfectly localized mirror, its quantum state can be approximated as a Dirac delta wave function in the position space, having thus a momentum uncertainty that tends to infinity. Therefore no matter how much momentum it exchanges with a photon, its wave function can only acquire a global phase, not being shifted nor deformed – and this is consistent with the idea of a fixed mirror. Since an arbitrary quantum state for the mirror can be decomposed in the position eigenfunctions which are delta distributions, and since the Schrödinger equation is linear, if we know what the interaction does to every position eigenfunction, we know what it does to an arbitrary mirror state.

For the photon wave function we use the Bialynicki-Birula–Sipe formalism [12–15] described in Sec. 4.1, which allows us to bridge the photon problem to the reflection of a classical electromagnetic field via Maxwell's equations. The classical problem of a monochromatic electromagnetic wave being reflected by a fixed perfectly conducting plane is a traditional textbook problem [84], and this classical problem that we know how to

[4] In some cases the photon wave function formalism can be useful even when there is the absorption and generation of photons in a scattering process, as in the generation of entangled twin photons with parametric down conversion [15, 121].

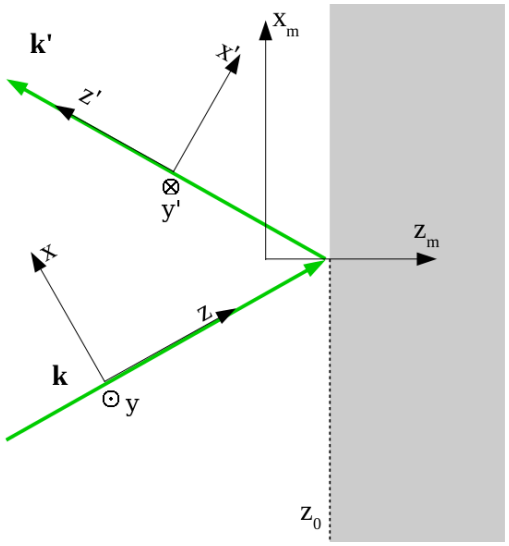

Figure 19 – An electromagnetic field with wave vector $\mathbf{k}$ is reflected by a perfect mirror, resulting in a reflected wave with wave vector $\mathbf{k}' = \mathbf{k} - 2(\mathbf{k} \cdot \hat{\mathbf{z}}_\mathbf{m})\hat{\mathbf{z}}_\mathbf{m}$.

solve has thus a perfect analogy to the reflection of a monochromatic photon (described with the Bialynicki-Birula–Sipe wave function) by a fixed mirror whose quantum state tends to a delta function in position space. With the solution of this quantum version of a classical problem we can build the solution for the general quantum case.

4.2.1 Photon state after reflection by a localized mirror

Let $z_m = z_0$ be the plane of the mirror interface, with the region $z_m > z_0$ being a perfect conductor, as shown in Fig. 19. It can be shown that the electromagnetic field inside the conductor falls to zero rapidly and there is no field propagation inside the conductor [84]. Also, Maxwell's equations demand the component of the electric field that is parallel to an interface of two different media to be continuous at the interface. These two facts combined ensure us that the component of the electric field that is parallel to the conductor surface is zero at the surface itself, when the penetration depth is much smaller than the field wavelength. Hence, by solving Maxwell's equations with the above conditions, we find that if there is a field

$$\mathbf{E}_\pm(\mathbf{r}, t) = \hat{\mathbf{u}}_{\mathbf{k}\pm} E_{0\mathbf{k}} \mathrm{e}^{i(\mathbf{k}\cdot\mathbf{r} - \omega t)} \tag{4.8}$$

in the $z_m < z_0$ region, called the incident field, then there must be a field

$$\mathbf{E}'_\mp(\mathbf{r}, t) = -\hat{\mathbf{u}}_{\mathbf{k}'\mp} E_{0\mathbf{k}} \mathrm{e}^{i(\mathbf{k}'\cdot\mathbf{r} - \omega t)} \mathrm{e}^{2i(\mathbf{k}\cdot\hat{\mathbf{z}}_\mathbf{m})z_0}, \tag{4.9}$$

called the reflected field, in the same region. This guarantees that, at the interface, the component of the electric field parallel to it is zero. In the above equations, we use a complex field notation, in which the real electric field is given by the real part of the complex field. The vectors $\hat{\mathbf{u}}_{\mathbf{k}\pm}$ are the circular polarization unit vectors relative to the direction of $\mathbf{k}$.

Also, $\mathbf{k}' = \mathbf{k} - 2(\mathbf{k}\cdot\hat{\mathbf{z}}_\mathbf{m})\hat{\mathbf{z}}_\mathbf{m}$, which indicates the inversion of the component of the field propagation in the direction characterized by $\hat{\mathbf{z}}_\mathbf{m}$, the unit vector perpendicular to the surface of reflection and pointing inward the conductor. Given the reference frames (x, y, z) and (x', y', z') indicated in Fig. 19, we define $\hat{\mathbf{u}}_{\mathbf{k}\pm} = (\hat{\mathbf{x}} \pm i\hat{\mathbf{y}})/\sqrt{2}$ and $\hat{\mathbf{u}}_{\mathbf{k}'\pm} = (\hat{\mathbf{x}}' \pm i\hat{\mathbf{y}}')/\sqrt{2}$.

With the solution of the classical problem in hand, we can now proceed to the construction of the solution of the quantum version of the problem. The modulus of the electric field of a circularly polarized monochromatic electromagnetic wave defines its magnetic field in a way that we can write

$$\mathbf{\Psi}_\pm(\mathbf{r}, t) = \hat{\mathbf{u}}_{\mathbf{k}\pm} A \mathrm{e}^{i(\mathbf{k}\cdot\mathbf{r}-\omega t)} \tag{4.10}$$

as the quantum version of the classical field of Eq. (4.8), based on the photon wave function of Eq. (4.2), and where A is a complex number.

Therefore, in the same spatial configuration as that of Fig. 19, the boundary conditions imposed by Maxwell's equations demand that if the incident photon in this space is described by Eq. (4.10) in the region $z_m \leq z_0$, then in that same region there must be a reflected part of the wave function given by

$$\mathbf{\Psi'}_\mp(\mathbf{r}, t) = -\hat{\mathbf{u}}_{\mathbf{k}'\mp} A \mathrm{e}^{i(\mathbf{k}'\cdot\mathbf{r}-\omega t)} \mathrm{e}^{2i(\mathbf{k}\cdot\hat{\mathbf{z}}_\mathbf{m})z_0}, \tag{4.11}$$

with $\mathbf{k}' = \mathbf{k} - 2(\mathbf{k}\cdot\hat{\mathbf{z}}_\mathbf{m})\hat{\mathbf{z}}_\mathbf{m}$, analogously to Eq. (4.9).

From now on, we represent the state of a photon with wave vector $\mathbf{k}$ and helicity $\pm$ in the Dirac notation as $|\mathbf{k}\pm\rangle$. The reflection described by Eqs. (4.10) and (4.11) thus implies that, for every $|\mathbf{k}\pm\rangle$ component of the field, there must be another component $|\mathbf{k}'\mp\rangle$ with the same amplitude and a phase difference $-\mathrm{e}^{2i(\mathbf{k}\cdot\hat{\mathbf{z}}_\mathbf{m})z_0}$ in order to satisfy the boundary conditions. Of course, the wave function must be zero for $z_m > z_0$.

Up to now we have been dealing with plane waves, which extend themselves with the same amplitude throughout all times and all space, but in our problem the interaction takes place during a finite time and in a restricted region of the mirror. So in order to talk about before and after the reflection of the photon and to consider that the mirror surface is larger than the beam diameter, we make use of the superposition principle and allow the state of the photon to be a superposition of different wave vectors, therefore confining it in space and time. For an incident photon in a beam state

$$|\psi\rangle = \int \psi(\mathbf{k})(c_{\mathbf{k}+}|\mathbf{k}+\rangle + c_{\mathbf{k}-}|\mathbf{k}-\rangle)\, d^3k, \tag{4.12}$$

with $|c_{\mathbf{k}+}|^2 + |c_{\mathbf{k}-}|^2 = 1$ for every $\mathbf{k}$ and $\int |\psi(\mathbf{k})|^2 d^3k = 1$, our treatment implies that, apart from a global phase, the reflected photon state must be

$$|\psi'\rangle = \int \psi(\mathbf{k})(c_{\mathbf{k}-}|\mathbf{k}'+\rangle + c_{\mathbf{k}+}|\mathbf{k}'-\rangle)\mathrm{e}^{2i(\mathbf{k}\cdot\hat{\mathbf{z}}_\mathbf{m})z_0}\, d^3k. \tag{4.13}$$

We have thus arrived at the general solution for the quantum state of a photon being reflected by a localized fixed mirror, i.e. a mirror whose position wave function can be approximated by a delta function and acquires at most a phase upon reflection. In this scenario, the mirror does not exchange any useful information with the photon and we cannot use it to investigate the photon momentum. We then proceed to generalize the mirror state, so that it does not need to be fixed anymore.

4.2.2 Photon state after reflection by a mirror in an arbitrary state: entanglement and radiation pressure

We are finally ready to include the wave function for the z position of the quantum mirror in the description. Eqs. (4.12) and (4.13) correspond to the situation of a fixed mirror at position $z_m = z_0$, that is, its state is described by the wave function $\langle z_m|z_0\rangle = \delta(z_m - z_0)$. Hence, for a mirror in an arbitrary state $|\phi\rangle$ with wave function $\phi(z_m) = \langle z_m|\phi\rangle$, the composite state of the light–mirror system before the interaction is

$$|\Psi\rangle = \int \psi(\mathbf{k})(c_{\mathbf{k}+}|\mathbf{k}+\rangle + c_{\mathbf{k}-}|\mathbf{k}-\rangle)\, d^3k \otimes \int \phi(z_m)|z_m\rangle\, dz_m, \tag{4.14}$$

which leads us to the state after the reflection

$$|\Psi'\rangle = \iint \psi(\mathbf{k})\ \phi(z_m)\ \mathrm{e}^{2i(\mathbf{k}\cdot\hat{\mathbf{z}}_\mathbf{m})z_m}\ (c_{\mathbf{k}-}|\mathbf{k}'+\rangle + c_{\mathbf{k}+}|\mathbf{k}'-\rangle)|z_m\rangle\ d^3k\ dz_m, \tag{4.15}$$

up to a global phase. The state described in Eq. (4.15) has a different phase factor for each ket $|\mathbf{k}\pm\rangle|z_m\rangle$ of the composite system state. This phase depends on the eigenvalues $\mathbf{k}$ and z_m correspondent respectively to the photon and the mirror, which means that this is a non-separable – or entangled – state between the two systems. So in general there are non-classical correlations between the photon and the quantum mirror after the photon reflection.

We can also write the state of Eq. (4.15) in the linear momentum basis for the mirror $\{|p_m\rangle\}$, given that $\langle p_m|z_m\rangle = (2\pi\hbar)^{-\frac{1}{2}}\mathrm{e}^{-ip_m z_m/\hbar}$ [46]. By applying the identity $\mathbb{I}_{\mathrm{ph}} \otimes \int |p_m\rangle\langle p_m| dp_m$ to Eq. (4.15), where $\mathbb{I}_{\mathrm{ph}}$ is an identity in the photon space, we get

$$|\Psi'\rangle = \iint \psi(\mathbf{k})\ \left[\int \phi(z_m)\ \frac{\mathrm{e}^{2i(\mathbf{k}\cdot\hat{\mathbf{z}}_\mathbf{m})z_m}\mathrm{e}^{-ip_m z_m/\hbar}}{\sqrt{2\pi\hbar}} dz_m\right]\ (c_{\mathbf{k}-}|\mathbf{k}'+\rangle + c_{\mathbf{k}+}|\mathbf{k}'-\rangle)|p_m\rangle\ d^3k\ dp_m. \tag{4.16}$$

The term in square brackets is the Fourier transform of $\phi(z_m)\mathrm{e}^{2i(\mathbf{k}\cdot\hat{\mathbf{z}}_\mathbf{m})z_m}$, and thus for $\tilde{\phi}(p_m) \equiv (2\pi\hbar)^{-\frac{1}{2}} \int \phi(z_m)\mathrm{e}^{-ip_m z_m/\hbar} dz_m$ we get

$$|\Psi'\rangle = \iint \psi(\mathbf{k})\ \tilde{\phi}(p_m - 2\hbar(\mathbf{k}\cdot\hat{\mathbf{z}}_\mathbf{m}))\ (c_{\mathbf{k}-}|\mathbf{k}'+\rangle + c_{\mathbf{k}+}|\mathbf{k}'-\rangle)|p_m\rangle\ d^3k\ dp_m, \tag{4.17}$$

where $\tilde{\phi}(p_m)$ is a wave function for the mirror in momentum space, $\tilde{\phi}(p_m) = \langle p_m|\phi\rangle$.

From Eq. (4.17) it is clear that every component $|\mathbf{k}\pm\rangle$ pushes the mirror by transferring a momentum $2\hbar(\mathbf{k}\cdot\hat{\mathbf{z}}_\mathbf{m})$ to it. This is the exact necessary amount to conserve momentum, given that the momentum of a monochromatic photon is $\hbar\mathbf{k}$, since the reflection simply inverts every photon wave vector component in the z_m direction. It is interesting to note that we arrived at this result of the momentum transfer from the photon to the mirror simply by imposing boundary conditions on the photon reflection. No specification of the photon momentum was ever made. In other words, if we assume momentum conservation, we can conclude that the photon momentum is given by the expression $\hbar\mathbf{k}$ simply by computing the momentum transfer to the mirror upon reflection.

The spatial phase relation between incident and reflected fields, imposed by Maxwell's equations boundary conditions at the surface of the mirror, is translated into a momentum kick when we go to the quantum domain. The quantum canonical relation between position and momentum connects phases on the spatial wave function with displacements on the momentum wave function. This becomes clear when we see that the imposed phase $\mathrm{e}^{2i(\mathbf{k}\cdot\hat{\mathbf{z}}_\mathbf{m})z_m}$ has the same shape as a momentum translation operator [46], where z_m in in the place of the operator that acts on the wave function of the mirror, weighted by the quantity $2(\mathbf{k}\cdot\hat{\mathbf{z}}_\mathbf{m})$.

4.2.3 Can this kind of photon-mirror entanglement be detected?

We can analyze some separable limits of the quantum state of Eqs. (4.15) and (4.17). In the case when the mirror position wave function approximates a delta function, Eq. (4.15) reduces to Eq. (4.13) for the reflected photon, with the mirror state unaltered by the photon reflection. This is not surprising, since a localized fixed mirror was one of our first assumptions in order to be able to derive the result. In Eq. (4.17) where we use the momentum basis, the aforementioned approximation is valid whenever the mirror momentum uncertainty is much larger than the momentum gained by the reflection of each $\mathbf{k}$ component of the photon state. Equivalently, since $\Delta p_m \Delta z_m \sim \hbar$, this disentangled approximation is reached whenever the mirror position uncertainty is much smaller than the wavelengths that compose the photon state. For an optical photon with average wavelength $\lambda \sim 500$ nm, it means that the mirror should have a position uncertainty around $\Delta x \sim 10^{-7}$m or larger for significant entanglement effects to appear. It is important to note that the momentum transfer from the photon to the quantum mirror can be increased by a factor of F if the quantum mirror is one of the mirrors of a cavity with a finesse F. This is because the photon is reflected on average F times by the quantum mirror before leaving the cavity. Entanglement effects may arise in that way with for instance $\Delta x \sim 10^{-10}$m, when $F \sim 10^3$.

If the mirror is trapped in a harmonic potential and is initially in the ground state, the relation between its mass m_0, its resonance frequency ω_0 and its position uncertainty

is $\Delta x = \sqrt{\hbar/2m_0\omega_0}$ [46]. In that sense, $m_0\omega_0$ gets smaller as Δx grows larger, hence entanglement effects arise whenever $m_0\omega_0 \sim 10^{-8}$kg/s or smaller. A look at Table II of Ref. [99] shows us that the suspended mirrors with smallest $m_0\omega_0$ by 2014 have it of order 10^{-6}kg/s, but their finesse is extremely small, around unity [122], while mirrors with $F \sim 10^4$ are associated with larger $m_0\omega_0 \sim 1$ kg/s [123]. Some recently fabricated mirrors with a very small effective mass can achieve a higher finesse of order 10^3, but they have $m_0\omega_0 \sim 10^{-6}$kg/s [124], still two orders of magnitude larger than necessary. So it is still not possible to significantly entangle spatial modes of a photon and a mirror upon reflection.

Another separable state limit occurs if the photon propagates as a nearly monochromatic beam along an arbitrary direction $\mathbf{k_0}$ (but non-monochromatic enough so that the interaction is still much faster than any evolution due to the free mirror Hamiltonian), i.e. the photon is pretty much a plane wave with a transversal envelope. In a rough approximation, the mirror interacts only with the main plane wave component $\mathbf{k_0}$ of the photon, the whole mirror momentum wave function is displaced by $2\hbar(\mathbf{k_0}\cdot\hat{\mathbf{z}}_\mathbf{m})$, and thus the system final state of Eq. (4.17) is almost disentangled,

$$|\Psi'\rangle \approx \int \psi(\mathbf{k})\ (c_{\mathbf{k_0}-}|\mathbf{k}'+\rangle + c_{\mathbf{k_0}+}|\mathbf{k}'-\rangle)\ d^3k\ \otimes \int \tilde{\phi}(p_m - 2\hbar(\mathbf{k_0}\cdot\hat{\mathbf{z}}_\mathbf{m}))|p_m\rangle\ dp_m. \quad (4.18)$$

Intermediate regimes account for mirror position uncertainty of the order of the average wavelength of non-monochromatic light, and those generally result in a non-separable state, as evident in Eq. (4.17). Following the discussions of the above paragraphs, such regimes can in principle be achieved by engineering cavities with larger finesse tuned to smaller light wavelengths. But since a high finesse is associated with highly monochromatic light allowed in the cavity, present technology seems to be in a deadlock to try to probe this kind of entanglement.

It is important to note, though, that if a cavity with the quantum mirror is in one arm of an interferometer, as proposed in Ref. [103], entanglement between the photon and the mirror could be generated due to the superposition of the single photon propagating on each arm of the interferometer. In the proposal of Ref. [103] (see Fig. 20), a vertically polarized photon enters a Michelson interferometer via a polarizing beam splitter (PBS), and is split into a coherent superposition of two paths by a 50:50 beam splitter (BS). The PBS is a device that reflects the vertically polarized component of the electromagnetic field, while transmitting the horizontally polarized one. In the horizontal path, the photon enters a regular cavity with fixed mirrors, while in the vertical path it enters a cavity of which one of the mirrors is attached to a tiny oscillator (M), whose motion must be described by quantum mechanics. The mirror motion is thus affected by the photon superposition state. The quantum superposition of the path in which the photon interacts with the mirror and transfers momentum to it with the path in which the photon does not interact and does not transfer momentum to the mirror may result in an entangled state. The photon

then leaks out of the cavities and a quarter-wave plate ($\lambda/4$) makes sure it is directed into one of the two detectors (D). If there is any entanglement the photon interference pattern will have a decreased visibility, but the coherent evolution of the system allows for the recovery of an unentangled state as time passes. Thus, after many rounds of the experiment performed with many different interaction times, one can plot the visibility of the photon interference pattern as a function of time. If there is a rise in the visibility as time passes, it means that the initial lowering of the visibility is due to the creation of entanglement by the coherent evolution of the photon–mirror system, and not due to some other decoherence process that could never lead to a recovery of the visibility. An experimental realization of this proposal, however, has not yet been accomplished.

In chapter 2 we used this kind of superposition effect of having a positive force and a null force acting on a quantum system in order to propose an experiment that could detect not entanglement, but an anomalous (negative) momentum transfer to the system, which we called quantum interference of force.

4.3 Connection with the Abraham–Minkowski debate

Now we briefly address the historical Abraham–Minkowski debate, which concerns how the linear momentum carried by light behaves when it propagates through a dielectric

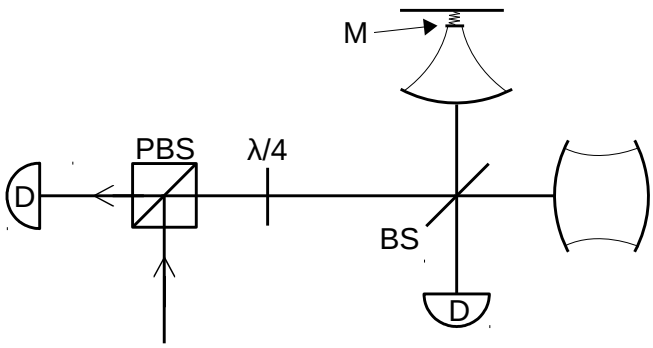

Figure 20 – The interferometric experiment proposed in Ref. [103]. A photon enters a Michelson interferometer via a polarizing beam splitter (PBS), and is split into a coherent superposition of two paths by a 50:50 beam splitter (BS). In the horizontal path, the photon enters a regular cavity with fixed mirrors, while in the vertical path it enters a cavity of which one of the mirrors is attached to a tiny oscillator (M), whose motion must be described by quantum mechanics. The photon propagation modes and the mirror motion thus get entangled. The photon leaks out of the cavities and a quarter-wave plate ($\lambda/4$) makes sure it is directed into one of the two detectors (D). The detection of the photon carries information about the entanglement between mirror and photon.

medium [20, 21]. Hermann Minkowski's formulation [117, 118] of the light momentum in a medium proposes the expression $\mathbf{D} \times \mathbf{B}$ for the momentum density, where $\mathbf{D} = \epsilon\mathbf{E}$ is the electric displacement field when the medium has electric permittivity ϵ. This expression leads to a momentum density *directly* proportional to the medium refractive index n, i.e. the electromagnetic momentum carried by the light proposed by Minkowski increases when the light propagates through a medium with $n > 1$, when compared to the vacuum momentum. In turn, Max Abraham's formulation [119, 120] uses different considerations and arrives at the expression $\mathbf{E} \times \mathbf{H}/c^2$ for the momentum density, where $\mathbf{H} = \mathbf{B}/\mu$ is the magnetic field when the medium has magnetic permeability μ and c is the speed of light in vacuum. This leads to the conclusion that the momentum density is *inversely* proportional to the refractive index n and decreases in the medium with $n > 1$ when compared to the vacuum, which seems to be in contradiction with Minkowski's conclusion.

Minkowski's formulation leads to an asymmetric energy-momentum tensor [20], which raises suspicion over it, but on the other hand it is the one that fits reflection-off-of-a-mirror experiments [22,23]. Abraham's formulation leads to a symmetric energy-momentum tensor [20] and therefore it fits well rotation experiments that involve conservation of angular momentum [125, 126]. It can be shown, however, that there is no universal way of splitting the energy-momentum tensor between electromagnetic and material tensors [20, 127, 128], with conservation laws being universally applied only to the total electromagnetic+material tensor. Therefore there is some freedom in which part of the momentum is associated with the light and which is associated with the medium. When appropriate medium considerations are taken, all experiments can be explained by any of the two momenta, either Abraham's or Minkowski's. In fact, there are phenomena that are not accounted in any of the two formulations [20], e.g. the electrostrictive effect, which is the change in the shape of an object when an electric field is applied to it.

Recently Barnett showed how the Abraham and Minkowski momenta can be respectively associated with the kinetic and canonical momentum of the field [21, 113]. It is clear that, according to equation (4.17), the momentum gained by every component $|p_m\rangle$ of the mirror is proportional to the wave vector component $\mathbf{k}$. If $\hat{\boldsymbol{\kappa}}$ is the unitary vector along the direction of $\mathbf{k}$, then we can write $\mathbf{k} = n(\omega/c)\hat{\boldsymbol{\kappa}}$, where n is the refractive index of the medium in which the photon is propagating. Clearly, this corresponds to the Minkowski momentum for the photon, which is directly proportional to n. As mentioned, this behavior was observed in the experiments with classical light being reflected by classical mirrors immersed in dielectric media [22, 23], and we present a fully quantum justification here.

Under Barnett's view, the answer to why the Minkowski momentum is the one that appears in our case lies in the fact that quantum mechanics is a Hamiltonian theory, based on canonical relations between position and momentum. The phase acquired upon reflection by the photon on Eq. (4.13), which is dependent on the mirror position and

is directly proportional to the medium refractive index n, is shared by both mirror and photon on Eq. (4.15). Therefore the acquired phase demanded by boundary conditions on the electromagnetic field is transformed in a momentum kick that is also proportional to n when we look at its effect on the mirror. As discussed previously, the canonical commutation relations in quantum mechanics define translation operators with the same form as these phase factors [46], hence turning phase factors into momentum kicks, which is explicit on the basis change from Eq. (4.15) to Eq. (4.17). It is natural then that our system will reveal the canonical momentum of the photon, which corresponds to the Minkowski momentum.

4.4 Chapter remarks

In summary, we have treated a single-photon reflection by a quantum mirror using the photon wave function formalism. This allowed us to treat the problem using boundary conditions on the photon wave equation instead of using the second quantization formalism for light.

By computing the momentum transferred from the photon to the mirror, we concluded that a photon with wavevector $\mathbf{k}$ must have momentum $\hbar\mathbf{k}$ in order to achieve momentum conservation in the system, as expected. We also showed that in the case that the photon is not monochromatic and its average wavelength is of the order of the mirror position uncertainty, entanglement between them might appear with the reflection process.

Finally we addressed a contribution to the Abraham-Minkowski debate by showing, with a quantum treatment from first principles, that the momentum transferred from a photon to a mirror immersed in a dielectric medium upon reflection is proportional to the medium refractive index. This result associates the photon momentum with the Minkowski momentum. This is natural given that the Minkowski momentum is associated with the canonical momentum of light, which is the momentum that should appear in a quantum treatment.

The results presented in this chapter are published in Ref. [24].

5 Final remarks

We have approached three substantially different subjects in this Thesis: the quantum interference of force in chapter 2 (see Refs. [1, 2]), the fermionic Hanbury Brown and Twiss interference in free space with two independent electron sources in chapter 3, and the reflection of a photon by a quantum mirror in chapter 4 (see Ref. [24]).

In chapter 2 we have presented the phenomenon of *quantum interference of force*. We have shown how the quantum superposition of a positive force with no force on a quantum particle may result in a "negative force" on that particle. In the first part of the chapter, we have explored the situation in which the force is caused by an external classical device, and this was used to present proposals for feasible experiments that could verify this anomalous momentum transfer to a quantum particle with available technology. Currently, there have been talks with experimental groups regarding the possibility of realizing an experiment with a Bose-Einstein condensate that could detect the quantum interference of force. The feasibility of such experiment is clear, and it is only a matter of time for it to be done. In the last part of the chapter, we investigated a setup in which the force that the quantum particle feels is caused by another quantum particle. Namely, we showed how two electrons propagating in a Mach-Zehnder interferometer could experience an effective attraction between them, under suitable post-selection. It would be challenging to implement such a setup, but we have argued that it could in principle be done with current technology.

In chapter 3 we have presented the work developed during the 12-month Sandwich PhD period in the group of Prof. Joachim von Zanthier, at the University of Erlangen-Nuremberg. The work consists of the proposal of an experiment that is able to unambiguously detect the Hanbury Brown and Twiss interference effect with electrons in free space. With the use of tungsten nanotips, it should be possible to have two independent electron sources than can have the emission time coordinated. This setup should be able to rule out the Coulomb repulsion as an explanation to the experimental results, an achievement that relies on the much larger distance between the two sources, in relation to a previous experiment. The distance between the tips causes a great number of oscillations in the two-particle interference pattern, which can be unambiguously distinguished from the effect of Coulomb repulsion. This technique opens a new path on electron imaging, where incoherent electron sources can be used to construct images based on intensity correlation measurements, just like the Hanbury Brown and Twiss technique has allowed for incoherent imaging with light. An experiment with the implementation of the proposal is currently being set up at the University of Erlangen-Nuremberg, in collaboration with the experimental group of Prof. Peter Hommelhoff at that university.

Finally, with the work presented in chapter 4 we were able to use a photon wave function formalism to theoretically treat from first principles the reflection of a single photon by a quantum mirror. By using boundary conditions, the final state of the photon-mirror system was found and shown to be in general entangled. Furthermore, the photon momentum could be derived from the treatment, which also led us to the conclusion that the Minkowski momentum appears in our quantum setting, in the context of the Abraham–Minkowski debate concerning the momentum of light when propagating through a material medium. This formalism we used avoids the complications of using the quantum field operators in the presence of boundary conditions, and it could be used to treat the dynamics of the interaction between the photon and the mirror. We have disregarded the evolution of the mirror during the reflection process, and the inclusion of the mirror dynamics could lead for instance to the description of non-linearities in the field dynamics mediated by the mirror.

Bibliography

1 CORRÊA, R.; CENNI, M. F. B.; SALDANHA, P. L. Quantum interference of force. *Quantum*, v. 2, p. 112, 2018. Cited 3 times on page 9, 13, and 79.

2 CENNI, M. F. B.; CORRÊA, R.; SALDANHA, P. L. Effective electrostatic attraction between electrons due to quantum interference. *arXiv:1808.07082*. Disponível em: <https://arxiv.org/abs/1808.07082>. Cited 3 times on page 9, 13, and 79.

3 BROWN, R. H.; JENNISON, R. C.; GUPTA, M. K. D. Apparent angular sizes of discrete radio sources. *Nature*, v. 170, p. 1061, 1952. Cited 3 times on page 10, 34, and 38.

4 BROWN, R. H.; TWISS, R. Q. A new type of interferometer for use in radio astronomy. *Phil. Mag.*, v. 45, p. 663, 1954. Cited 3 times on page 10, 34, and 38.

5 BROWN, R. H.; TWISS, R. Q. Correlation between photons in two coherent beams of light. *Nature*, v. 177, p. 27, 1956. Cited 3 times on page 10, 34, and 38.

6 BROWN, R. H.; TWISS, R. Q. A test of a new type of stellar interferometer on Sirius. *Nature*, v. 178, p. 1046, 1956. Cited 4 times on page 10, 34, 38, and 39.

7 HENNY, M.; OBERHOLZER, S.; STRUNK, C.; HEINZEL, T.; ENSSLIN, K.; HOLLAND, M.; SCHÖNENBERGER, C. The fermionic hanbury brown and twiss experiment. *Science*, v. 284, p. 296, 1999. Cited 2 times on page 10 and 34.

8 OLIVER, W. D.; KIM, J.; LIU, R. C.; YAMAMOTO, Y. Hanbury brown and twiss-type experiment with electrons. *Science*, v. 284, p. 299, 1999. Cited 2 times on page 10 and 34.

9 KIESEL, H.; RENZ, A.; HASSELBACH, F. Observation of hanbury brown-twiss anticorrelations for free electrons. *Nature*, v. 418, p. 392, 2002. Cited 3 times on page 10, 34, and 63.

10 KODAMA, T.; OSAKABE, N.; TONOMURA, A. Correlation in a coherent electron beam. *Phys. Rev. A*, American Physical Society, v. 83, p. 063616, Jun 2011. Cited 4 times on page 10, 34, 35, and 63.

11 BAYM, G.; SHEN, K. Hanbury Brown-Twiss interferometry with electrons: Coulomb vs. quantum statistics. *arXiv:1212.4008*. Cited 6 times on page 10, 34, 35, 63, 64, and 65.

12 BIALYNICKI-BIRULA, I. On the wave function of the photon. *Acta Phys. Pol. A*, v. 86, p. 97, 1994. Cited 4 times on page 10, 67, 69, and 70.

13 SIPE, J. E. Photon wave functions. *Phys. Rev. A*, v. 52, p. 1875, 1995. Cited 3 times on page 10, 67, and 70.

14 SMITH, B. J.; RAYMER, M. G. Photon wave functions, wave-packet quantization of light, and coherence theory. *New J. Phys.*, v. 9, p. 414, 2007. Cited 3 times on page 10, 67, and 70.

15 SALDANHA, P. L.; MONKEN, C. H. Interaction between light and matter: a photon wave function approach. *New J. Phys.*, v. 13, n. 073015, 2011. Cited 5 times on page 10, 67, 68, 69, and 70.

16 GLAUBER, R. J.; LOWENSTEIN, M. Quantum optics of dielectric media. *Phys. Rev. A*, v. 43, p. 467, 1991. Cited 3 times on page 10, 67, and 69.

17 HUTTNER, B.; BARNETT, S. M. Quantization of the electromagnetic field in dielectrics. *Phys. Rev. A*, v. 43, p. 4306, 1992. Cited 3 times on page 10, 67, and 69.

18 SCHEEL, S.; BUHMANN, S. Y. Macroscopic quantum electrodynamics – concepts and applications. *Acta Phys. Slovaca*, v. 58, p. 675, 2008. Cited 3 times on page 10, 67, and 69.

19 PHILBIN, T. G. Canonical quantization of macroscopic electromagnetism. *New J. Phys.*, v. 12, p. 123008, 2010. Cited 3 times on page 10, 67, and 69.

20 PFEIFER, R. N. C.; NIEMINEN, T. A.; HECKENBERG, N. R.; RUBINSZTEIN-DUNLOP, H. Colloquium: Momentum of an electromagnetic wave in dielectric media. *Rev. Mod. Phys.*, v. 79, p. 1197, 2007. Cited 4 times on page 10, 66, 69, and 77.

21 BARNETT, S. M.; LOUDON, R. The enigma of optical momentum in a medium. *Phil. Trans. R. Soc. A*, v. 368, p. 927, 2010. Cited 3 times on page 10, 66, and 77.

22 JONES, R. V. Radiation pressure in a refracting medium. *Nature*, v. 167, p. 439, 1951. Cited 3 times on page 11, 66, and 77.

23 JONES, R. V.; LESLIE, B. The measurement of optical radiation pressure in dispersive media. *Proc. R. Soc. Lond. A*, v. 360, p. 347, 1978. Cited 3 times on page 11, 66, and 77.

24 CORRÊA, R.; SALDANHA, P. L. Photon reflection by a quantum mirror: a wave-function approach. *Phys. Rev. A*, v. 93, p. 023803, 2016. Cited 4 times on page 11, 67, 78, and 79.

25 FEYNMAN, R. P.; LEIGHTON, R. B.; SANDS, M. *The Feynman Lectures on Physics*. New York: Basic Books, 2010. III. Cited on page 12.

26 TONOMURA, A.; ENDO, J.; MATSUDA, T.; KAWASAKI, T.; EZAWA, H. Demonstration of single-electrion buildup of an interference pattern. *Am. J. Phys.*, v. 57, p. 117, 1989. Cited on page 12.

27 BACH, R.; POPE, D.; LIOU, S.-H.; BATELAAN, H. Controlled double-slit electron diffraction. *New J. Phys.*, v. 15, p. 033018, 2013. Cited on page 12.

28 WHEELER, J. A. *Mathematical foundations of quantum theory*. [S.l.]: Academic Press, 1978. 9 to 48 p. Cited on page 12.

29 JACQUES, V.; WU, E.; GROSSHANS, F.; TREUSSART, F.; GRANGIER, P.; ASPECT, A.; ROCH, J.-F. Experimental realization of Wheeler's delayed-choice gedanken experiment. *Science*, v. 315, p. 966, 2007. Cited on page 12.

30 MANNING, A. G.; KHAKIMOV, R. I.; DALL, R. G.; TRUSCOTT, A. G. Wheeler's delayed-choice gedanken experiment with a single atom. *Nat. Phys.*, v. 11, p. 539, 2015. Cited on page 12.

31 VEDOVATO, F.; AGNESI, C.; SCHIAVON, M.; DEQUAL, D.; CALDERARO, L.; TOMASIN, M.; MARANGON, D. G.; STANCO, A.; LUCERI, V.; BIANCO, G.; VALLONE, G.; VILLORESI, P. Extending Wheeler's delayed-choice experiment to space. *Sci. Adv.*, v. 3, p. 1701180, 2017. Cited on page 12.

32 SCULLY, M. O.; ENGLERT, B.-G.; WALTHER, H. Quantum optical tests of complementarity. *Nature*, v. 351, p. 111, 1991. Cited on page 12.

33 HERZOG, T. J.; KWIAT, P. G.; WEINFURTER, H.; ZEILINGER, A. Complementarity and the quantum eraser. *Phys. Rev. Lett.*, v. 75, p. 3034, 1995. Cited on page 12.

34 DURR, S.; NONN, T.; REMPE, G. Fringe visibility and which-way information in an atom interferometer. *Phys. Rev. Lett.*, v. 81, p. 5705, 1998. Cited on page 12.

35 WALBORN, S. P.; CUNHA, M. O. T.; PÁDUA, S.; MONKEN, C. H. Double-slit quantum eraser. *Phys. Rev. A*, v. 65, p. 033818, 2002. Cited on page 12.

36 ELITZUR, A. C.; VAIDMAN, L. Quantum mechanical interaction-free measurements. *Found. Phys.*, v. 23, n. 7, p. 987, 1993. Cited on page 12.

37 KWIAT, P.; WEINFURTER, H.; HERZOG, T.; ZEILINGER, A.; KASEVICH, M. A. Interaction-free measurement. *Phys. Rev. Lett.*, v. 74, p. 4763, 1995. Cited on page 12.

38 PEISE, J.; LUCKE, B.; PEZZÉ, L.; DEURETZBACHER, F.; ERTMER, W.; ARLT, J.; SMERZI, A.; SANTOS, L.; KLEMPT, C. Interaction-free measurements by quantum Zeno stabilization of ultracold atoms. *Nat. Commun.*, v. 6, p. 6811, 2015. Cited on page 12.

39 IONICIOIU, R.; TERNO, D. R. Proposal for a quantum delayed-choice experiment. *Phys. Rev. Lett.*, v. 107, p. 230406, 2011. Cited on page 12.

40 PERUZZO, A.; SHADBOLT, P.; BRUNNER, N.; POPESCU, S.; O'BRIEN, J. L. A quantum delayed-choice experiment. *Science*, v. 338, p. 634, 2012. Cited on page 12.

41 KAISER, F.; COUDREAU, T.; MILMAN, P.; OSTROWSKY, D. B.; TANZILLI, S. Entanglement-enabled delayed-choice experiment. *Science*, v. 338, p. 637, 2012. Cited on page 12.

42 AHARONOV, Y.; BOTERO, A.; NUSSINOV, S.; POPESCU, S.; TOLLAKSEN, J.; VAIDMAN, L. The classical limit of quantum optics: not what it seems at first sight. *New J. Phys.*, v. 15, p. 093006, 2013. Cited 7 times on page 12, 13, 14, 15, 16, 18, and 20.

43 AHARONOV, Y.; DAVIDOVICH, L.; ZAGURY, N. Quantum random walks. *Phys. Rev. A*, v. 48, p. 1687, 1993. Cited on page 12.

44 AHARONOV, Y.; ALBERT, D. Z.; VAIDMAN, L. How the result of a measurement of a component of the spin of a spin-$\frac{1}{2}$ particle can turn out to be 100. *Phys. Rev. Lett.*, v. 60, p. 1351, 1988. Cited on page 15.

45 DRESSEL, J.; MALIK, M.; MIATTO, F. M.; JORDAN, A. N.; BOYD, R. W. Colloquium: Understanding quantum weak values: Basics and applications. *Rev. Mod. Phys*, v. 86, p. 307, 2014. Cited on page 15.

46 COHEN-TANNOUDJI, C.; DIU, B.; LALOE, F. *Quantum Mechanics*. 2nd (in english). ed. Paris: Hermann by John Wiley & Sons, 1977. Cited 9 times on page 21, 32, 42, 43, 73, 74, 75, 78, and 91.

47 MARTON, L.; SIMPSON, J. A.; SUDDETH, J. A. An electron interferometer. *Rev. Sci. Instr.*, v. 25, n. 11, p. 1099, 1954. Cited on page 22.

48 RAUCH, H.; TREIMER, W.; BONSE, U. Test of a single crystal neutron interferometer. *Phys. Lett. A*, v. 47, n. 5, p. 369, 1974. ISSN 0375-9601. Cited on page 22.

49 KEITH, D. W.; EKSTROM, C. R.; TURCHETTE, Q. A.; PRITCHARD, D. E. An interferometer for atoms. *Phys. Rev. Lett.*, American Physical Society, v. 66, p. 2693, May 1991. Cited on page 22.

50 CRONIN, A. D.; SCHMIEDMAYER, J.; PRITCHARD, D. E. Optics and interferometry with atoms and molecules. *Rev. Mod. Phys.*, American Physical Society, v. 81, p. 1051, Jul 2009. Cited on page 22.

51 GODUN, R. M.; D'ARCY, M. B.; SUMMY, G. S.; BURNETT, K. Prospects for atom interferometry. *Contemp. Phys.*, v. 42, p. 77, 2001. Cited 3 times on page 22, 32, and 33.

52 GRONNIGER, G.; BARWICK, B.; BATELAAN, H. A three-grating electron interferometer. *New J. Phys.*, v. 8, p. 224, 2006. Cited 4 times on page 22, 23, 32, and 33.

53 EKSTROM, C. R.; SCHMIEDMAYER, J.; CHAPMAN, M. S.; HAMMOND, T. D.; PRITCHARD, D. E. Measurement of the electric polarizability of sodium with an atom interferometer. *Phys. Rev. A*, v. 51, p. 3883, 1995. Cited on page 22.

54 ROBERTS, T. D.; CRONIN, A. D.; TIBERG, M. V.; PRITCHARD, D. E. Dispersion compensation for atom interferometry. *Phys. Rev. Lett.*, v. 92, p. 060405, 2004. Cited on page 22.

55 MIFFRE, A.; JACQUEY, M.; BUCHNER, M.; TRÉNEC, G.; VIGUÉ, J. Measurement of the electric polarizability of lithium by atom interferometry. *Phys. Rev. A*, v. 73, p. 011603(R), 2006. Cited on page 22.

56 RAUCH, H.; WENER, S. *Neutron interferometry*. 2nd. ed. Oxford: Oxford University Press, 2015. Cited on page 23.

57 HASEGAWA, Y.; RAUCH, H. Quantum phenomena explored with neutrons. *New J. Phys.*, v. 13, p. 115010, 2011. Cited on page 23.

58 GEPPERT, H.; DENKMAYR, T.; SPONAR, S.; LEMMEL, H.; HASEGAWA, Y. Improvement of the polarized neutron interferometer setup demonstrating violation of a Bell-like inequality. *Nucl. Instrum. Methods Phys. Res.*, v. 763, p. 417, 2014. Cited on page 23.

59 DENKMAYR, T.; GEPPERT, H.; LEMMEL, H.; WAEGELL, M.; DRESSEL, J.; HASEGAWA, Y.; SPONAR, S. Experimental demonstration of direct path state characterization by strongly measuring weak values in a matter-wave interferometer. *Phys. Rev. Lett.*, v. 118, p. 010402, 2017. Cited on page 23.

60 COHEN-TANNOUDJI, C.; DUPONT-ROC, J.; GRYNBERG, G. *Atom-Photon Interactions: Basic Processes and Applications*. Weinheim: Wiley-VCH Verlag GrnbH & Co. KGaA, 1998. ISBN 9780471293361. Cited on page 24.

61 MATTHEWS, M. R.; HALL, D. S.; JIN, D. S.; ENSHER, J. R.; WIEMAN, C. E.; CORNELL, E. A.; DALFOVO, F.; MINNITI, C.; STRINGARI, S. Dynamical response of a Bose-Einstein condensate to a discontinuous change in internal state. *Phys. Rev. Lett.*, American Physical Society, v. 81, p. 243–247, Jul 1998. Cited on page 24.

62 HARDY, L. Quantum mechanics, local realistic theories, and Lorentz-invariant realistic theories. *Phys. Rev. Lett.*, v. 68, p. 2981, 1992. Cited on page 25.

63 AHARONOV, Y.; BOTERO, A.; POPESCU, S.; REZNIK, B.; TOLLAKSEN, J. Revisiting Hardy's paradox: counterfactual statements, real measurements, entanglement and weak values. *Phys. Lett. A*, v. 301, p. 130, 2002. Cited 2 times on page 25 and 30.

64 HOMMELHOFF, P.; KEALHOFER, C.; KASEVICH, M. A. Ultrafast electron pulses from a tungsten tip triggered by low-power femtosecond laser pulses. *Phys. Rev. Lett.*, v. 97, p. 247402, 2006. Cited 5 times on page 32, 33, 35, 64, and 65.

65 BARWICK, B.; CORDER, C.; STROHABER, J.; CHANDLER-SMITH, N.; UITERWAAL, C.; BATELAAN, H. Laser-induced ultrafast electron emission from a field emission tip. *New J. Phys.*, v. 9, n. 5, p. 142, 2007. Cited 4 times on page 32, 33, 35, and 64.

66 EHBERGER, D.; HAMMER, J.; EISELE, M.; KRUGER, M.; NOE, J.; HOGELE, A.; HOMMELHOFF, P. Highly coherent electron beam from a laser-triggered tungsten needle tip. *Phys. Rev. Lett.*, v. 114, p. 227601, 2015. Cited 7 times on page 32, 33, 35, 56, 62, 64, and 65.

67 LOUGOVSKI, P.; BATELAAN, H. Quantum description and properties of electrons emitted from pulsed nanotip electron sources. *Phys. Rev. A*, v. 84, p. 023417, 2011. Cited 8 times on page 32, 34, 35, 59, 62, 63, 64, and 65.

68 GLAUBER, R. J. Nobel lecture: One hundred years of light quanta. *Rev. Mod. Phys.*, American Physical Society, v. 78, p. 1267–1278, Nov 2006. Cited on page 34.

69 MORGAN, B. L.; MANDEL, L. Measurement of photon bunching in a thermal light beam. *Phys. Rev. Lett.*, v. 16, n. 22, p. 1012, 1966. Cited 2 times on page 34 and 58.

70 PFLEEGOR, R. L.; MANDEL, L. Interference of independent photon beams. *Phys. Rev.*, v. 159, p. 1084, 1967. Cited on page 34.

71 KIMBLE, H. J.; DAGENAIS, M.; MANDEL, L. Photon antibunching in resonance fluorescence. *Phys. Rev. Lett.*, v. 39, n. 11, p. 691, 1977. Cited 2 times on page 34 and 58.

72 HONG, C. K.; OU, Z. Y.; MANDEL, L. Measurement of subpicosecond time intervals between two photons by interference. *Phys. Rev. Lett.*, v. 59, p. 2044, 1987. Cited 3 times on page 34, 54, and 58.

73 LIU, J.; SHIH, Y. Nth-order coherence of thermal light. *Phys. Rev. A*, v. 79, p. 023819, 2009. Cited on page 34.

74 OPPEL, S.; BÜTTNER, T.; KOK, P.; ZANTHIER, J. von. Superresolving multiphoton interferences with independent light sources. *Phys. Rev. Lett.*, v. 109, p. 233603, 2012. Cited 3 times on page 34, 35, and 53.

75 WIEGNER, R.; OPPEL, S.; BHATTI, D.; ZANTHIER, J. von; AGARWAL, G. S. Simulating superradiance from higher-order-intensity-correlation measurements: single atoms. *Phys. Rev. A*, v. 92, p. 033832, 2015. Cited 3 times on page 34, 50, and 53.

76 BHATTI, D.; OPPEL, S.; WIEGNER, R.; AGARWAL, G. S.; ZANTHIER, J. von. Simulating dicke-like superradiance with classical light sources. *Phys. Rev. A*, v. 94, p. 013810, 2016. Cited 3 times on page 34, 50, and 53.

77 CLASSEN, A.; WALDMANN, F.; GIEBEL, S.; SCHNEIDER, R.; BHATTI, D.; MEHRINGER, T.; ZANTHIER, J. von. Superresolving imaging of arbitrary one-dimensional arrays of thermal light sources using multiphoton interference. *Phys. Rev. Lett.*, v. 117, p. 253601, 2016. Cited 2 times on page 34 and 35.

78 SCHNEIDER, R.; MEHRINGER, T.; MERCURIO, G.; WENTHAUS, L.; CLASSEN, A.; BRENNER, G.; GOROBTSOV, O.; BENZ, A.; BHATTI, D.; BOCKLAGE, L.; FISCHER, B.; LAZAREV, S.; OBUKHOV, Y.; SCHLAGE, K.; SKOPINTSEV, P.; WAGNER, J.; WALDMANN, F.; WILLING, S.; ZALUZHNYY, I.; WURTH, W.; VARTANYANTS, I. A.; RÖHLSBERGER, R.; ZANTHIER, J. von. Quantum imaging with incoherently scattered light from a free-electron laser. *Nat. Phys*, v. 14, p. 126–129, 2018. Cited 2 times on page 34 and 35.

79 JELTES, T.; MCNAMARA, J. M.; HOGERVORST, W.; VASSEN, W.; KRACHMALNICOFF, V.; SCHELLEKENS, M.; PERRIN, A.; CHANG, H.; BOIRON, D.; ASPECT, A.; WESTBROOK, C. I. Comparison of the Hanbury Brown-Twiss effect for bosons and fermions. *Nature*, v. 445, p. 402, 2007. Cited on page 34.

80 BOCQUILLON, E.; FREULON, V.; BERROIR, J.-M.; DEGIOVANNI, P.; PLAÇAIS, B.; CAVANNA, A.; JIN, Y.; FÈVE, G. Coherence and indistinguishability of single electrons emitted by independent sources. *Science*, v. 339, p. 1054, 2013. Cited on page 34.

81 KERAMATI, S.; JONES, E. R.; ARMSTRONG, J.; BATELAAN, H. Partially coherent quantum degenerate electron matter waves. *arXiv:1811.09743*. Disponível em: <https://arxiv.org/abs/1811.09743>. Cited 2 times on page 35 and 63.

82 MANDEL, L.; WOLF, E. *Optical coherence and quantum optics*. [S.l.]: Cambridge University Press, 1995. Cited 15 times on page 36, 39, 40, 41, 42, 43, 44, 45, 46, 47, 48, 50, 51, 52, and 58.

83 MANDEL, L. Quantum theory of interference effects produced by independent light beams. *Phys. Rev.*, v. 134, p. A10, 1964. Cited on page 38.

84 JACKSON, J. D. *Classical Electrodynamics*. 3rd. ed. New York: John Wiley & Sons, 1999. Cited 4 times on page 39, 40, 70, and 71.

85 GOLDSTEIN, H.; POOLE, C.; SAFKO, J. *Classical mechanics*. 3rd. ed. [S.l.]: Addison-Wesley, 2001. Cited on page 41.

86 MILONNI, P. W. *The quantum vacuum: an introduction to quantum electrodynamics*. San Diego: Academic Press, 1994. Cited on page 44.

87 SUDARSHAN, E. C. G. Equivalence of semiclassical and quantum mechanical descriptions of statistical light beams. *Phys. Rev. Lett.*, American Physical Society, v. 10, p. 277–279, Apr 1963. Cited on page 45.

88 GLAUBER, R. J. Photon correlations. *Phys. Rev. Lett.*, American Physical Society, v. 10, p. 84–86, Feb 1963. Cited on page 45.

89 GLAUBER, R. J. The quantum theory of optical coherence. *Phys. Rev.*, v. 130, p. 2529, 1963. Cited 2 times on page 45 and 50.

90 PIZA, A. F. R. d. T. *Mecânica quântica*. 2nd. ed. São Paulo: Editora da Universidade de São Paulo, 2009. Cited 2 times on page 47 and 55.

91 GRIFFITHS, J. D. *Introduction to quantum mechanics*. 2nd. ed. New Jersey: Pearson Prentice Hall, 2005. Cited on page 47.

92 MANDEL, L. Sub-poissonian photon statistics in resonance fluorescence. *Opt. Lett.*, v. 4, p. 205, 1979. Cited on page 52.

93 MANDEL, L. Photon interference and correlation effects produced by independent quantum sources. *Phys. Rev. A*, v. 28, p. 929, 1983. Cited 3 times on page 53, 55, and 62.

94 OPPEL, S.; WIEGNER, R.; AGARWAL, G. S.; ZANTHIER, J. von. Directional superradiant emission from statistically independent incoherent nonclassical and classical sources. *Phys. Rev. Lett.*, v. 113, p. 263606, 2014. Cited on page 53.

95 MAHRLEIN, S.; OPPEL, S.; WIEGNER, R.; ZANTHIER, J. von. Hong-Ou-Mandel interference without beam splitters. *J. Mod. Opt.*, v. 64, p. 921, 2016. Cited 4 times on page 55, 56, 58, and 59.

96 OU, Z. Y.; MANDEL, L. Further evidence of nonclassical behavior in optical interference. *Phys. Rev. Lett.*, v. 62, p. 2941, 1989. Cited on page 55.

97 AGARWAL, G. S. *Quantum statistical theories of spontaneous emission and their relation to other approaches*. Berlin, Heidelberg: Springer-Verlag, 1974. v. 70. (Springer tracts in modern physics, v. 70). Cited on page 56.

98 WIEGNER, R.; ZANTHIER, J. von; AGARWAL, G. S. Quantum-interference-initiated superradiant and subradiant emission from entangled atoms. *Phys. Rev. A*, v. 84, p. 023805, 2011. Cited on page 56.

99 ASPELMEYER, M.; KIPPENBERG, T. J.; MARQUARDT, F. Cavity optomechanics. *Rev. Mod. Phys.*, v. 86, p. 1391, 2014. Cited 2 times on page 66 and 75.

100 JACOBS, K.; TOMBESI, P.; COLLETT, M. J.; WALLS, D. F. Quantum-nondemolition measurement of photon number using radiation pressure. *Phys. Rev. A*, v. 49, p. 1961, 1994. Cited on page 66.

101 MANCINI, S.; MAN'KO, V. I.; TOMBESI, P. Ponderomotive control of quantum macroscopic coherence. *Phys. Rev. A*, v. 55, p. 3042, 1997. Cited on page 66.

102 BOSE, S.; JACOBS, K.; KNIGHT, P. L. Scheme to probe the decoherence of a macroscopic object. *Phys. Rev. A*, v. 59, p. 3204, 1999. Cited on page 66.

103 MARSHALL, W.; SIMON, C.; PENROSE, R.; BOUWMEESTER, D. Towards quantum superpositions of a mirror. *Phys. Rev. Lett.*, v. 91, p. 130401, 2003. Cited 3 times on page 66, 75, and 76.

104 BASSI, A.; IPPOLITI, E.; ADLER, S. L. Towards quantum superpositions of a mirror: an exact open systems analysis. *Phys. Rev. Lett.*, v. 94, p. 030401, 2005. Cited on page 66.

105 STEUERNAGEL, O. Imprinting interference fringes in massive optomechanical systems. *Phys. Rev. A*, v. 84, p. 064101, 2011. Cited on page 66.

106 VITALI, D.; GIGAN, S.; FERREIRA, A.; BOHM, H. R.; TOMBESI, P.; GUERREIRO, A.; VEDRAL, V.; ZEILINGER, A.; ASPELMEYER, M. Optomechanical entanglement between a movable mirror and a cavity field. *Phys. Rev. Lett.*, v. 98, p. 030405, 2007. Cited on page 66.

107 PATERNOSTRO, M.; VITALI, D.; GIGAN, S.; KIM, M. S.; BRUKNER, C.; EISERT, J.; ASPELMEYER, M. Creating and probing multipartite macroscopic entanglement with light. *Phys. Rev. Lett.*, v. 99, p. 250401, 2007. Cited on page 66.

108 HOFER, S. G.; WIECZOREK, W.; ASPELMEYER, M.; HAMMERER, K. Quantum entanglement and teleportation in pulsed cavity optomechanics. *Phys. Rev. A*, v. 84, p. 052327, 2011. Cited on page 66.

109 PALOMAKI, T. A.; HARLOW, J. W.; TEUFEL, J. D.; SIMMONDS, R. W.; LEHNERT, K. W. Coherent state transfer between itinerant microwave fields and a mechanical oscillator. *Nature*, v. 495, p. 210, 2013. Cited on page 66.

110 COHEN, J. D.; MEENEHAN, S. M.; MCCABE, G. S.; GROBLACHER, S.; SAFAVI-NAEINI, A. H.; MARSILI, F.; SHAW, M. D.; PAINTER, O. Phonon counting and intensity interferometry of a nanomechanical resonator. *Nature*, v. 520, p. 522, 2015. Cited on page 66.

111 MARINKOVIć, I.; WALLUCKS, A.; RIEDINGER, R.; HONG, S.; ASPELMEYER, M.; GRÖBLACHER, S. Optomechanical bell test. *Phys. Rev. Lett.*, v. 121, p. 220404, Nov 2018. Cited on page 66.

112 LAW, C. K. Interaction between a moving mirror and radiation pressure: A Hamiltonian formulation. *Phys. Rev. A*, v. 51, p. 2537, 1995. Cited on page 66.

113 BARNETT, S. M. Resolution of the Abraham-Minkowski dilemma. *Phys. Rev. Lett.*, v. 104, p. 070401, 2010. Cited 2 times on page 66 and 77.

114 NEWTON, T. D.; WIGNER, E. P. Localized states for elementary systems. *Rev. Mod. Phys.*, American Physical Society, v. 21, p. 400, Jul 1949. Cited on page 67.

115 JORDAN, T. F. What happens to the position, spin, and parity when the mass goes to zero. *J. Math. Phys.*, v. 23, n. 12, p. 2524, 1982. Cited on page 67.

116 BIALYNICKI-BIRULA, I. Photon wave function. *Progress in Optics*, XXXVI, 1996. Cited 2 times on page 68 and 69.

117 MINKOWSKI, H. Die Grundgleichungen für die elektromagnetische Vorgänge in bewegten Körpen. *Nachr. Ges. Wiss. Goettingen*, v. 1908, p. 53, 1908. Cited 2 times on page 69 and 77.

118 MINKOWSKI, H. *The Fundamental Equations for Electromagnetic Processes in Moving Bodies*. Calcuta: University Press, 1920. In: The Principle of Relativity. Translated by M. Saha. Disponível em: <https://en.wikisource.org/wiki/Translation:The_Fundamental_Equations_for_Electromagnetic_Processes_in_Moving_Bodies>. Cited 2 times on page 69 and 77.

119 ABRAHAM, M. Zur Elektrodynamik Bewegter Körpe. *Rend. Circ. Mat. Palermo*, v. 28, p. 1, 1909. Cited 2 times on page 69 and 77.

120 ABRAHAM, M. Sull'elettrodinamica di Minkowski. *Rend. Circ. Mat. Palermo*, v. 30, p. 33, 1910. Cited 2 times on page 69 and 77.

121 SALDANHA, P. L.; MONKEN, C. H. Energy and momentum entanglement in parametric downconversion. *Am. J. Phys.*, v. 81, p. 28, 2013. Cited on page 70.

122 THOMPSON, J. D.; ZWICKL, B. M.; JAYICH, A. M.; MARQUARDT, F.; GIRVIN, S. M.; HARRIS, J. G. E. Strong dispersive coupling of a high-finesse cavity to a micromechanical membrane. *Nature*, v. 452, p. 72, 2008. Cited on page 75.

123 ARCIZET, O.; COHADON, P.-F.; BRIANT, T.; PINARD, M.; HEIDMANN, A. Radiation-pressure cooling and optomechanical instability of a micromirror. *Nature*, v. 444, p. 71, 2006. Cited on page 75.

124 NORTE, R. A.; MOURA, J. P.; GROBLACHER, S. Mechanical resonators for quantum optomechanics experiments at toom temperature. *Phys. Rev. Lett.*, v. 116, p. 147202, 2016. Cited on page 75.

125 WALKER, G. B.; LAHOZ, D. G. Experimental observation of Abraham force in a dielectric. *Nature*, v. 253, p. 339, 1975. Cited on page 77.

126 WALKER, G. B.; LAHOZ, D. G.; WALKER, G. Measurement of the Abraham force in a barium titanate specimen. *Can. J. Phys.*, v. 53, n. 23, p. 2577–2586, 1975. Cited on page 77.

127 PENFIELD, P.; HAUS, H. A. *Electrodynamics of moving media*. Cambridge: M.I.T. Press, 1967. Cited on page 77.

128 GROOT, S. R. de; SUTTORP, L. G. *Foundations of electrodynamics*. Amsterdam: North-Holland Publishing Company, 1972. Cited on page 77.

Appendix

APPENDIX A – Effect of an impulsive force on a momentum wave function

In this appendix we want to derive what happens to the wave function of a quantum particle when a linear potential acts over it during a very short period of time – this is equivalent to saying that the particle suffered an impulsive force. We will show that, apart from a global phase, the momentum wave function of the particle is displaced by the classically expected amount, without distorting its shape.

Consider a quantum particle with mass m, described by the state $|\psi_0\rangle$ whose momentum wave function is $\psi_0(p) = \langle p|\psi_0\rangle$, and that evolves under the Hamiltonian

$$H = \frac{p^2}{2m} + V(x). \tag{A.1}$$

We demand that the potential $V(x)$ is linear, that is, it corresponds to the application of a constant force F in the x direction and can be written as

$$V(x) = V_0 - Fx, \tag{A.2}$$

where V_0 is a constant factor. According to Schrödinger's equation [46], the momentum wave function of the particle after some time t is given by

$$\psi(p,t) = \langle p|e^{-iHt}|\psi_0\rangle = \langle p|e^{-i\left[\frac{p^2}{2m}+V(x)\right]t}|\psi_0\rangle, \tag{A.3}$$

where we have used $\hbar = 1$.

We now assume that the interaction time t is so small that, in comparison with the potential term $V(x)$ in the Hamiltonian, the free evolution term $p^2/2m$ will cause a negligible change in the wave function and we can thus approximate $H \approx V(x)$. Implicit in this approximation is the assumption that $\psi_0(p)$ has negligible amplitude for momentum values that are too large and which could compensate for the smallness of t. One can therefore say that the evolution of the momentum wave function in this regime is approximately given by

$$\psi(p,t) \approx e^{-iV_0t}\langle p|e^{i(Ft)x}|\psi_0\rangle \tag{A.4}$$

We immediately note that $e^{i(Ft)x}$ has the form of a momentum displacement operator [46], with $\langle p|e^{i\lambda x} = \langle p-\lambda|$. We can therefore say that

$$\psi(p,t) \approx e^{-iV_0t}\ \psi_0(p - Ft), \tag{A.5}$$

which is what we wanted to prove.

We have thus showed that, under a constant force F that acts during a very short period of time t, the momentum wave function of a particle is simply displaced by the classically expected amount Ft, apart from a phase factor.